

**INVESTIGATIONS INTO USE OF CARBON NANOTUBES IN  
POLYMER MEMBRANES FOR FILTRATION AND OTHER  
APPLICATIONS**

**Thesis Submitted to  
THE MAHARAJA SAYAJIRAO UNIVERSITY OF BARODA**

**For the degree of  
Doctor of Philosophy  
In  
Applied Chemistry**

**Submitted by  
Prachi Shah**



**APPLIED CHEMISTRY DEPARTMENT  
FACULTY OF TECHNOLOGY & ENGINEERING  
THE M. S. UNIVERSITY OF BARODA  
VADODARA-390 001, INDIA**

**September 2013**

## CERTIFICATE

This is to certify that the thesis entitled “**INVESTIGATIONS INTO USE OF CARBON NANOTUBES IN POLYMER MEMBRANES FOR FILTRATION AND OTHER APPLICATIONS**” submitted by Mrs. Prachi Shah to The M.S. University of Baroda, Vadodara for the award of **Ph.D.** degree in Applied Chemistry incorporates the original research work carried out by him under my supervision.

Dr. C. N. Murthy

Research Guide  
Applied Chemistry Department

Head

Applied Chemistry Department  
Faculty of Technology and Engineering  
The M. S. University of Baroda

Dean

Faculty of Technology and Engineering  
The M. S. University of Baroda

## DECLARATION

I state that the work presented in this thesis entitled “**INVESTIGATIONS INTO USE OF CARBON NANOTUBES IN POLYMER MEMBRANES FOR FILTRATION AND OTHER APPLICATIONS**” comprises of independent investigations carryout out by me under the guidance of Prof.C. N. Murthy. Wherever references have been made to the work of others, it has been clearly indicated with the source of information under the references selection. The matter presented in this thesis has not been submitted elsewhere for the award of any other degree.

Signature of the candidate

Prachi Shah

## ACKNOWLEDGEMENTS

I sincerely express my deep sense of gratitude and thank my guide Prof. C. N. Murthy, Applied Chemistry Department, for his invaluable guidance, expert suggestions throughout my research work. He is responsible to inspire me for developing the sense of commitment and firmness to carry out this work. I also thank him for his constant encouragement, help and providing necessary facilities throughout this work.

I deeply thank Prof. P. T. Deota, Head, Applied Chemistry Department, Faculty of Technology and Engineering, M. S. U. for their continual support and encouragement during my research work.

I deeply thank The M. S. University of Baroda, Vadodara for providing me the opportunity to carry out this research work and especially Applied Chemistry department to provide necessary facilities to carry out my research work in their research lab.

I deeply thank DRDO (Defense Research Development Organization) for funding my project and helping in metal removal studies.

I thank Dr. Vandana Rao, Metallurgy Department, Faculty of Technology and Engineering, M. S. U. for her guidance and help conducting out SEM and EDX studies.

I deeply thank Choksi Laboratories, Munjmahuda, Vadodara to help me carry out NMR studies.

I deeply thank Dr. A. V. R. Reddy of CSMCRI (Central Salt and Marine Chemicals Research Institute) Bhavnagar to help me carry out Capillary porometry studies.

I am thankful to all the teachers and non-teaching staff of the Applied Chemistry Department for supporting me throughout the research work.

I thank all my fellow colleagues Dr. Santosh Kumar, Dr. Vinod Bhoi, Dr. Murali, Vaishali Suthar, T. Gangadhar, Renu Singh for their continuous support and encouragement throughout my research work.

My deepest gratitude and indebtedness belong to my sweet Daughter, my Husband, father, mother, brother, sister and in-laws for their patience, endless love, encouragement and understanding during the different phases of my work and made it possible to complete this thesis.

Prachi Shah

*Dedicated to my Husband and Daughter*

# Contents

	<b>Page No.</b>
Chapter 1 Introduction	17
1.1 Carbon nanotubes	17
1.1.1 Single walled carbon nanotubes	19
1.1.2 Double walled carbon nanotubes	21
1.1.3 Multi-walled carbon nanotubes	21
1.1.4 Torus	23
1.1.5 Nanobud	23
1.1.6 Graphenated carbon nanotubes (g-CNTs)	23
1.1.7 Nitrogen Doped Carbon Nanotubes	25
1.1.8 Peapod	26
1.1.9 Cup-stacked carbon nanotubes	26
1.1.10 Extreme carbon nanotubes	26
1.2 Synthesis techniques of nanotubes	27
1.2.1 High Pressure Carbon Monoxide Method	27
1.2.2 Arc discharge	29
1.2.3 Laser ablation	31
1.2.4 Plasma torch	32
1.2.5 Chemical vapor deposition (CVD)	34
1.2.6 Super-growth CVD	36
1.2.7 Flame pyrolysis	36
1.3 Potential applications	37
1.3.1 Mechanical and structural applications	37
1.3.2 Antiballistic materials	38
1.3.3 Medical	38
1.3.4 Electrical circuits	38
1.3.5 Solar cells	39
1.3.6 Lighting Elements	39
1.3.7 Hydrogen Storage	40
1.3.8 Memory device	40

1.3.9	Ultracapacitors	40
1.3.10	Radar absorption	40
1.3.11	Optical power detectors	41
1.3.12	Adsorption	42
1.4	“Water” : Transparent Gold	45
1.5	Toxic ions present in surface and ground water	46
1.6	Sources and Health effects of Toxic Metals	46
1.6.1	Arsenic	46
1.6.2	Cadmium	47
1.6.3	Chromium	48
1.6.4	Cobalt	49
1.6.5	Lead	50
1.6.6	Mercury	51
1.6.7	Nickel	52
1.7	Consumption guidelines by WHO & BIS	53
1.8	Different technologies used in water purification	56
1.8.1	Chemical precipitation	56
1.8.2	Sulphide Precipitation	56
1.8.3	Carbonate precipitation	57
1.8.4	Chemical Reduction	57
1.8.5	Solvent Extraction	57
1.8.6	Cementation	58
1.8.7	Electro-deposition	58
1.8.8	Ultrafiltration & Nanofiltration	58
1.8.9	Electro dialysis	59
1.8.10	Reverse Osmosis hyperfine filtration	59
1.8.11	Evaporation	60
1.8.12	Xanthate process	60
1.8.13	Adsorption on Solid Surfaces	60
1.8.14	Ion Exchange Resins	61
1.9	Advanced Materials Introduced in Water Purification	61
1.9.1	Resins Functionalized with Novel Chelating groups	62

1.9.2	Biomaterials and their scope in water purification applications	63
1.9.3	Carbon nanotubes	63
Chapter 2	Nanotube cleaning, functionalization, characterization, metal removal and adsorption isotherm studies	65
2.1	Introduction	65
2.2	Materials	67
2.3	Experiments	67
2.3.1	Surface cleaning of nanotubes	67
2.3.2	Functionalization of CNTs	70
2.3.3	Preparation of stocks and Batch method studies	71
2.4	Characterization	73
2.5	Results and discussion	73
2.5.1	Characterization of nanotubes	73
2.5.2	Adsorption kinetics	86
2.5.3	Adsorption isotherm studies with batch method	106
2.6	Conclusion	114
Chapter 3	Comparative study of surface cleaning and modification of MWNT's using various oxidizing agents	115
3.1	Introduction	115
3.2	Materials	116
3.3	Experiment	117
3.3.1	Treatment with acid piranha solution	117
3.3.2	Treatment with HNO <sub>3</sub> +H <sub>2</sub> SO <sub>4</sub> Mixture	119
3.3.3	Treatment with base Piranha	119
3.3.4	Treatment with KMnO <sub>4</sub> + CH <sub>3</sub> COOH in presence of phase transfer catalyst	119
3.3.5	Titration analysis of functionalized CNT's	119
3.4	Characterization	119
3.5	Results	120
3.5.1	Electron microscopy	120
3.5.2	FT-IR	124
3.5.3	Thermo-gravimetric analysis	126
3.5.4	Raman Spectroscopy	126

3.5.5	Volumetric titration	132
3.6	Conclusions	134
Chapter 4	Preparation of MWNT/PSf composite membranes and its effect on metal removal	135
4.1	Introduction	135
4.2	Materials	138
4.3	Experiments	138
4.3.1	Purification and functionalization of MWNTs	138
4.3.2	Blending of CNT's into polysulfone to form nanocomposite membranes	140
4.3.3	Preparation of asymmetric flat sheet membranes	142
4.3.4	Capillary flow porometry	142
4.3.5	Permeation test	144
4.3.6	Zeta Potential measurement	145
4.4	Characterization	147
4.5	Results and Discussion	147
4.5.1	Membrane casting by phase-inversion process	147
4.5.2	Characterization of composite polysulfone membranes	148
4.5.3	Heavy metal removal	157
4.6	Conclusions	173
Chapter 5	ATRP using functionalized nanotubes /Acetyl Chloride as radical initiators	174
5.1	Introduction	174
5.2.	Materials	178
5.3	Experimental	179
5.3.1	Polymerization of MMA	179
5.4	Characterization	181
5.5	Results and Discussion	183
5.5.1	Polymerization of MMA and Styrene	183
5.5.2	Characterization	183
5.6	Conclusions	218
	Summary of thesis	219
	References	224
	List of Publications & Presentations	237
	List of Awards	238

# List of Figures

Figures	Title	Page No.
<b>Chapter 1 Introduction</b>		
1.1	Bucky ball Fullerene and cylindrical nanotubes	2
1.2	Rolling of graphene sheet along different directions to get different nanotubes	4
1.3	Double-walled carbon nanotubes	6
1.4	Torus	8
1.5	High Pressure Carbon Monoxide Method	12
1.6	Arc discharge method	14
1.7	Laser ablation Process	17
1.8	Chemical vapor deposition (CVD) process	19
1.9	Availability of renewable fresh water in India	39
<b>Chapter 2 Nanotube cleaning, functionalization, characterization, metal removal and adsorption isotherm studies</b>		
2.1	SEM image of commercially available Pristine CNTs	53
2.2	Schematic representation of functionalization of nanotubes	56
2.3	Raman spectra (a) Pristine (b) Purified CNTs	59
2.4	TEM images (a) Pristine (b) Oxidized (c) Acylated (d) Amide (e) Azide functionalized CNTs	61
2.5	FT-IR spectras (a) Pristine (b) Oxidized (c) Acylated (d) Amide (e) Azide functionalized CNTs	63
2.6	EDS spectras (a) Pristine (b) Oxidized (c) Azide functionalized CNTs	65
2.7	XRD spectra of oxidized and functionalized CNTs	67
2.8	Thermo-gravimetric studies of Purified CNT's and various functionalized CNT's	69
2.9	Plots of (a) % Removal of metal ions v/s time (b,c) $\ln(1-Ut)$ v/s Time(h) for removal of heavy metals by unfunctionalized CNTs	71
2.10	Plots of (a) % Removal of metal ions v/s time (b,c) $\ln(1-Ut)$ v/s Time(h) for for removal of heavy metals by acylated CNTs	72
2.11	Plots of (a) % Removal of metal ions v/s time (b,c) $\ln(1-Ut)$ v/s Time(h) for for removal of heavy metals by amide functionalized CNTs	73
2.12	Plots of (a) % Removal of metal ions v/s time (b,c) $\ln(1-Ut)$ v/s Time(h) for for removal of heavy metals by azide functionalized CNTs	74
2.13	Removal of Cr+6 ions at diff. pH by (a)amide and (b) azide functionalized CNTs	87
2.14	Freundlich and Langmuir adsorption isotherm of Chromium onto	94

2.15	amide functionalized CNTs Freundlich and Langmuir adsorption isotherm of Chromium onto azide functionalized CNTs	95
------	--	----

### **Chapter 3 Comparative study of surface cleaning and modification of MWNT's using various oxidizing agents**

3.1	Effect of washing on the behavior of nanotubes towards magnetic needle	102
3.2	SEM images of MWNT's (a) pristine (b) H <sub>2</sub> SO <sub>4</sub> /HNO <sub>3</sub> treated (c) Base piranha treated (d) Acid piranha treated (e) KMnO <sub>4</sub> /CH <sub>3</sub> COOH treated in absence of PTC (f) KMnO <sub>4</sub> /CH <sub>3</sub> COOH treated in presence of PTC	105
3.3	Pictures of the dispersion of the MWCNTs (10 mg) in water (10 ml). 1-H <sub>2</sub> SO <sub>4</sub> /HNO <sub>3</sub> -treated MWCNTs; 2-KMnO <sub>4</sub> -PTC treated MWCNTs; 3-base piranha treated MWCNTs; 4-acid piranha treated MWCNTs; 5-Pristine MWNT's. Samples were kept for 100 days. MWCNTs were dispersed in water by sonication for 1h	107
3.4	FT-IR spectra of MWNT's (a) Purified (b) H <sub>2</sub> SO <sub>4</sub> /HNO <sub>3</sub> treated (c) Base Piranha treated (d) Acid Piranha treated (e) KMnO <sub>4</sub> /CH <sub>3</sub> COOH treated in presence of PTC	109
3.5	TGA curves of the MWCNT samples: (a) MWCNT-HNO <sub>3</sub> , (b) MWCNT-NH <sub>4</sub> OH/H <sub>2</sub> O <sub>2</sub> , (c) MWCNT-H <sub>2</sub> SO <sub>4</sub> /H <sub>2</sub> O <sub>2</sub> , (d) MWCNT-KMnO <sub>4</sub> -PTC	111
3.6	Raman spectra of the MWCNT samples: (a) MWCNT-HNO <sub>3</sub> , (b) MWCNT-NH <sub>4</sub> OH/H <sub>2</sub> O <sub>2</sub> , (c) MWCNT-H <sub>2</sub> SO <sub>4</sub> /H <sub>2</sub> O <sub>2</sub> , (d) MWCNT-KMnO <sub>4</sub> -PTC	113
3.7	Raman spectra of differently oxidized MWCNT samples	114

### **Chapter 4 Preparation of MWNT/PSf composite membranes and its effect on metal removal**

4.1	FT-IR scans of MWNTs (a) carboxylated MWNT and (b) azide functionalized MWNTs	125
4.2	Hydrogen bonding between the possible arrangement of functional groups on nanotubes and polysulfone	127
4.3	Charge development on surface of membrane or dispersed particle in a dispersion medium	130
4.4	FESEM images of CNT/PSf composite membranes (a) 0.0% (b) 0.1% (c) 1% functionalized MWNTs	133
4.5	FT-IR of (a) oxidized CNT/PSF (b) amide functionalized CNT/PSF blend membranes	135
4.6	TGA data composite polysulfone membranes with different percentages of amide functionalized MWNTs	137
4.7	Flow rate at different pressures for different amide MWCNT/PSf membranes at acidic pH 2.6	146
4.8	%Removal of metal ions at different pressure (a) %amide CNT/PSf (b) %azide CNT/PSf composite membranes at pH 2.6	150

4.9	Removal studies of Cr+6 ions at different pH for (a) oxidized (b) amide (c) azide functionalized MWCNT/PSf. at pressure of 0.49MPa	152
-----	--	-----

## Chapter 5 ATRP using a Novel Initiator :Acetyl Chloride/Acylated nanotubes

5.1	Schematic presentation of general mechanism of controlled radical polymerization (CRP) method	159
5.2	Reaction scheme employed in the process where $K_a$ , $K_p$ , $K_t$ are rate coefficients for activation, propagation and termination	164
5.3	FTIR of (a)PMMA (b) Styrene initiated from acetyl chloride/acylated nanotubes	168
5.4	NMR of acetylchloride/acylated nanotubes initiated PMMA	170
5.5	$^{13}\text{C}$ NMR of PMMA obtained from labeled acetyl chloride used as initiator	171
5.6	$^{13}\text{C}$ NMR of Polystyrene obtained from acetyl chloride used as initiator	173
5.7	Thermogravimetric analysis of PMMA, obtained by (a) acetyl chloride (b) acylated nanotubes as initiator	175
5.8	Thermogravimetric analysis of Polystyrene by acylated nanotubes as initiator	176
5.9	DSC curve for PMMA (glass transition temperature:135°C)	178
5.10	DSC curve for PS (glass transition temperature:109°C)	179
5.11	SEM images of polymer PMMA depict the foamy fibrous texture of the polymer	181
5.12	SEM images of polymer PMMA initiated by acylated CNT	182
5.13	SEM images of polymer PS initiated by acylated CNT	183
5.14	SEC curves for different sets S1, S2, S3, S4 depicting the peak apex and weight average molecular weight	186
5.15	SEC curves for different sets PMNS and PMVLS depicting the peak apex and weight average molecular weight	187
5.16	(a) SEC curve for acetyl chloride initiated ATRP of MMA depicting $2.83 \times 10^5$ and $2.84 \times 10^5$ as peak apex and weight average molecular weight respectively (b) PD and Mn as a function of monomer conversion ; reaction conditions: Temperature = 60°C and $[M]_0/[M]_t^sX/[L]_0/I_0 = [PMMA]_0/[Cu(1)Br]_0/[2,2'$ bipyridyl] $]_0/[CH_3COCl]_0 = 100:0.5:1:0.625$ and surfactant (Brij-98)concentration =1.64gm/10 mL of distilled water	190
5.17	(a) SEC curve for acetyl chloride initiated ATRP of MMA depicting $8.0 \times 10^5$ and $7.2 \times 10^5$ as peak apex and weight average molecular weight respectively (b) PD as a function of %Conversion(c) $\ln[M]_0/[M]$ versus time and (d)Mn as a function of %Conversion; reaction conditions: Temperature = 28°C and $[M]_0/[M]_t^sX/[L]_0/I_0 = [PMMA]_0/[Cu(1)Br]_0/[2,2'$ bipyridyl] $]_0/[CH_3COCl]_0 = 100:0.5:1:0.625$ and surfactant (Brij-98)concentration =0.82gm/10 mL of distilled water	193

5.18	(a) Mn as a function of %Conversion (b) PD as a function of %Conversion for polystyrene at room temperature (c) Mn as a function of %Conversion (b) PD as a function of %Conversion for polystyrene at high temperature: $[M]_0/[M_t^s X]_0/[L]_0/I_0 = [PS]_0/[Cu(1)Br]_0/[2,2' \text{ bipyridyl}]_0/[CH_3COCl]_0 = 100:0.5:1:0.625$ and surfactant (Brij-98) concentration = 1.64gm/10 mL of distilled water	197
5.19	Activation energies for decomposition acyl radicals and formation of acyl radical	199
5.20	Action of acyl radical on double bond(a) and subsequent propagation to help in polymerization of ethene(b)	200

## List of Tables

Tables	Title	Page No.
<b>Chapter 1 Introduction</b>		
1.1	Permissible Limits of Different Metal Ions for Potable Water (in mg/L)	38
<b>Chapter 2 Nanotube cleaning, functionalization, characterization, metal removal and adsorption isotherm studies</b>		
2.1	% removal of metal ions with time for unfunctionalized nanotubes	75
2.2	% removal of metal ions with time for acylated nanotubes	76
2.3	% removal of metal ions with time for amide functionalized nanotubes	77
2.4	% removal of metal ions with time for azide functionalized nanotubes	78
2.5	Comparative study of different MWNTs	79
2.6	Values of $\ln(1-Ut)$ for unfunctionalized nanotubes at various times	81
2.7	Values of $\ln(1-Ut)$ for acylated nanotubes at various times	82
2.8	Values of $\ln(1-Ut)$ for amide functionalized nanotubes at various times	83
2.9	Values of $\ln(1-Ut)$ for azide functionalized nanotubes at various times	84
2.10	Comparative study of different MWNTs	85
2.11	% Removal of metal ions with dosage of functionalized nanotubes	89
2.12	Showing $X_e$ , $Q_e$ , $C_e$ , $1/X_e$ , $1/Q_e$ , $1/C_e$ , $\log Q_e$ , $\log C_e$ for different initial concentrations of $Cr^{+6}$ solution when their adsorption was studied onto amide CNTs, to study Langmuir and Freundlich isotherms	91
2.13	Showing $X_e$ , $Q_e$ , $C_e$ , $1/X_e$ , $1/Q_e$ , $1/C_e$ , $\log Q_e$ , $\log C_e$ for different initial concentrations of $Cr^{+6}$ solution when their adsorption was studied onto azide CNTs, to study Langmuir and Freundlich isotherms	92
2.14	The regression equations parameters $Q_0$ , $K$ , $R^2$ and $1/n$ for functionalized CNTs	97
<b>Chapter 3 Comparative study of surface cleaning and modification of MWNT's using various oxidizing agents</b>		
3.1	ID/IG ratios for differently oxidized MWNT's samples	115
3.2	Carbonyl group concentration for differently oxidized MWNT's samples	117

## **Chapter 4 Preparation of MWNT/PSf composite membranes and its effect on metal removal**

4.1	Variation of the pore size with amount of amide functionalized CNT's	139
4.2	Variation of the smallest pore diameter (micron) and required pressure (MPa) with weight % of CNT's	140
4.3	Values of Zeta potential developed at the surface of PSf/ % carboxylated CNT composite membranes when in contact with an electrolyte solution	142
4.4	Values of Zeta potential developed at the surface of PSf/ % amide functionalized CNT composite membranes when in contact with an electrolyte solution	143
4.5	Permeate flow for different membranes at different pressures	145
4.6	Removal studies of metal ions at pH 2.6 for amide functionalized MWCNT/PSf. at pressure of 0.49MPa and 0.882MPa	148
4.7	Removal studies of metal ions at pH 2.6 for azide functionalized MWCNT/PSf. at pressure of 0.49MPa and 0.882MPa	149
4.8	Removal studies of toxic metal ions at pH 2.6 for oxidized MWCNT/PSf at pressure of 0.49MPa	154
4.9	Removal studies of toxic metal ions at pH 2.6 for amide functionalized MWCNT/PSf at pressure of 0.49MPa	155
4.10	Removal studies of toxic metal ions at pH 2.6 for azide functionalized MWCNT/PSf at pressure of 0.49MPa	156

## **Chapter 5 ATRP using a Novel Initiator :Acetyl Chloride/Acylated nanotubes**

5.1	Various sets performed to obtain polymers	166
5.2	% conversions, weight average molecular weights and polydispersities for different sets where Monomer(M) = MMA (methyl-methacrylate), Catalyst(C) = CuCl, Ligand(L) = 2,2' bipyridyl, Initiator(I) = acetyl chloride, Surfactant= Brij 98, Solvent = water	185
5.3	Kinetic study of ATRP of PMMA at 60°C using acetyl chloride as initiator	189
5.4	Kinetic study of ATRP of PMMA at low surfactant concentration (PMLS) using acetyl chloride as initiator	192
5.5	Kinetic study of ATRP of PS at room temperature using acetyl chloride as initiator	195
5.6	Kinetic study of ATRP of PS at high temperature (60°C) using acetyl chloride as initiator	196

## ***1.1 Carbon nanotubes***

Carbon nanotubes (CNTs) are allotropes of carbon with a cylindrical nanostructure. Nanotubes have been constructed with length-to-diameter ratio of up to 132,000,000:1<sup>1</sup>this ratio called as aspect ratio is significantly larger than that of any other material. These cylindrical carbon molecules have extremely unique and remarkable properties which find their use in various fields as bio-sensors, semi-conductors, electronics, optical sciences, nanotechnology, mechanical and materials science, astrology and thousands of other technologies. Carbon nanotubes have extraordinary mechanical strength, thermal and electrical conductivity, which make them useful as additives. CNT exhibits extraordinary mechanical properties: the Young's modulus is over 1 Tera Pascal. It is stiff as diamond. The estimated tensile strength is 200 Giga Pascal. These properties are ideal for reinforced composites, Nanoelectro-mechanical systems (NEMS).

Researchers have been working on using carbon nanotubes to make transistors instead of silicon. *Recently a team at USC has created a carbon nanotube transistor that has an extrinsic frequency (which defines its practical performance limit) of 25 GHz – 40% faster than the current record holder, which operates at 15 GHz. That makes the team's nanotube transistor the fastest in the world.* The extremely small lengths possible due to use of CNT reduce the time it takes for the electrons to travel through the transistors, thus making them faster by reducing the parasitic capacitance of the circuit and also decreasing the channel length of the transistor.

Nanotubes are members of the fullerene (Figure 1.1) structural family. Their walls are formed by one-atom-thick sheets of carbon, called graphene ( $sp^2$  hybridized). These sheets are rolled at specific and

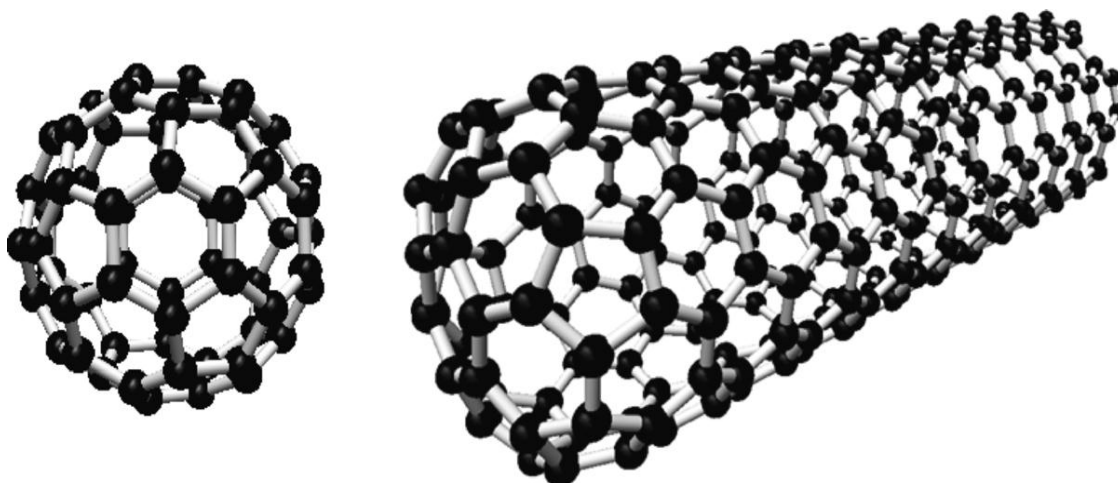


**Figure 1.1** Bucky ball Fullerene and cylindrical nanotubes.

discrete ("chiral") angles, and the combination of the rolling angle and radius decides the nanotube properties; for example, whether the individual nanotube shell is a metal or semiconductor. Applied quantum chemistry, specifically, orbital hybridization best describes chemical bonding in nanotubes. The chemical bonding of nanotubes is composed entirely of  $sp^2$  bonds, similar to those of graphite. These bonds, which are stronger than the  $sp^3$  bonds found in alkanes and diamond, provide nanotubes with their unique strength.

The end cap of the nanotube can be thought as an incomplete fullerene with five and six membered carbon rings. Nanotubes are categorized as single-walled nanotubes (SWNTs) and multi-walled nanotubes (MWNTs). Individual nanotubes naturally align themselves into "ropes" held together by van der Waals forces, more specifically, pi-stacking.

### 1.1.1 Single walled carbon nanotubes

The structure of a SWNT can be conceptualized by wrapping a one-atom-thick layer of graphite called graphene into a seamless cylinder. The way the graphene sheet is wrapped is represented by a pair of indices  $(n,m)$ . The integers  $n$  and  $m$  denote the number of unit vectors along two directions in the honeycomb crystal lattice of graphene. If  $m = 0$ , the nanotubes are called zigzag nanotubes, and if  $n = m$ , the nanotubes are called armchair nanotubes (Figure 1.2). Otherwise, they are called chiral. The diameter of an ideal nanotube can be calculated from its  $(n, m)$  indices as follows

$$d = \frac{a}{\pi} \sqrt{(n^2 + nm + m^2)} = 78.3 \sqrt{((n + m)^2 - nm)} \text{ pm.}$$

where  $a = 0.246 \text{ nm}$ .

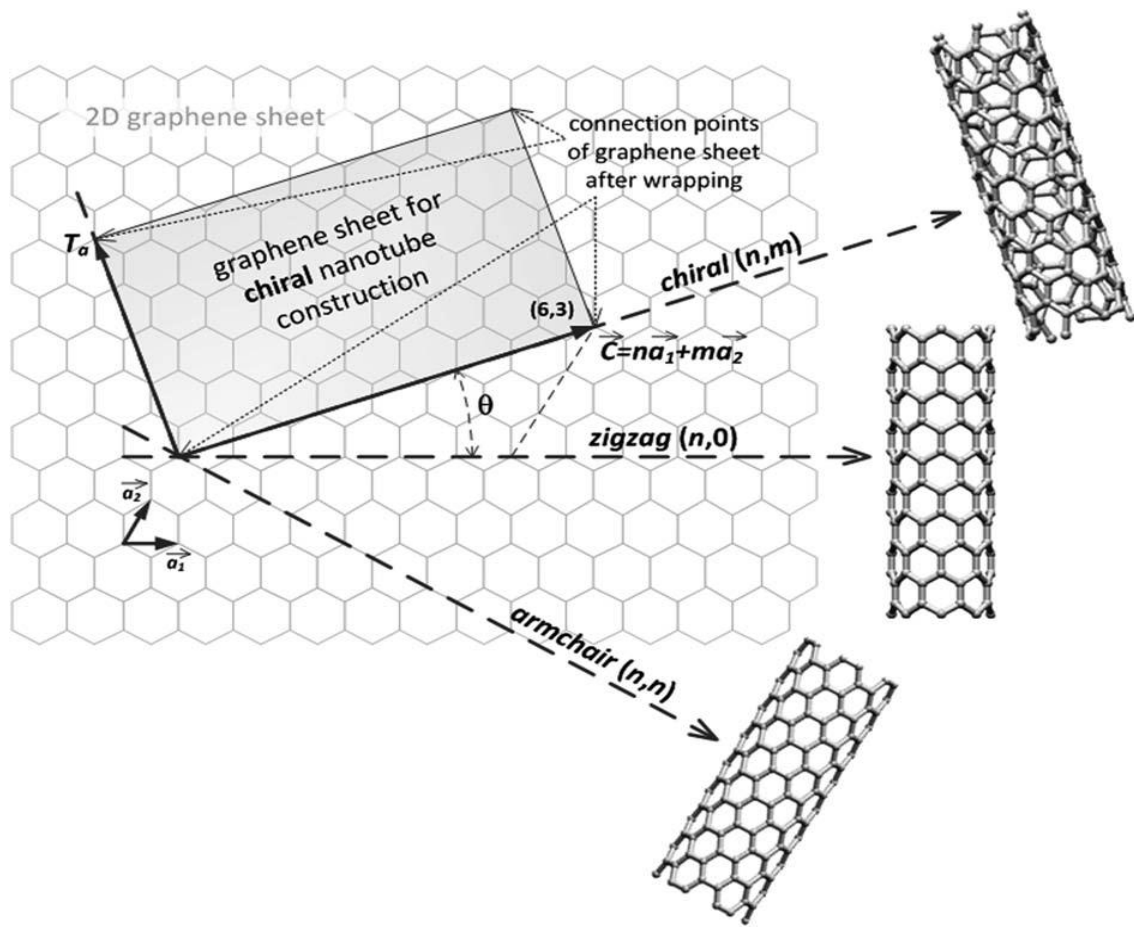


**Figure 1.2** Rolling of graphene sheet along different directions to get different nanotubes.

### **1.1.2 Double walled carbon nanotubes**

Double-walled carbon nanotubes (DWNT) form a special class of nanotubes (Figure 1.3) because their morphology and properties are similar to those of SWNT but their resistance to chemicals is significantly improved. This is especially important when functionalization is required (this means grafting of chemical functions at the surface of the nanotubes) to add new properties to the CNT. In the case of SWNT, covalent functionalization will break some C=C double bonds, leaving "holes" in the structure on the nanotube and, thus, modifying both its mechanical and electrical properties. In the case of DWNT, only the outer wall is modified. DWNT synthesis on the gram-scale was first proposed in 2003<sup>2</sup> by the CCVD technique, from the selective reduction of oxide solutions in methane and hydrogen.

The telescopic motion ability of inner shells<sup>3</sup> and their unique mechanical properties<sup>4</sup> will permit the use of MWNT and SWNT's as main movable arms in coming nanomechanical devices. Retraction force that occurs to telescopic motion caused by the Lennard-Jones interaction between shells and its value is about 1.5 nN<sup>5</sup>.

### **1.1.3 Multi-walled carbon nanotubes**

Multi-walled nanotubes (MWNT) consist of multiple rolled layers (concentric tubes) of graphene. Its individual shells can be described as SWNTs, which can be metallic or semiconducting. Because of statistical probability and restrictions on the relative diameters of the individual tubes, one of the shells, and thus the whole MWNT, is usually a zero-gap metal.

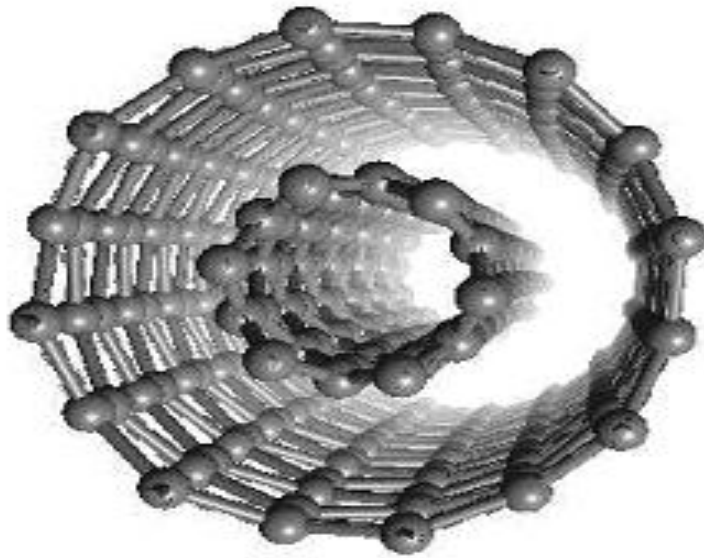


**Figure 1.3** Double-walled carbon nanotubes.

#### **1.1.4 Torus**

In theory, a nanotorus is a carbon nanotube bent into a torus (doughnut shape). Nanotori (Figure 1.4) are predicted to have many unique properties, such as magnetic moments 1000 times larger than previously expected for certain specific radii<sup>6</sup>. Properties such as magnetic moment, thermal stability, etc. vary widely depending on radius of the torus and radius of the tube<sup>6,7</sup>.

#### **1.1.5 Nanobud**

Carbon nanobuds are a newly created material combining two previously discovered allotropes of carbon: carbon nanotubes and fullerenes. In this new material, fullerene-like "buds" are covalently bonded to the outer sidewalls of the underlying carbon nanotube. This hybrid material has useful properties of both fullerenes and carbon nanotubes. In particular, they have been found to be exceptionally good field emitters. In composite materials, the attached fullerene molecules may function as molecular anchors preventing slipping of the nanotubes, thus improving the composite's mechanical properties.

#### **1.1.6 Graphenated carbon nanotubes (g-CNTs)**

Carbon filter papers(Hsu *et al.*)<sup>10</sup> and carbon nanotubes develop some leaf like structures on their sidewalls. These structures are produced following some special conditions of time and temperatures. These are graphene structures bonded chemically to CNT walls reported by Yu *et al.*<sup>8</sup>. Stoner *et al.*<sup>9</sup> have made a detailed study on extraordinary supercapacitor performance of these structures known as "graphenated CNTs". The foliate density can vary as a function of deposition conditions (e.g. temperature and time) with their structure ranging from few layers of graphene (< 10) to thicker, more graphite-like<sup>11</sup>.



**Figure 1.4** Torus.

Presence of these structures makes a very complicated structure with a three-dimensional arrangement, thereby increasing the reactive surface area. The graphene edges arising out are supposed to possess very high density. Graphene edges provide significantly higher charge density and reactivity than the basal plane, but they are difficult to arrange in a three-dimensional, high volume-density geometry. CNTs are readily aligned in a high density geometry (i.e., a vertically aligned forest) but lack high charge density surfaces<sup>12</sup>. The sidewalls of the CNTs are similar to the basal plane of graphene and exhibit low charge density except where edge defects exist. Depositing a high density of graphene foliates along the length of aligned CNTs can significantly increase the total charge capacity per unit of nominal area as compared to other carbon nanostructures.

### **1.1.7 Nitrogen Doped Carbon Nanotubes**

Nitrogen doped carbon nanotubes (N-CNT's), can be produced through 5 main methods, Chemical Vapor Deposition, high-temperature and high-pressure reactions, gas-solid reaction of amorphous carbon with  $\text{NH}_3$  at high temperature<sup>13</sup> solid reaction, and solvothermal synthesis<sup>14</sup>.

N-CNTs can also be prepared by a CVD method of pyrolyzing melamine under Argon at elevated temperatures of  $800^\circ\text{C}$  -  $980^\circ\text{C}$ . However synthesis via CVD and melamine results in the formation of bamboo structured CNTs. XPS spectra of grown N-CNT's reveals nitrogen in five main components, pyridinic nitrogen, pyrrolic nitrogen, quaternary nitrogen, and nitrogen oxides. Furthermore synthesis temperature affects the type of nitrogen configuration.

Nitrogen doping plays a pivotal role in Lithium storage. N-doping provides defects in the walls of CNT's allowing for Li ions to diffuse into interwall space. It also increases capacity by providing more favorable bind of N-doped sites. N-CNT's are also much more reactive to metal oxide nanoparticle

deposition which can further enhance storage capacity, especially in anode materials for Li-ion batteries. However Boron doped nanotubes have been shown to make batteries with triple capacity.

### **1.1.8 Peapod**

A Carbon peapod is a novel hybrid carbon material<sup>15</sup> which traps fullerene inside a carbon nanotube. It can possess interesting magnetic properties with heating and irradiating. It can also be applied as an oscillator during theoretical investigations and predictions.

### **1.1.9 Cup-stacked carbon nanotubes**

Cup-stacked carbon nanotubes (CSCNTs) differ from other quasi-1D carbon structures, which normally behave as quasi-metallic conductors of electrons. CSCNTs exhibit semiconducting behaviors due to the stacking microstructure of graphene layers<sup>16</sup>.

### **1.1.10 Extreme carbon nanotubes**

The observation of the *longest* carbon nanotubes (18.5 cm long) was reported in 2009. These nanotubes were grown on Si substrates using an improved chemical vapor deposition (CVD) method and represent electrically uniform arrays of single-walled carbon nanotubes.

The *shortest* carbon nanotube is the organic compound cycloparaphenylene, which was synthesized in early 2009.

The *thinnest* carbon nanotube is armchair (2,2) CNT with a diameter of 3 Å. This nanotube was grown inside a multi-walled carbon nanotube. Assigning of carbon nanotube type was done by combination of high-resolution transmission electron microscopy (HRTEM), Raman spectroscopy and density functional theory (DFT) calculations<sup>17</sup>.

Another structural aspect of tubes is their self-organization into "*ropes*," which causes many (typically, 10-100) tubes held together by van der Waals forces. Ropes are far longer than any individual tube in them (Tubes : 100-1000 nm in length, Ropes: endless, branching off from one another, then joining others). These ropes are useful in providing very long conductive pathways. These rope formation and interactive forces hinder, stable colloidal suspension in various protic and aprotic solvents. These forces overcome any other repulsive forces (e.g., electrostatic or steric), and make dispersed colloidal suspensions thermodynamically unstable, which limits the use of CNTs. However, surface active agents (surfactants, polymers or other colloidal particles) can modify the particles-suspending medium interface and change some rheological surface properties which contribute to increasing the stability of the colloidal suspension.

## ***1.2 Synthesis techniques of nanotubes***

Techniques have been developed to produce nanotubes in sizeable quantities, including arc discharge, laser ablation, high-pressure carbon monoxide disproportionation (HiPco), and chemical vapor deposition (CVD). Most of these processes take place in vacuum or with process gases. CVD growth of CNTs can occur in vacuum or at atmospheric pressure. Large quantities of nanotubes can be synthesized by these methods; advances in catalysis and continuous growth processes are making CNTs more commercially viable.

### **1.2.1 High Pressure Carbon Monoxide Method**

The high pressure carbon monoxide (HiPCO) method (Figure 1.5) can produce large quantities of carbon nanotubes. Catalysts for SWNT growth form in situ by thermal decomposition of iron pentacarbonyl in a heated flow of carbon monoxide at pressures of 1-10atm and temperatures of 800-1200 °C. Previous methods for growing CNTs using hydrocarbons as source have resulted large

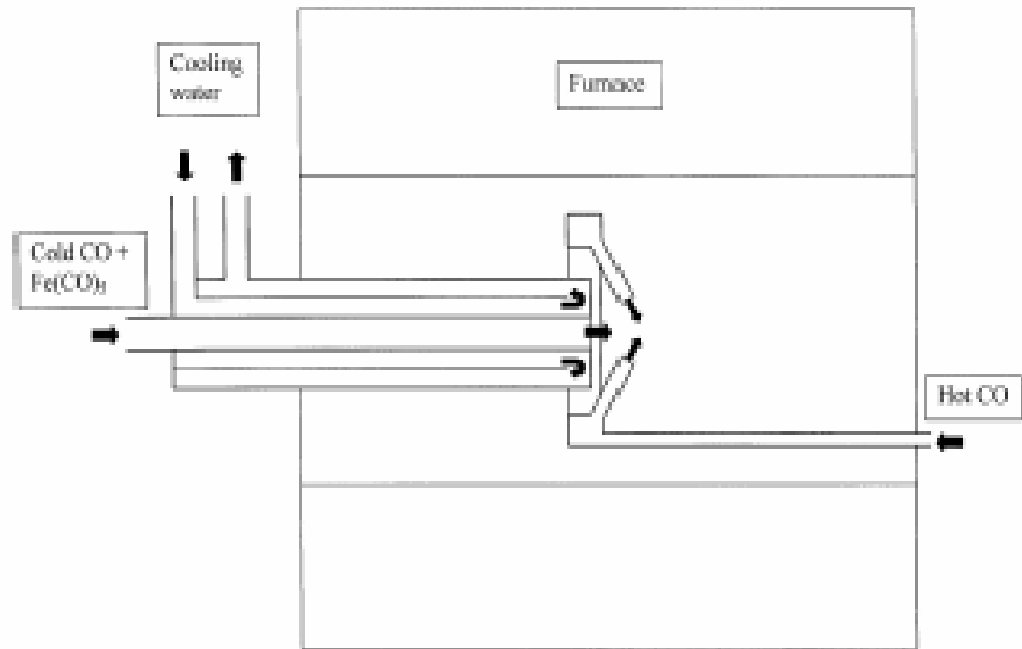
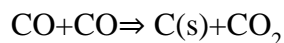


**Figure 1.5** High Pressure Carbon Monoxide Method.

quantities of amorphous carbon and graphitic deposits due to the thermal breakdown of hydrocarbons at high temperatures. The amorphous carbon overcoating would have to be removed in subsequent steps. The HiPCO method uses carbon monoxide as the carbon feedstock and  $\text{Fe}(\text{CO})_5$  as the iron-containing catalyst precursor<sup>18</sup>.

The products of the  $\text{Fe}(\text{CO})_5$  thermal decomposition react to produce iron clusters in gas phase. SWNTs nucleate and grow on these clusters. The solid carbon is formed through CO disproportionation, also known as the Boudouard reaction:



This reaction occurs catalytically on the surface of the iron particles. The iron particles promote the formation of the tube's characteristic graphitic carbon lattice.

### **1.2.2 Arc discharge**

Nanotubes were observed in 1991, but first macroscopic production of carbon nanotubes was made in 1992 by two researchers at NEC's Fundamental Research Laboratory<sup>19</sup>. Arc discharge (Figure 1.6) belongs to the methods that use higher temperatures (above 1700°C) for CNT synthesis<sup>20</sup> which usually causes the growth of CNTs with fewer structural defects in comparison with other techniques.

#### **A. MWNTs synthesis.**

The arc discharge synthesis of MWNTs uses DC arc discharge between two graphite water-cooled electrodes with diameters between 6 and 12 mm in a chamber filled with helium at sub atmospheric pressure. Different atmospheres markedly influence the final morphology of CNTs. Wang et al.<sup>21</sup> used DC arc discharge of graphite electrodes in He and methane. By evaporation under high pressured  $\text{CH}_4$  gas and high arc current, thick nanotubes embellished with many carbon nanoparticles can be

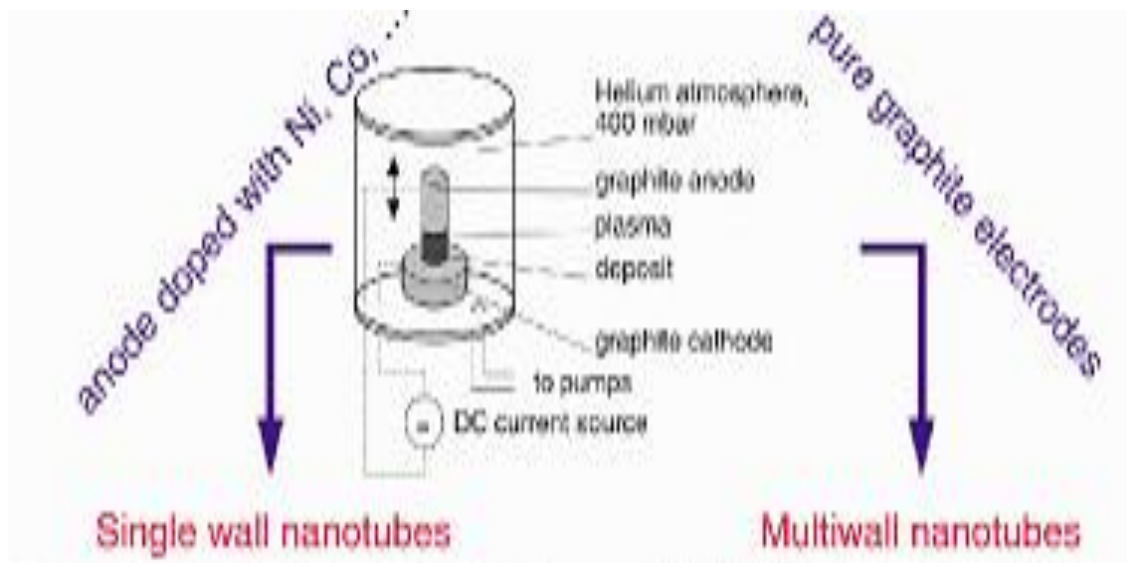


**Figure 1.6** Arc discharge method.

obtained. Thin and long MWNTs can be obtained under a  $\text{CH}_4$  gas pressure of 50 Torr. Arc discharges in the three organic atmospheres (ethanol, acetone and hexane) produce more MWNTs, by two times at least, than those in the He atmosphere. Shimotani et al.<sup>22</sup> said that acetone, ethanol and hexane can be ionized and the molecules can be decomposed into hydrogen and carbon atoms. These ionized species may contribute the synthesis of MWNTs, so the higher yield of CNTs is produced. MWNTs obtained are highly crystalline, with a well-ordered structure and free of defects. They obtained MWNTs with an outer diameter of 10–20 nm and an interlayer distance of approximately 0.35 nm between graphene layers.

### **B. SWNTs synthesis**

Usually the MWNTs are produced when no catalyst is used. On the other hand, the SWNTs are produced when the transition metal catalyst is used. The process of SWNTs growth in arc discharge utilizes a composite anode, usually in hydrogen or argon atmosphere. The anode is made as a composition of graphite and a metal, such as Ni, Fe, Co, Pd, Ag, Pt, etc. or mixtures of Co, Fe, Ni with other elements like Co–Ni, Fe–Ni, Fe–No, Co–Cu, Ni–Cu, Ni–Ti, etc. The metal catalyst plays a significant role in the process yield. To ensure high efficiency, the process also needs to be held on a constant gap distance between the electrodes which ensures stable current density and anode consumption rate. According to growth patterns and morphology of SWNTs, they divided the synthesis results into three groups: the tubes tangled with each other to form “highway junction” pattern for Co and Fe/Ni, long and thin tubes radially growing from Ni particles, and short and thick tubes growing from lanthanide compound particles<sup>23</sup>.

### **1.2.3 Laser ablation**

In the laser ablation process, a pulsed laser vaporizes a graphite target in a high-temperature reactor while an inert gas is bled into the chamber. Nanotubes develop on the cooler surfaces of the reactor as

the vaporized carbon condenses. A water-cooled surface may be included in the system to collect the nanotubes. Laser ablation, as crucial step of PLD, is one of the superior methods to grow SWNTs with high-quality and high-purity. In this method, which was first demonstrated by Dr. Richard Smalley and co-workers at Rice University in 1995<sup>24</sup> the principles and mechanisms are similar to the arc discharge with the difference that the energy is provided by a laser hitting a graphite pellet containing catalyst materials (usually nickel or cobalt)<sup>25</sup>.

The laser ablation method (Figure 1.7) yields around 70% and produces primarily single-walled carbon nanotubes with a controllable diameter determined by the reaction temperature. However, it is more expensive than either arc discharge or chemical vapor deposition.

#### **1.2.4 Plasma torch**

Single-walled carbon nanotubes can be synthesized by the induction thermal plasma method, discovered in 2005 by groups from the University of Sherbrooke and the National Research Council of Canada<sup>26</sup>. The method is similar to the arc-discharge process in that both use ionized gas to reach the high temperature necessary to vaporize carbon containing substances and the metal catalysts necessary for the ensuing nanotube growth. The thermal plasma is induced by high frequency oscillating currents in a coil, and is maintained in flowing inert gas. Typically, a feedstock of carbon black and metal catalyst particles is fed into the plasma, and then cooled down to form single-walled carbon nanotubes. Different single-wall carbon nanotube diameter distributions can be synthesized.

The induction thermal plasma method can produce up to 2 grams of nanotube material per minute, which is higher than the arc-discharge or the laser ablation methods.

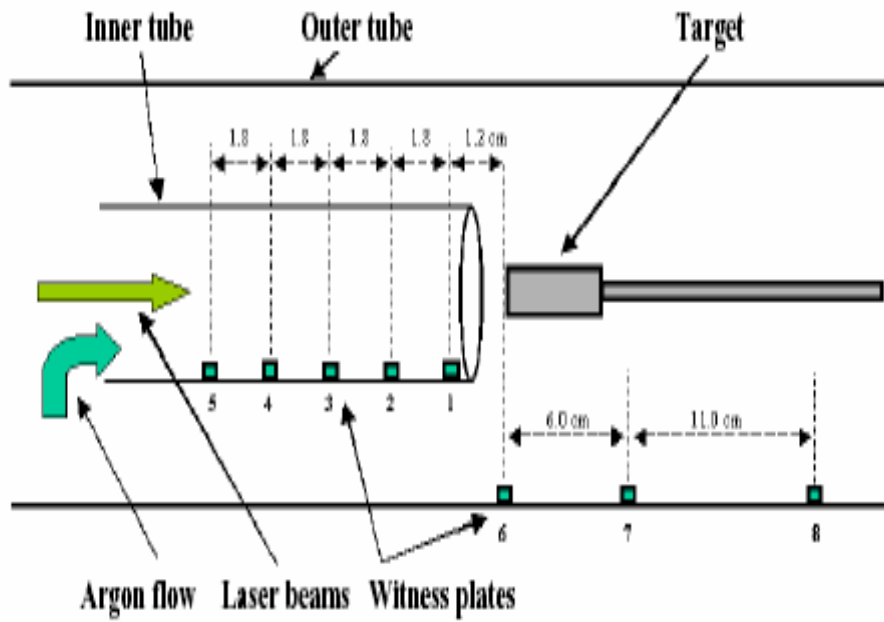


**Figure 1.7** Laser ablation Process.

### 1.2.5 Chemical vapor deposition (CVD)

Carbon nanotubes were first prepared by this process in 1993, though the discovery of this process lies long back in 50's. For CVD (Figure 1.8) a substrate/reactor bed is prepared with a layer of metal catalyst particles, most commonly nickel, cobalt, iron, or a combination<sup>27</sup>. Size of the metal particles used decides the diameters of the nanotubes that are produced. The substrate is heated to approximately 700°C or high temperature annealing is done. A combination of two gases, inorganic or process gas, which is generally N<sub>2</sub> or H<sub>2</sub>, and a organic gas, basically methane, ethene, or ethyne is used as initiator for growth of nanotubes at metal particles. The catalyst particles can stay at the tips of the growing nanotube during the growth process, or remain at the nanotube base, depending on the adhesion between the catalyst particle and the substrate<sup>28</sup>. Thermal catalytic decomposition of hydrocarbon has become an active area of research and can be a promising route for the bulk production of CNTs. Fluidized bed reactor is the most widely used reactor for CNT preparation. A combination of metal nanoparticles such as MgO or Al<sub>2</sub>O<sub>3</sub> and catalyst increases the surface area for higher yield. New water soluble catalyst particles are now preferred, due to the ease of their removal.

Use of a strong electric field during the growth process produces plasma (plasma enhanced chemical vapor deposition), and the nanotube growth follows the direction of the electric field. By adjusting the geometry of the reactor it is possible to synthesize vertically aligned carbon nanotubes<sup>29</sup> (i.e., perpendicular to the substrate), a morphology that has been of interest to researchers interested in the electron emission from nanotubes. CVD produces great interest because of its price/unit ratio, and because CVD is capable of developing nanotubes of desired diameters, length, and alignment and on desired catalyst support. In 2007, a team from Meijo University demonstrated a high-efficiency CVD technique for growing carbon nanotubes from camphor<sup>30</sup>.

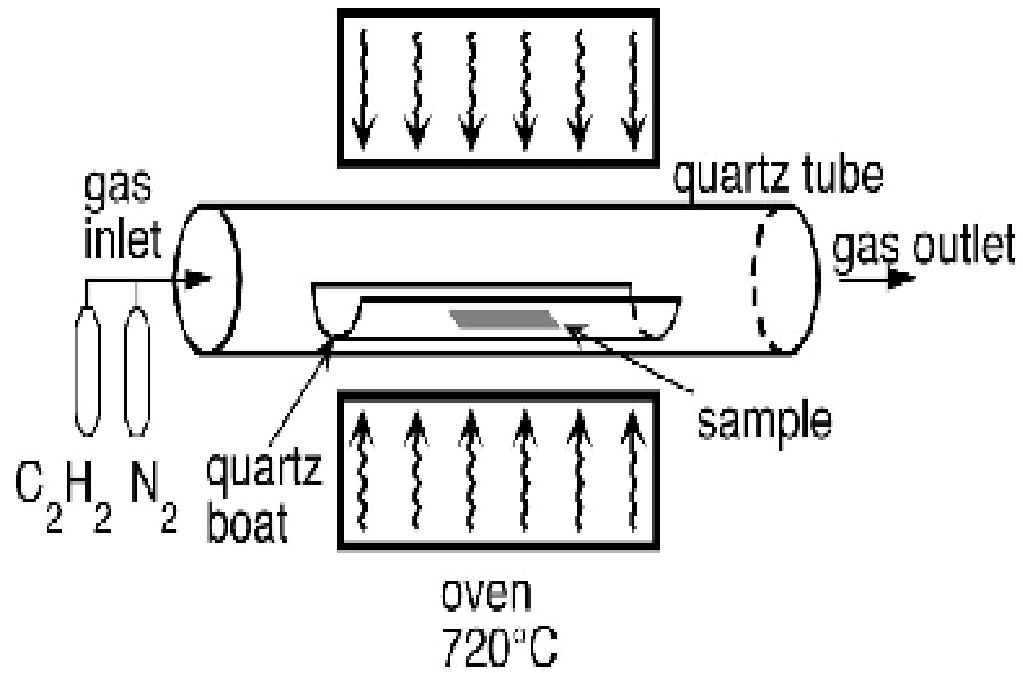


**Figure 1.8** Chemical vapor deposition (CVD) process.

### 1.2.6 Super-growth CVD

Super-growth CVD (water-assisted chemical vapor deposition) process was developed by Kenji Hata, Sumio Iijima and co-workers at AIST, Japan<sup>31</sup>. In this process, the activity and lifetime of the catalyst are enhanced by addition of water into the CVD reactor.

Their specific surface exceeds 1,000 m<sup>2</sup>/g (capped) or 2,200 m<sup>2</sup>/g (uncapped), SWNT forests can be easily separated from the catalyst, yielding clean SWNT material (purity >99.98%) without further purification. Patterned highly organized single-walled nanotube structures were successfully fabricated using the super-growth technique.

The mass density of super-growth CNTs is about 0.037 g/cm<sup>3</sup>. It is much lower than that of conventional CNT powders (~1.34 g/cm<sup>3</sup>), probably because the latter contain metals and amorphous carbon.

The vertically aligned nanotube forests originate from a "zipping effect" when they are immersed in a solvent and dried. The zipping effect is caused by the surface tension of the solvent and the van der Waals forces between the carbon nanotubes. The packed carbon nanotubes are more than 1 mm long and have a carbon purity of 99.9% or higher; they also retain the desirable alignment properties of the nanotubes forest<sup>32</sup>.

### 1.2.7 Flame pyrolysis

This technique is presented very uniquely by the research group of Liu et al.<sup>33</sup> as a new method for mass CNTs production using simple equipment and experimental conditions. The authors called it V-type pyrolysis flame. They captured successfully CNTs with less impurities and high yield using carbon monoxide as the carbon source. Acetylene/air premixed gas provided heat by combustion. Pentacarbonyl was used as the catalyst and hydrogen/helium premixed gas acted as diluted and

protection gas. The diameter of obtained CNTs was approximately between 10 nm and 20 nm, and its length was dozens of microns. Moreover they studied the effect of sampling time, hydrogen and helium to the CNTs growth process.

### ***1.3 Potential applications***

The strength and flexibility of carbon nanotubes makes them of potential use in controlling other nanoscale structures, which suggests they will have an important role in nanotechnology engineering. The highest tensile strength of an individual multi-walled carbon nanotube has been tested to be is 63 Gpa<sup>34</sup>.

#### **1.3.1 Mechanical and structural applications**

Carbon nanotubes have superior mechanical properties, and so find use and space in everyday items like clothes and sports gear to combat jackets and space elevators. Work done by Ray H. Baughman at the NanoTech Institute has shown that single and multi-walled nanotubes can produce materials with extremely high toughness<sup>35</sup>.

Unmatched mechanical properties (~1 TPa in modulus, and ~100 GPa in strength) allowed them to be used to produce continuous CNT yarns from CVD grown CNT aerogels by Windle *et al.*<sup>36</sup>. With this technology, they fabricated CNT yarns with strengths as high as ~9 GPa at small gage lengths of ~1 mm, however, defects resulted in a reduction of specific strength to ~1 GPa at 20 mm gage length.

The fundamental properties of these extremely fine yarns are being studied using techniques borrowed from CSIRO's multi-fibre research and development (R&D) capability. They are also studying the production methods and properties of extruded fibres made from polymers blended with carbon nanotubes, with an emphasis on the uniform dispersal of the nanotubes in polymers, before extrusion

into yarn. CNT's could help create stab-proof and bulletproof clothing. The nanotubes would effectively stop the bullet from penetrating the body.

### **1.3.2 Antiballistic materials**

CSIRO is working with the Defence Science and Technology Organisation (DSTO), Defence Capability and Technology Demonstrator (CTD) Program to demonstrate the capabilities of carbon nanotubes as strong, lightweight antiballistic materials.

### **1.3.3 Medical**

In the Kanzius cancer therapy, single-walled carbon nanotubes are inserted around cancerous cells, then excited with radio waves, which causes them to heat up and kill the surrounding cells. Researchers<sup>37</sup> at Rice University, Radboud University Nijmegen Medical Centre and University of California, Riverside have shown that carbon nanotubes and their polymer nanocomposites are suitable scaffold materials for bone cell proliferation and bone formation.

### **1.3.4 Electrical circuits**

Nanotube-based transistors, also known as carbon nanotube field-effect transistors (CNTFETs), have been made to operate at using a single electron, at room temperature and that are capable of digital switching band gap. Semiconducting nanotubes can be used to build molecular field-effect transistors (FETs) while metallic nanotubes can be used to build single-electron transistors.

The recent CNFETs<sup>38</sup> are now built with top-gate geometry and resemble more conventional silicon CMOS devices. The SWNT transistors consist of a semiconducting carbon nanotube about 1 nm in diameter bridging two closely separated metal electrodes on a silicon surface coated with SiO<sub>2</sub>.

One major obstacle to realization of nanotubes has been the lack of mass production. IBM researchers demonstrated how metallic nanotubes can be destroyed, leaving semiconducting ones behind for use

as transistors. Their process is called "constructive destruction". An approach<sup>39</sup> to produce transistors using random networks of carbon nanotube, that would help to average out all of their electrical differences was studied. Large structures of carbon nanotubes can be used for thermal management of electronic circuits. An approximately 1 mm–thick carbon nanotube layer was used as a special material to fabricate coolers, this material has very low density, ~20 times lower weight than a similar copper structure, while the cooling properties are similar for the two materials.

### **1.3.5 Solar cells**

The different type of nanotubes, SWNT ,MWNT, and DWNT's have the capability to absorb various types of electromagnetic radiations such as Ultraviolet radiations, Visible and IR rays, making them useful in solar and radar panels. Solar cells<sup>40</sup> developed at the New Jersey Institute of Technology use a carbon nanotube complex, formed by a mixture of carbon nanotubes and carbon buckyballs (known as fullerenes) to form snake-like structures. The fullerenes or carbon nanotubes can be complexed with some polymers, which then results in structures which could trap electrons and cause them to flow. There are many types of photexcitable electron donors known like porphrin which when combined to fullerene and nanotube composition to create hybrid solar panels, would definitely give rise to increased efficiency.

### **1.3.6 Lighting Elements**

Nanotubes are excellent electron sources, thus they are useful in the creation of light elements. The electrons produced by nanotubes are used to bombard a surface coated with phosphor in order to produce light. The brightness of this light is usually 2 times brighter than conventional lighting elements (due to the high electron efficiency).

### **1.3.7 Hydrogen Storage**

Another property of carbon nanotubes is their ability to quickly adsorb high densities of hydrogen at room temperature and atmospheric pressure. The research group at the National Renewable Energy Laboratory already confirms that SWNTs are capable of storing hydrogen at densities of more than  $63\text{kg/m}^3$ . Researchers have found that the interaction of hydrogen and SWNT is between the Van der Waals force of the SWMT and the chemical bonds of the hydrogen molecule (as opposed to being due to hydrogen dissociation)<sup>41</sup>.

### **1.3.8 Memory device**

Because of its ability to store information as a single electronic charge, nanotubes have the potential to be used in the design of memory devices. A single electron is discrete, and thus needs less energy in order to change the state of the memory. Such a design would also take advantage of the high mobility of SWMT, which is ten times greater than that of silicon.

### **1.3.9 Ultracapacitors**

Ultracapacitors are storage devices which can store electric charges. The surface area available for storing electric charge plays a valuable role. Introduction of nanotubes to modify these capacitors has been challenging and has been worked upon by MIT Laboratory and Electronic Systems uses. The conventional ultracapacitors which use activated charcoal has many limitations such as, a significant fraction of the electrode surface is not available for storage because the hollow spaces are not compatible with the charge's requirements. With a nanotube electrode the spaces may be tailored to size—few too large or too small—and consequently the capacity should be increased considerably<sup>42</sup>.

### **1.3.10 Radar absorption**

Radars work in the microwave frequency range, which can be absorbed by MWNTs. Applying the MWNTs to the aircraft would cause the radar to be absorbed and therefore seem to have a smaller

signature. One such application could be to paint the nanotubes onto the plane. Recently there has been some work done at the University of Michigan regarding carbon nanotubes usefulness as stealth technology on aircraft. It has been found that in addition to the radar absorbing properties, the nanotubes neither reflect nor scatter visible light, making it essentially invisible at night, much like painting current stealth aircraft black except much more effective. Current limitations in manufacturing, however, mean that current production of nanotube-coated aircraft is not possible. One theory to overcome these current limitations is to cover small particles with the nanotubes and suspend the nanotube-covered particles in a medium such as paint, which can then be applied to a surface, like a stealth aircraft<sup>43</sup>.

### **1.3.11 Optical power detectors**

A spray-on mixture of carbon nanotubes and ceramic demonstrates unprecedented ability to resist damage while absorbing laser light. Such coatings that absorb as the energy of high-powered lasers without breaking down are essential for optical power detectors that measure the output of such lasers. These are used, for example, in military equipment for defusing unexploded mines. The composite consists of multiwall carbon nanotubes and a ceramic made of silicon, carbon and nitrogen. Including boron boosts the breakdown temperature. The nanotubes and graphene-like carbon transmit heat well, while the oxidation-resistant ceramic boosts damage resistance. Creating the coating involves dispersing the nanotubes in toluene, to which a clear liquid polymer containing boron was added. The mixture was heated to 1,100°C (2,010 °F). The result is crushed into a fine powder, dispersed again in toluene and sprayed in a thin coat on a copper surface. The coating absorbed 97.5 percent of the light from a far-infrared laser and tolerated 15 kilowatts per square centimeter for 10 seconds. Damage tolerance is about 50 percent higher than for similar coatings, e.g., nanotubes alone and carbon paint.

### 1.3.12 Adsorption

Carbon nanotubes, functionalized or unfunctionalized have very high adsorptivity. Functionalization of Carbon nanotubes, generates active sites on the surface of nanotubes. These charged sites help to associate with the metal ions by chelate formation. Thus an added advantage of functionalization, increases the retention power of the nanotubes towards heavy metal ions.

HNO<sub>3</sub> treated Carbon nanotubes (CNTs) have been employed as adsorbent<sup>44</sup> to study the adsorption characteristics of some divalent metal ions (Cu, Co, Cd, Zn, Mn, Pb). Multi-walled carbon nanotubes have been used successfully for the removal of Copper(II), Lead(II), Cadmium(II), and Zinc(II) from aqueous solution, and effect of solution temperature on this process has been studied<sup>45</sup>. It has been confirmed that the % adsorption increases by raising the solution temperature due to the endothermic nature of the adsorption. The values of the free energies for the reactions are negative, which indicates that adsorption process is spontaneous, and this spontaneity increases by raising the solution temperature. The changes in entropy values are positive, which indicate the increase in randomness due to the physical adsorption of heavy metal ions from the aqueous solution to the carbon nanotubes surface. Enthalpy values are positive for all metal ions, but the free energies are negative, and the adsorption is a spontaneous one, which indicates that the heavy metal adsorption of Multi-walled carbon nanotubes is an entropy-driving process. Similar works on heavy metal adsorption has been done by Y. H. Li and co-workers<sup>46</sup>.

Though most of the studies have been done with nanotubes containing carboxyl groups(-COOH), many studies have been done on nanotubes, developing different functional moieties containing different hetero atoms such as nitrogen, chlorine, sulfur, phosphorus etc. These hetero atoms increase

the chelate formation tendency due to presence of lone pairs in hetero atoms and also due to their small sizes.

Multiwalled nanotubes functionalized with iminodiacetic acid (IDA) have been studied<sup>47</sup> for heavy metal detection in biological samples. Detection limit (3 s) was achieved at 1.3, 1.2, 0.70, 0.40, 2.5, 3.4, 0.79 ng L(-1), respectively. At the 1.0 µg L(-1) level, the precision (RSD, %) for 11 replicate measurements was from 1.0 to 4.0. this shows that carbon nanotubes could be used with good accuracy. A novel Schiff base-chitosan-grafted multiwalled carbon nanotubes (S-CS-MWCNTs) solid-phase extraction adsorbent has been<sup>48</sup> synthesized by covalently grafting a Schiff base-chitosan (S-CS) onto the surfaces of oxidized MWCNTs and used for detection of heavy metals.

Carbon nanotubes show a great affinity for protein adsorption and human complement activation<sup>49</sup> and thus interact with a part of the human immune system. Fibrinogen and apolipoproteins (AI, AIV and CIII) bound to carbon nanotubes in greatest quantity. Similarly light membranes composed of single-walled carbon nanotubes (SWNTs) can serve as efficient nanoscale vessels for encapsulation of tetrafluoromethane<sup>50</sup> on their surface as compared to currently used activated carbons and zeolites,

As an advancement procedure functionalized CNT sheets<sup>51</sup> synthesized by chemical vapor deposition of cyclohexanol and ferrocene have been studied as adsorbent for water treatment. Using the oxidized CNT sheets for waste water treatment without CNT leakage into water is economically feasible. Therefore, CNT sheets have good potential application in environmental protection. In some other research works Carbon nanotubes (CNTs) have been grown on the surface of microsized Al<sub>2</sub>O<sub>3</sub> particles in CH<sub>4</sub> atmosphere at 700°C under the catalysis of Fe-Ni nanoparticles<sup>52</sup>. As grown CNTs have been tested for adsorbing heavy metals from test solutions and the results compared with active carbon powders, commercial carbon nanotubes, and Al<sub>2</sub>O<sub>3</sub> particles. The as-grown CNTs/Al<sub>2</sub>O<sub>3</sub>, have

demonstrated extraordinary absorption capacity with oxidation, as well as hydrophilic ability that unoxidized CNTs lacked.

The 1-D nanomaterials composed of various ratios of carbon nanotubes (CNT) and titanate nanotubes (TNT) (CNT/TNT) have been prepared<sup>53</sup> by alkaline hydrothermal method. The nanocomposites may have different shapes and morphologies as nanoparticles/nanosheets, nanotubes, nanowires and nanoribbon depending on used temperatures (60 - 230°C). In addition, the CNT/TNT nanomaterials have a good capability toward heavy metal adsorption. The Langmuirian maximum adsorption capacities of nanomaterials were in the range 83-124 mg/g for Cu<sup>2+</sup> and 192-588 mg/g for Pb<sup>2+</sup>, which is superior to that of CNT. Thus it could be said that nanocomposites are a promising nano-adsorbent for coupled removal of organic as well as heavy metal ions in solution.

CNTs also have found immense applications in nanocomposite science. CNT/polycarbonate matrix composite membranes have been found to have good hydrogen separation properties<sup>54</sup>. Unmodified MWCNT/polysulfone microporous conductive membranes have also been prepared by sonication technique<sup>55</sup>. *The use of carbon nanotubes in pure or composite forms the major base of present study. The nanosize materials also have the capacity of altering the pore diameters of polymeric membranes. This property has been used for heavy metal rejection studies using CNT/Polysulfone nanocomposite membranes, where effect of addition of CNTs to polysulfone has been recorded in terms of porosity and hydrophilicity variation.*

CNTs have also found use in chemisorptions of polymers and macromolecules<sup>56,57</sup>, as well as in in situ ATRP “grafting from” approach to functionalize themselves<sup>58</sup>. *Apart from traditional initiators of ATRP, new macro initiators and some simple initiators have been used and reported as a part of study in the thesis.*

#### **1.4 “Water” : Transparent Gold**

“Water” is elixir to life. Survival is impossible without it. Population explosion, industrialization and globalization has made clean drinking water an “endangered requirement” for the world. There is water all around us, 10 x 10<sup>8</sup> billion cubic meters water, covering 75% of the surface of earth. Most of this is highly saline water and flows into rivers, seas and oceans making it unavailable for drinking. Out of the remaining 2.8%, a major portion is locked in polar ice and glaciers. Only 0.5% is available for human use. Access to clean water is increasingly becoming the most important issue around the world. A large population is dependent on rain water and stagnant water (at some places) for quenching their thirst. A large population lacks access to sufficient amount of clean water and adequate sanitation<sup>59</sup>. The combination of poor sanitation and unhealthy water quality is one of the largest causes of disease and death in the world.

World health organization (WHO),has set standards for potable water defining a permissible limit for various constituents as heavy metals, salts, organic chemicals, minerals, essential metals ions, algae and various other suspended impurities. Concentrations above this permissible limit make water unfit for drinking<sup>60</sup>.

With the growth of technology, the concentration of heavy metals in surface water has increased considerably. Metals ions allowed to pass into the environment are persistent, and cannot be biodegraded. These metals are adsorbed into the soil, runoff into rivers or lakes or leach in the ground water which is an important source of drinking water. These heavy metals tend to build their homes in animals, plants and humans tissues.

### ***1.5 Toxic ions present in surface and ground water***

The ions which are not metabolized by our body and accumulate in the soft tissues are referred as toxic ions. Arsenic, mercury, cadmium, chromium and lead are fall in this category. All over the globe tons of toxic ions add to waters every year.

Agency for Toxic Substance and Disease Registry (ATSDR), Department of Health and Human Services (US), identified some ions as toxic ions and arranged them in the form of a list called ATSDR's "Top 20 List of Hazardous Substances"<sup>61</sup>.

### ***1.6 Sources and Health effects of Toxic Metals***

The presence of heavy metals such as chromium, cadmium, copper, nickel, lead, mercury etc. in aqueous environment may result in a major concern due to their toxicity and carcinogenicity, which may cause damage to various systems of the human body.

#### **1.6.1 Arsenic**

##### **A. Sources**

Erosion from local rocks seeps into ground water and adds Arsenic to it. A large number of minerals and ores also are a source of arsenic to ground water<sup>62</sup>. Whereas, the occurrence of arsenic in surface water is generally believed to be due to the domestic waste water. Other major sources include sewage sludge, manufacturing processes, and smelting and refining.

##### **B. Health Effects**

###### **i. Toxicity**

ATSDR placed arsenic, on number 1 in the "Top 20 List of Hazardous Substances". It is the most common cause of acute heavy metal poisoning in humans and characterized by central nervous system effects, leading to coma and eventual death. The respiratory tract, gastrointestinal tract and skin are

also affected during the bouts of sever poisoning. Chronic intoxication results in neurological disorders, muscular weakness, loss of appetite, nausea, and skin disorders such as hyper-pigmentation and keratosis. Low level ingestion of arsenic (1-10 mg/L) over extended periods may leads to the onset of acute toxicity.

## **ii. Carcinogenicity**

Inorganic arsenic was associated with the genesis of skin cancer as early as 1888<sup>63</sup>. The international agency for research on cancer currently classifies inorganic as in group1: Inadequate evidence for carcinogenicity in animals and sufficient evidence of carcinogenicity (skin and lungs) in humans. The earliest manifestation of arsenicosis such as pigmentation and lesions on skin have often played havoc in the social situation of those affected owing to ignorance and misleading information. In rural areas skin pigmentation caused by consumption of arsenic contaminated water is often believed to be contagious and hereditary. Further arsenicosis is often mistaken for leprosy or other highly communicable skin disease<sup>64,65</sup>.

## **1.6.2 Cadmium**

### **A. Sources**

Among the toxic metals cadmium is of considerable environmental and health significance because of its increasing mobilization and human toxicity. The major sources for the introduction of cadmium in water are smelting and refining of nonferrous metals, manufacturing processes related to chemicals and metals and domestic waste water<sup>66</sup>. The atmospheric deposition which contributes about 15% cadmium contamination, from natural sources such as volcanoes, windborne soil particles and biogenic particles cannot be ignored.

## **B. Health Effects**

### **i. Toxicity**

In humans acute exposure to cadmium leads to nausea, vomiting, salivation, diarrhoea and muscular cramps. Sever to fatal cases may show the symptoms of liver injury, convulsions, shock, renal failure and cardiopulmonary depression.

### **ii. Carcinogenicity**

The international agency for research on cancer has classified cadmium for carcinogenicity in humans and no evidence for carcinogenicity in animals since there is no or little evidence that it is carcinogenic via oral route <sup>67</sup>.

## **1.6.3 Chromium**

### **A. Sources**

Chromium another common pollutant with its toxicity and mutagenic effect is introduced into natural waters from domestic waste water, sewage sludge and a variety of industrial processes such as electroplating, metal finishing industries (hexavalent chromium) and tanneries (trivalent chromium). Chromium occurs most frequently as Cr (VI) and Cr (III) in aqueous solutions. Both valences of chromium are potentially harmful but Cr (VI) possesses a greater risk due to its carcinogenic properties<sup>68</sup>.

## **B. Health Effects**

### **i. Toxicity**

Compounds of hexavalent chromium are more toxic than trivalent chromium to humans. The toxic and genotoxic nature of Cr(VI) ion were established a long time ago<sup>69,70</sup>. Acute exposure to Cr(VI) produces nausea, diarrhoea, liver and kidney damage, internal haemorrhage, dermatitis and respiratory problems. Cases of acute poisoning by Cr(III) compounds are extremely rare, reflecting their low toxicity to human population.

## **ii. Carcinogenicity**

The IARC (1980) has evaluated the carcinogenicity of chromium compounds and found the compounds of Cr(VI) cancer producing but not yet categorized it as carcinogenic groups due to insufficient evidences for its carcinogenicity to humans. R. Sanz has established that the workers exposed to Cr(VI) compounds in stainless steel welding, chrome pigment production and other industrial occupations can suffer skin lesions, lung disease and various forms of cancer<sup>71</sup>.

## **1.6.4 Cobalt**

### **A. Sources**

Cobalt is introduced to water mainly by the burning of fossil fuels approximately 55 %. Municipal effluents may also contain relatively high residues, particularly in the cities dominated by the metal-working industries. Contribution of cobalt through fly ash and sewage sludge may not be ignored.

### **B. Health Effects**

#### **i. Toxicity**

Water polluted with cobalt may result in asthma like allergy, damage to heart, causing heart failure damage to thyroid and liver. Acute exposure to cobalt may lead to depression to the iodine uptake.

Neurotoxicological symptoms including peripheral neuritis and changes in reflexes have also been reported<sup>72</sup>. It may also cause mutation in living cells.

## **ii. Carcinogenicity**

There does not appear to be any evidence for carcinogenicity of cobalt in humans, even those exposed occupationally through the inhalation route.

### **1.6.5 Lead**

#### **A. Sources**

The primary sources of lead include manufacturing processes, atmospheric deposition and domestic wastewater. Combustion of leaded fuels, pyrometallurgical nonferrous metal processes and coal combustion are also responsible lead introduction in water stream.

#### **B. Health Effects**

##### **i. Toxicity**

Lead number 2 on the ATSDRs list, accounts for the most of the cases of paediatric heavy metal poisoning and targets the bones, brain, thyroid gland and kidney. Acute poisoning by it is rare and is generally restricted to occupational settings.

##### **ii. Carcinogenicity**

Some examples for carcinogenicity of lead are available but they are insufficient to prove or disprove its carcinogenicity<sup>73</sup>. The IARC classified lead into group 3: inadequate evidence for carcinogenicity in humans and sufficient evidence for carcinogenicity in animals.

## **1.6.6 Mercury**

### **A. Sources**

Mercury pollution of water occurs due to various reasons like discharge from coal burning power plants, chemical manufacturing processes and discharge from municipal and industrial sources etc. Its contamination of aquatic ecosystem is widespread globally due primarily to atmospheric deposition<sup>74</sup>. The majority of atmospherically deposited Hg is in the inorganic form which can be converted to highly bio-available methyl mercury (MeHg) through natural processes in water bodies and watersheds.

### **B. Health Effects**

#### **i. Toxicity**

Mercury, placed on number 3 on ATSDR's "Top 20 List", exists in three forms; elemental mercury, organic mercury and inorganic mercury. It shows its harmful effects on brain and kidneys. Since mercury is one of the most hazardous heavy metals having very high binding capacity with proteins and mainly affects renal & nervous systems<sup>75</sup>.

#### **ii. Carcinogenicity**

Although methyl mercury may cause chromosome aberrations, there are inadequate evidences for its carcinogenicity.

### **1.6.7 Nickel**

#### **A. Sources**

Nickel, another pollutant is the major part of municipal wastewater followed by waste of smelting and refining of nonferrous metals Beucemma et al. reported that the total amount of nickel discharged into the Netherlands part of the North sea amounted to 1100 metric tons per year<sup>76</sup>.

#### **B. Health Effects**

##### **i. Toxicity**

The primary acute effect of nickel exposure is dermatoses, including contact dermatitis, atopic dermatitis and allergic sensitization. No clinical epidemiological studies are available on the acute effects of oral ingestion of nickel.

##### **ii. Carcinogenicity**

Nickel in some forms is likely to be carcinogenic in humans and in fact statistically significant elevations in the incidence of respiratory cancers have been found in nickel refinery workers<sup>77</sup>. However, no evidence of carcinogenicity exists for ingestion of nickel in either food or water.

The harmful and toxic effects of these ions on human body compel the environmentalists, scientists and policy makers to work in the area of environmental protection in last three decades. All developed countries have initiated efforts for clean water supply to their population which is having these contaminants not more than permissible limits as decided by the WHO in 1980s.

## ***1.7 Consumption guidelines by WHO & BIS***

Bureau of Indian Standards (BIS), Indian Council of Medical Research (ICMR) and World Health Organization (WHO) have decided certain limits for different parameters such as pH, Hardness, Total Dissolved Solids, Turbidity, Colour, Odour, concentration of anions and cations including toxic metal ions. The potable water is the water in which these parameters present below permissible limits. Since our work is related to the removal of toxic ions from water for which the permissible limits decided by different agencies are shown in Table 1.1.

India, a large developing country is also making all out efforts for clean water supply to its population for quite some time. But lack of resources and place to place variation in surface and ground water quality due to large geographical area make this task difficult. Figure 1.9 insight on availability of fresh water in India and predict it as the acute scarcity region by year 2025. Rajasthan region is having large amount of nitrates in its ground water whereas West Bengal and some territories in UP are facing arsenic problem<sup>78</sup>. In present situation, therefore a need exists to develop technologies which can fulfil the needs of water purification at low cost and as per requirements of particular area. All of these goals can be achieved only when the cost effective and ion selective materials are developed and optimized for water purification.

**Table 1.1 Permissible Limits of Different Metal Ions for Potable Water (in mg/L).**

<b>S. No.</b>	<b>Metal</b>	<b>WHO</b>	<b>BIS</b>	<b>Other Agency</b>
1.	Arsenic	0.05	0.05	-
2.	Cadmium	0.005	0.01	-
3.	Chromium (VI)	0.05	0.05	-
5.	Lead	0.05	0.1	-
6.	Mercury	0.001	0.001	0.002 (EPA, US)
7.	Nickel	-	-	0.2 (EPA, US)

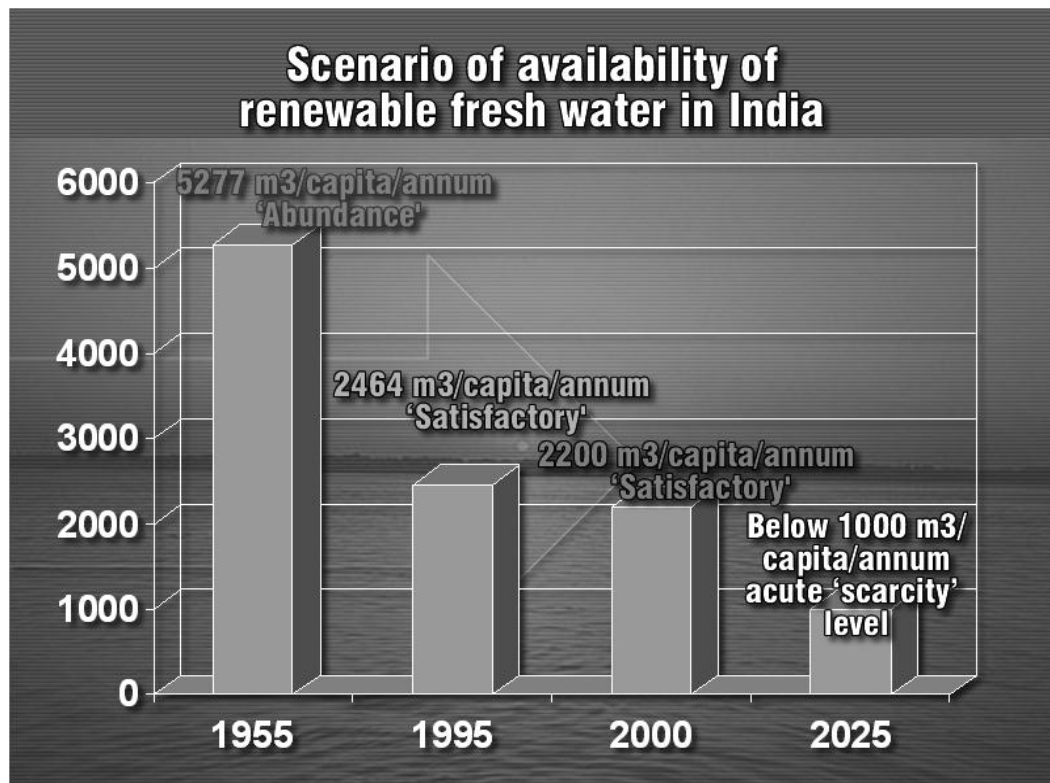


**Figure 1.9** Availability of renewable fresh water in India.

## ***1.8 Different technologies used in water purification***

Many treatment processes such as chemical precipitation, evaporation, ion exchange, adsorption, electro-dialysis, reverse osmosis and ultra-filtration are currently used in various water treatment plants; but all of them are having their own limitations. The brief introductions of above processes are mentioned below:

### **1.8.1 Chemical precipitation**

Precipitation of heavy metals as their hydroxides using lime, or sodium hydroxide, is widely used. Lime is generally chosen for precipitation purposes due to its low cost, ease of pH control in the range 8.0 – 10.0 and the presence of excess of lime also serves as an adsorbent for the removal of other metal ions<sup>79</sup>. The precipitation method has been used for the removal of iron, copper, zinc, tin, cadmium and nickel from the effluents of metal finishing industry and for the removal of aluminium and iron from sewage water<sup>80</sup>. Sorg.Et. al. Evaluated the use of lime for the removal of lead and cadmium from water and wastewaters and concluded that the effluents after treatment meet the requirements prescribed by Environmental Protection Agency (EPA), USA. But the major drawback with precipitation is sludge production<sup>81</sup>.

### **1.8.2 Sulphide Precipitation**

Excellent metal removal can be achieved by sulphide precipitation because most of the heavy metals form stable sulphides. The advantage of sulphide precipitation is that the solubility of metal sulphide is generally low resulting in a higher efficiency. In the sulphide precipitation method, the metal level is reduced to 0.01 mg/L for cadmium, copper and zinc and 0.05 mg/L for cadmium and nickel<sup>82</sup>. Mercury containing wastewaters have been treated using sodium sulphide in the pH range of 6.0 – 10.0 using ferric hydroxide as the collector<sup>83</sup>.

### **1.8.3 Carbonate precipitation**

The use of carbonate precipitation as a method for the removal of metals from wastewater is limited. Patterson et al.<sup>84</sup>, used carbonate precipitation for cadmium (II) and lead (II) removal from electroplating effluents. At pH 7.5, the concentration of lead (II) and cadmium were reduced 0.6 and 0.25 mg/L respectively. Apart from low pH of precipitation, the relative filtration rates for carbonate precipitates were found to be approximately twice that of hydroxide precipitation<sup>85</sup>.

### **1.8.4 Chemical Reduction**

The hexavalent chromium in the chromate waste is reduced to trivalent chromium under acidic conditions (pH=3) followed by precipitation of Cr(III) hydroxide under slightly alkaline conditions<sup>86</sup>, the removal of mercury, cadmium, lead, silver and gold by reduction process may be accomplished by use of sodium borohydride<sup>87</sup>.

### **1.8.5 Solvent Extraction**

Introduction of selective complexing agents has gained widespread usage for waste reprocessing and effluent treatment<sup>88</sup>. Liquid-liquid extraction of metals from aqueous solutions involves an organic and an aqueous phase. The aqueous solution containing the metal or metals of interest is mixed intimately with the appropriate organic solvent and the metal passes into the organic phase. In order to recover the extracted metal, the organic solvent is contacted with an aqueous solution whose composition is such that the metal is stripped from the organic phase and re-extracted into the stripping solution.

Knock et al<sup>89</sup>, investigated the extraction of chromium (III), cadmium (II), copper (II), nickel (II) and zinc (II) from solutions containing 100 mg/L of each ion with 0.5 M solution of 8-Hydroxy quinoline into chloroform. At pH 5.4, 99 % of the cadmium (II) was reported to have extracted into chloroform layer. Back titration with dilute Hydrochloric acid solution showed that at pH 2.0, 79 % of the

cadmium could be stripped into aqueous phase. The extraction of nickel into chloroform was 95 % at pH 2.0, while the extraction of Chromium (III) was poor at all pH conditions.

### **1.8.6 Cementation**

Cementation is the displacement of a metal ion from aqueous solution by a metal higher in the electromotive series. The precipitation of silver from photo processing discharges, the precipitation of copper from printed etching solutions and the reduction of Cr (VI) in chromium plating and iriditing are some of the examples of cementation in wastewater treatment<sup>90</sup>.

### **1.8.7 Electro-deposition**

Recovery of metals found in waste solutions can be done by electro-deposition techniques using insoluble anodes, e.g. spent solutions resulting from sulphuric acid cleaning of copper may be saturated with the copper sulphate in the presence of residual acid. These are ideal for electro-winning where high quality copper cathode can be electrolytically deposited while free sulphuric acid is regenerated<sup>91</sup>.

### **1.8.8 Ultrafiltration & Nanofiltration**

Conventional ultrafiltration (UF, which can exclude particle size larger than 100 nm) and nanofiltration (NF, which can exclude the particle size larger than a few nanometers) filters for water treatments are based on porous membranes, typically manufactured by the phase immersion method<sup>92</sup>. These membranes have been reported for the removal of microbial contaminants from water due to their larger size and can efficiently remove heavy metal ions after complexation with appropriate complexing agents<sup>93-95</sup>. Polymer assisted ultrafiltration is another method to use UF membranes for toxic metal ion removal from water. Y. Uludag reported mercury removal by UF membrane using polyethyleneimine (PEI) as complexing agent, P. Canizares et al. has successfully used polyethyleneimine (PEI) and Poly (acrylic) acid (PAA) as complexing material for UF based

separation of Cu(II), Ni(II), Pb(II) and Cd(II) ions from industrial wastewater<sup>96</sup>. Polyethyleneimine (PEI), poly (acrylic) acid (PAA) and poly (dimethylamine-co-epichlorohydrin-co-ethylenediamine) have been comparatively studied by R. Molinari for Cu(II) removal from wastewater using ultrafiltration<sup>97</sup>. Similarly many ultra and nanofiltration membranes have been reported by various workers which can be used for chelating enhanced or polymer assisted removal of heavy metals from wastewater<sup>98,99</sup>.

Fibrous media in the form of non woven filters have been used extensively in water treatment as pre filters or to support the medium that does the separation. At present the use of non woven filter media is limited to pre filters and is not used further downstream as high performance filters. However it is expected that by reducing the fiber size in the nanometer range, higher filtration efficiency can be achieved. Non woven nanofibrous media is now introduced in liquid filtration with great possibility to replace the ultra filtration (UF that can exclude particle size larger than 100 nm) by nanofiltration (NF that can exclude particle size larger than few nm).

### **1.8.9 Electro dialysis**

Electro-dialysis process works under the influence of electric current and separates the ions from water resulting in potable water. It is a well versed technique for ground and surface water treatment and can be used at TDS as high as 5000 ppm. The technique is used in SUJALAM, a joint project of DRDO and Rajasthan state government in which 64 water desalination plants have been installed in extreme desert areas of state to provide the potable water to its civilians<sup>100</sup>.

### **1.8.10 Reverse Osmosis hyperfine filtration**

Reverse osmosis are thin sheet-like materials forming barrier in the feed water path. They are usually permeable to some species and impermeable to others. RO is the phenomenon of flow of solvent from concentrated side to dilute (pure) side through semi-permeable membranes by exerting external

pressure. This technique is successfully applied for desalination purposes by various workers<sup>101,102</sup>, used for removal of Cr, Pb, Fe, Ni, Cu and Zn from vehicle wash rack water<sup>103</sup>, and now successfully used in large scale & domestic water purification systems.

### **1.8.11 Evaporation**

Evaporators are used chiefly to concentrate and recover valuable plating chemicals in electroplating industries. In this process collected rinse stream is boiled till concentration and allowed to return to the plating bath. There are several evaporators available which permit the recovery of condensed steam for recycle as rinse water. Capital and operational, both costs of recovery systems are very high<sup>104</sup>.

### **1.8.12 Xanthate process**

Xanthates of cellulose and starch are commercially available, may be used for wastewater treatment. Wastewater containing lead, nickel, copper, chromium and iron when treated with cellulose xanthate resulted in minimum level of residual metals at pH range 6.5 to 9.5<sup>105</sup>.

Most of these methods are associated with high capital and operational cost, complex handling and problems of disposal of the residual metal sludge.

### **1.8.13 Adsorption on Solid Surfaces**

Sorption operations, including adsorption and ion exchange are potential alternatives for wastewater treatment. In an adsorption process, atom or ions (adsorbate) in a fluid phase diffuse to the surface of a solid (adsorbent), where they bond with the solid surface or are held there by weak intermolecular forces<sup>106</sup>. A number of investigators have studied the removal of inorganic metal ions namely cadmium, cobalt, zinc, silver, copper, mercury, chromium and lead from aqueous solution using different adsorbents<sup>107-109</sup>.

#### **1.8.14 Ion Exchange Resins**

Ion exchange resins are potential alternatives for wastewater treatment. An ion exchange resin is an insoluble matrix (or support structure), normally in the form of small (1-2 mm diameter) beads fabricated from an organic polymer substrate. The material has sites with easily trapped and released ions. In the process simultaneous trapping and releasing of other ions takes place till the equilibrium is reached. Functionalization with chelating ligands enhances its efficacy due to complex formation in favorable conditions. However the improved ion exchange capacity of ion exchange resins may have advantages over such non specific adsorbents. In this regard, ion exchange resins hold great potential for the removal of heavy metals from water and industrial wastewater<sup>110</sup>.

### ***1.9 Advanced Materials Introduced in Water Purification***

Presence of toxic ions in ground water and surface water above the permissible level decided by the WHO is the biggest problem facing the world. Lots of the people are suffering from supply of unhealthy drinking water which causes numerous disease and even death. Since water touches every aspect of human activity, from food, health and environment to local and global economies, the staggering importance of water treatment technologies cannot be ignored.

In present scenario due to advancement in technology it is easy to explore the utility of advanced nano materials in water purification as filter media and adsorbent as well. The pore size of filter media is obvious fundamental parameters as it determines the ability of the filter to trap particles of specific size range. The efficacy of water purification technology can be governed by reducing the size of filtration media or adsorbent from micro level to nano level and there surface modifications can be achieved by functionalizing them. Use of non woven nano fibrous filter media and functionalized carbon nanotubes are the new advancements in the water purification techniques with promising results. Nanotechnology opens new horizons for the researchers in the area of water purification.

Current water purification methods in wide use employ chemically intensive treatment that is relatively expensive, increases stress on watersheds and environment and is not translatable to the non industrialized world. This is the reason, which opens the door for material scientists and researchers for advanced materials and technology development. Some of the recent water purification advancements in the field of toxic ion removal from contaminated water are in R&D stage and showing promising results which are discussed below:

### **1.9.1 Resins Functionalized with Novel Chelating groups**

Adsorption process has been and actually is the most frequently applied method in the industries and consequently the most extensively studied. S. Rangaraj et. al. reported IRN77 cation exchange resin as efficient adsorbent for the removal of Co(II), Cr(III) and Ni(II) from their aqueous solutions. Author has also carried out the comparison of IRN77 and SKN1 resin for the removal of cobalt from aqueous solution and nuclear power plant water. They have extensively utilised 1200H, 1500H and IRN77 for chromium removal from electronic process wastewater. A wide range of chelating ion exchangers has been tested for Zn, Ni, Cu and Cd removal from metal plating rinse water by Risto Koivula et.al.<sup>111</sup>.

Though chelating ion exchangers are extensively used for water purification from long time and having great importance in selected ion removal, possibility exists for identification of new chelating ion exchangers and their property to selective complex formation can be explored in toxic metal ion removal from water at specific locations where there concentration in water is more than the permissible limit.

Chelating enhanced ultrafiltration membranes are also used extensively in toxic ion removal from water due to their complex forming capacity with toxic metal ions. K. Antonina et al have done work of cobalt and nickel removal using PEI (polyethylene imine) both branched and linear one.

### **1.9.2 Biomaterials and their scope in water purification applications**

Biosorption of metal ions is also a good alternative and may be proved its potentiality due to easy availability and low cost. G. S. Agarwal et. al. has achieved better removal of chromium by tamarind seed powder, the chromium removal was also reported on different bio-sorbents by different workers. R.S. bai has successfully removed chromium from fungal biomass, S. E. Baily et. al. has reviewed the work on low cost sorbents thoroughly.

### **1.9.3 Carbon nanotubes**

Carbon nanotubes (CNTs) rank amongst the most exciting developments in the modern science and engineering since their discovery by Iijima in 1991<sup>112</sup>. Carbon nanotubes are one of such type of material having vast scope in the future water purification technologies. CNTs possess hollow tubular structure, large surface area, show better suitability to work as supporting material for other molecules, ability to be functionalized with different groups and work as potential adsorbent. They have been used in many ways in water purification applications. CNTs have been predicted and experimentally proved to be a good material for the adsorption of gases and can be functionalized to explore their ability to adsorb metal ions from water also.

Adsorption heterogeneity and hysteresis are two widely recognized features of organic chemical-CNT interactions. Different mechanisms mainly hydrophobic interactions, pi-pi bonds, electrostatic interactions, hydrogen bonds, and adsorption of organic chemical adsorption on CNTs may account for adsorption behavior. Adsorption mechanisms will be better understood by investigating the effects of properties of both CNTs and organic chemicals along with environmental conditions. *Due to their adsorption characteristics CNTs have potential applications in separation sciences and water treatment.*

X. Peng et al. synthesized a novel adsorbent, ceria supported on carbon nanotubes (CeO<sub>2</sub>-CNTs) and successfully used the material in arsenate removal from water and suggest that it is a promising adsorbent for drinking water purification with having 94% regeneration efficiency<sup>113</sup>.

## **Chapter 2 Nanotube cleaning, functionalization, characterization, metal removal and adsorption isotherm studies**

### **2.1 Introduction**

There have been reports of existence of carbon nanotubes with nanometer diameters in seventies by scientists working on different forms of graphite, in France and Japan. In Russia, LV Radushkevich reported about carbon nanotubes in 1952. M Endo from Japan and A Oberlin from France first observed nanotubes in 1976. But these were brought into limelight by Iijima in 1991. Since then they have been the subject of increasing numbers of experimental and theoretical studies. Because of their unique mechanical, electrical, optical and thermal properties (as already discussed in previous chapter) CNTs can be used to prepare novel materials such as hydrogen storage materials, super conductors, reinforced materials etc. On the mass basis they have much larger surface area than bulk particles and can also be functionalized with various chemical groups to increase their affinity towards target species<sup>114</sup>.

Having known about the hazardous and mutagenic effects of traces of heavy metal ions in water, and a thousand approaches to remove them, the CNTs capture the title of being one of the most effective sources, for the purpose. Adsorption technique is very popular due to simplicity and low cost. In an adsorption process, atom or ions (adsorbate) in a fluid phase diffuse to the surface of a solid (adsorbent), where they bond with the solid surface or are held there by weak intermolecular forces. Although activated carbon<sup>115,116</sup> is frequently used as general adsorbent of inorganic and organic compounds, alternative adsorbents have been developed. Many adsorbents have been developed and used to remove metal ions from waste water such as hybrid EDTA-zirconium phosphate cation

exchanger<sup>117</sup>, hazelnut activated carbon<sup>118</sup>, peanut hulls<sup>119</sup> and chelating resin<sup>120</sup>. The use of activated carbon, metal oxides and silica with various reagents utilized for removal has also been frequently practiced<sup>121-123</sup>. CNTs, on account of large surface areas, very high adsorptive nature, hydrophobic inner walls and resistant to bacterial contamination have been introduced recently in water purification applications as an efficient adsorbent and reported for removal of different heavy metal ions like Pb(II), Cd(II), As(III) etc.<sup>124,125</sup>

However, there are many difficulties encountered in the synthesis of high quality nanotube samples and so their direct use can also be questioned. The various methods used for nanotube synthesis such as Arc discharge, Laser ablation, Chemical vapour deposition, High Pressure Carbon monoxide synthesis etc involve traces of heavy metals such as Fe, Co, Ni and many amorphous and carbonaceous forms of carbon. Furthermore, nanoparticles consisting of nested closed graphitic layers of polyhedral shape make up to one half in weight of the nanomaterial deposit. The nanotubes which are produced are of different dimensions. They are with a wide distribution of lengths, helicities of the layers, and diameters.

Up to now, the only available purification method was oxidation, either in gas-phase<sup>126,127</sup> or in liquid-phase<sup>128,129</sup>. The basal planes of graphite are subject to oxidation only if defects (vacancies/dislocations) are present. The tips of the tubes and the particles, incorporating reactive five-membered carbon rings, have a higher curvature and higher strain and will thus be preferentially attacked<sup>131</sup>. The tube ends get invariably opened or at least damaged during the purification process, and the outer tube layers are removed during the treatment, presumably because of defects in the hexagonal network<sup>130</sup>. Tube tips have electronic properties that differ from the cylindrical part of the nanotubes<sup>132</sup>, and they determine furthermore to a great extent the field emission properties and

various other properties of the tubes. It is so of great importance to obtain purified tubes with intact ends and non-damaged sidewalls.

Cleaning of nanotubes would help to explore the properties better. Surface purification followed by functionalization with various groups could help to increase the activity of nanotubes. This work is focused on exploring the adsorption properties of surface and chelation properties of the functional groups decorating their surface. These properties have been studied in detail for heavy metal rejection from aqueous solutions. Studies have been done varying the metal ion concentration, CNT dosage, time of contact of the two and pH of prepared solution. Modifications with different functional groups containing different atoms still increases the metal binding capacity of CNT (due to increased chelation or complexation) and helps to retain more heavy metal ions on the surface, and thus better rejection.

## **2.2 *Materials***

Carbon nanotubes (multi-walled carbon nanotubes, MWNTs) manufactured by HiPCO (supplied by Iljin Nanotech, Korea) whose purity was greater than 90%, were purchased from Sigma Aldrich. The MWNTs were of diameter 110-170 nm and length 5-9 microns. Conc. H<sub>2</sub>SO<sub>4</sub> (98%), conc. HNO<sub>3</sub> GR (69%) were purchased from MERCK. SOCl<sub>2</sub>, Ethylenediamine (>99%, Sigma Aldrich), Sodium azide (>99%, Sigma Aldrich) were used as it is.

## **2.3 *Experiments***

### **2.3.1 *Surface cleaning of nanotubes***

Cleaning of surface of these pristine CNTs with SDS (sodium dodecyl sulfate) has been previously reported<sup>133</sup>. A modified method for effective cleaning of surface was adopted and this method helps to remove the amorphous carbon soot and nearly all heavy metals present in the as purchased CNTs. In this process, 2g of the as purchased pristine nanotubes (HiPCO, >90%) were sonicated with 500 ml of

1% Brij 98 (a non-ionic surfactant) for about 2h. The sonicated solution was allowed to stand for about 6h. The added surfactant being greater than the CMC value, was able to make big micelle structures and remove the heavy soot by sedimentation (gravitational law). The sediment was rejected as soot associated with the nanotubes. The nanotubes were collected from the mother liquor by subsequent centrifugation and sedimentation at 3000 rpm for 15 minutes. This process was repeated 2-3 times to obtain nanotubes.

The surfactant associated with the nanotubes could be easily removed by alternate washing with water and brine solution. Some of the heavy metals that may have remain attached to the surface of the CNT's, were removed by converting these heavy metals into their soluble salts using 50% HCl solution. This separated the nanotubes from heavy metal chlorides thus giving a clean surface of the nanotubes. The yield was nearly 35% of the initial raw CNTs (2 g) used. The remaining 65% could be considered to be amorphous, other undesired carbonaceous material and heavy metal traces.

The obtained nanotubes do not get attracted to the magnetic needle showing that the nanotubes are free from traces of heavy metal ions. It differs from the pristine CNTs which contain Fe, Co, Ni and other trace metals, and get stuck to the magnetic needle. The SEM photograph of pristine nanotubes (Figure 2.1) clearly shows presence of amorphous and carbonaceous materials associated with nanotubes where pristine stock dominates and nanotubes are not visible. Purification and washing removes the unwanted carbonaceous material and metal ions and nanotube surfaces become clearly visible. Now these washed and dried nanotubes were used to treat with various functionalizing agents.

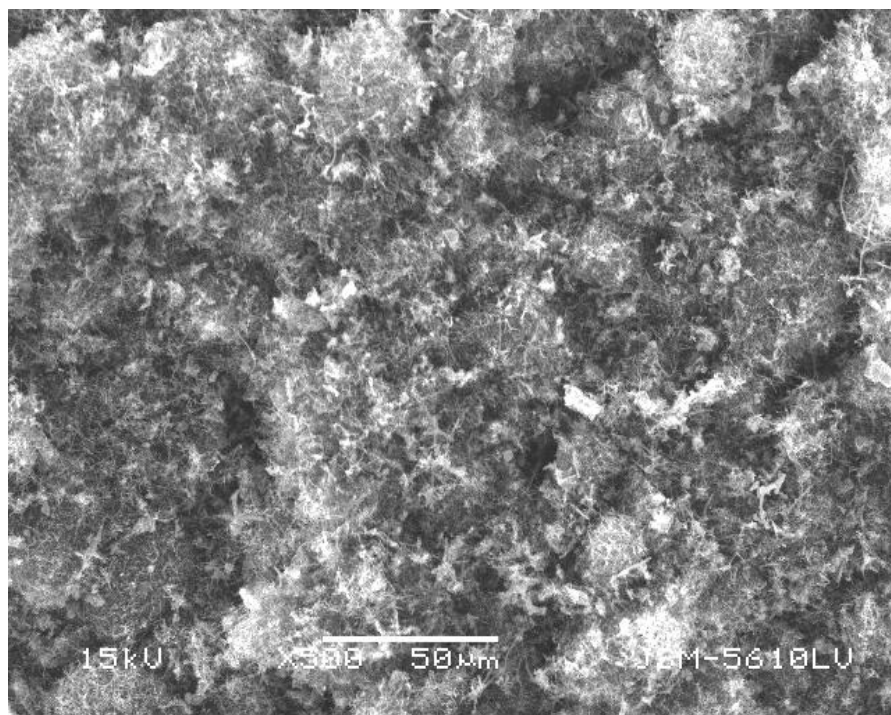


**Figure 2.1** SEM image of commercially available Pristine CNTs.

## **2.3.2 Functionalization of CNTs**

**2.3.2.1 Oxidation of Carbon Nanotubes:** The as-received and purified HiPCO MWNTs were first treated with a 3:1 mixture of concentrated nitric and sulfuric acid (40 mL). This acidic mixture is highly corrosive and reactive. This mixture was then stirred for 24 h at 40°C to introduce carboxylic acid groups on the MWCNT surface. The oxidized nanotubes were washed with double distilled water five times, to obtain oxidized clean surfaces of MWNT's.

Carboxylation is the most favored starting point because it can be covalently bonded to form ester or amide linkages easily. The sample was then dried in a vacuum oven at 80 °C for 4 h.

**2.3.2.2 Acylation of Carbon Nanotubes:** The oxidized nanotubes were treated with  $\text{SOCl}_2$  to introduce the acyl groups. 200 mg of obtained nanotubes were added to 20 mL of thionyl chloride and 2mL of DMF (dimethyl formamide) in 100 mL round bottom flask. The system was properly sealed with grease and teflon, to prevent any moisture contamination and then refluxed for 36 hrs. at 60°C. The whole set up was put in hood and the excess of thionyl chloride was removed by boiling it off in hood.

The product obtained was washed with toluene. The sample was then dried in a vacuum oven at 80 °C for 4 h.

### **2.3.2.3 Functionalization of Carbon Nanotubes with Ethylenediamine:**

Twenty milligrams of the acylated nanotubes (which contain  $-\text{COCl}$  distributed at places on the nanotube surface) were dispersed by sonication in 10 mL of ethylenediamine. The sonication was followed by stirring for 16 hrs. All processes were carried out at 60°C. The product was then diluted with 200 mL of methanol. The functionalized MWNTs were then dried in a vacuum oven at 80 °C for 4 h. This helped to introduce the amide groups on the CNT's.

#### **2.3.2.4 Azide functionalization of carbon nanotubes:**

Sodium Azide was used as a reagent to convert the  $-\text{COCl}$  group to  $-\text{CON}_3$ . 60 mg of acylated nanotubes were treated with 5 mg of  $\text{NaN}_3$  in DMF as solvent (Figure 2.2). The azide linkage is highly reactive and thus reactions were done in controlled conditions and in absence of water. The reaction was carried out at  $60^\circ\text{C}$  for 16h, and finally the product is precipitated in toluene. The product was dried in oven at  $80^\circ\text{C}$  for 4 h.

#### **2.3.3 Preparation of stocks and Batch method studies**

Aqueous solutions of salts of  $\text{Cr}^{+6}$ ,  $\text{Pb}^{+2}$ ,  $\text{Cd}^{+2}$ ,  $\text{As}^{+3}$ ,  $\text{Cu}^{+2}$  and  $\text{Ni}^{+2}$  were prepared to study the absorptive strength of nanotubes. Stock solutions of chromium and lead of 1000 mg/l concentration were prepared by dissolving, 2.848 g of  $\text{K}_2\text{Cr}_2\text{O}_7$ , 1.598 g of  $\text{Pb}(\text{NO}_3)_2$ , respectively in 1000 ml of ultrapure water (Elix, Millipore), whereas cadmium solution was prepared by dissolving 1 g of cadmium metal in minimum volume of (1 + 1) HCl and then making it up to 1000 ml with ultrapure water. Stock solution of nickel was prepared by dissolving 1.273 g of NiO in minimum volume of 10% (v/v) HCl and then diluted up to 1000 ml with ultrapure water. Standard working solutions of copper and arsenic were prepared from 1000 mg/L standard solution (Merck, Germany) and solutions of varying initial concentrations were prepared from a 1000 mg/L by serial dilution using distilled deionized water. In another series of experiments, the pH of Chromium metal ion solution was adjusted to 3.5 and 7.2 by the addition of 0.1N solution of NaOH during dilution process. Adsorption studies for other metal ions were done only at pH 3.5, as at basic pH they showed hydrolysis and hydroxides formation.

Batch experiments were carried out in different stoppered glass bottles at room temperature ( $25 \pm 1^\circ\text{C}$ ) using known amount, i.e. 10mg of differently functionalized CNTs in 10 ml of metal ion concentration ( $1000\mu\text{g/L}$ ) solution in ordinary mixing conditions using rotary shaker (Revotech) at the stirring

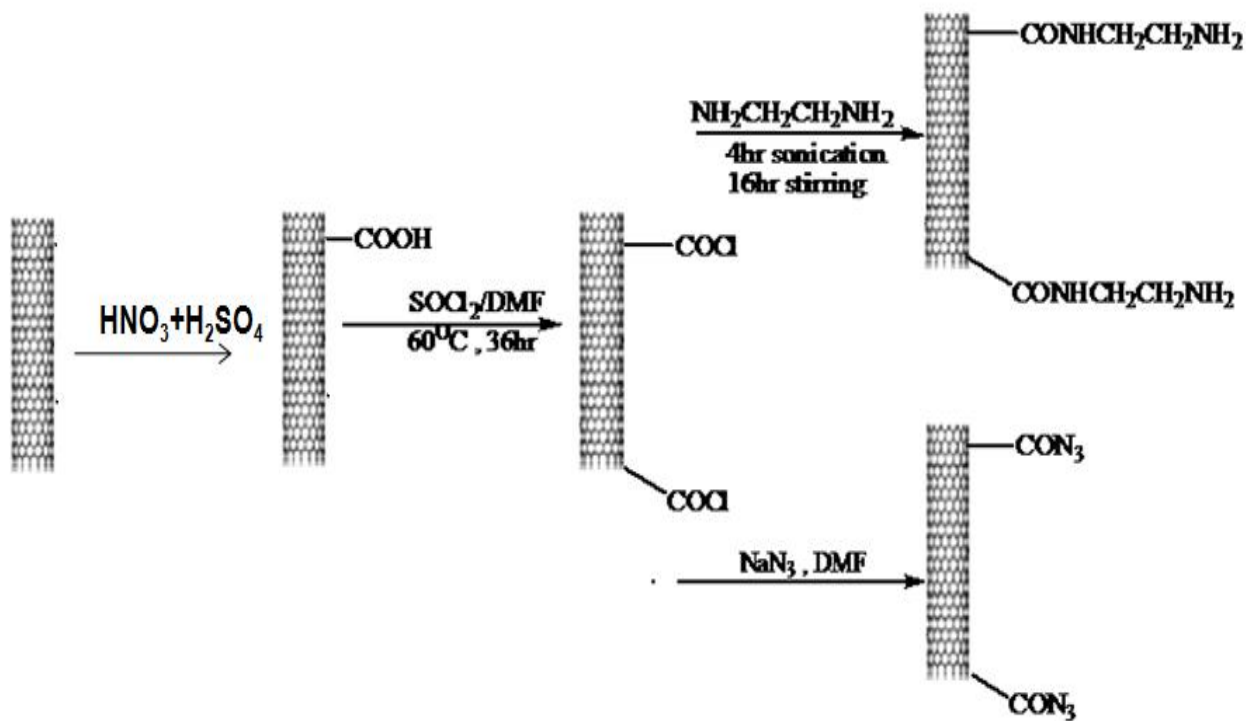


**Figure 2.2** Schematic representation of functionalization of nanotubes.

speed of 120 rpm. The samples were taken after regular time interval and filtered through Whatman's filter paper. Concentrations of metal ions in filtrates were determined by AAS. These data were used for comparative removal studies and kinetic establishment. The Arsenic ion concentration was measured in graphite furnace mode of AAS and other metal were measured in flame mode of AAS. Blank experiments (without CNT) were conducted to confirm, no adsorption onto container walls.

## **2.4 Characterization**

Concentrations of metal ions in filtrates were determined using Atomic Absorption Spectrophotometer (Analytikjena model Nova 400). AAS equipped with 100 mm burner, a cross flow nebulizer 5.0 ml/min and 1.2 mm slit was used throughout the experiments. IR spectra were recorded on Jasco FT-IR spectrometer model 610 by using KBr pellets. The pH measurements were made on a digital pH meter (HACH, sension 1, model 51935-00) equipped with a gel-filled pH electrode. The meter was calibrated with the buffers of 3.5 and 7.2. Raman spectra were recorded using microscope equipped triple monochromator combined with a peltier cooled charge couple device detector system. The spectra were acquired in the back-scattering geometry, while for excitation the 785 nm line of an Ar<sup>+</sup> laser was focused on the sample by means of an 80 $\times$  objective at a power of  $\sim$ 2mW, measured directly before the sample. The phonon frequencies were obtained by fitting Lorentzian line shapes to the experimental peaks after background subtraction.

## **2.5 Results and discussion**

### **2.5.1 Characterization of nanotubes**

#### **2.5.1.1 Raman spectroscopy**

It is a reliable technique for the characterization of carbon-based nanostructures. It points at the various radial breathing and tangential stretching modes of vibrations. The vibrations corresponding

to radial breathing mode at 785nm laser wavelength are very weak and not significant. The Raman spectra of MWNTs excited with this laser line show two characteristic bands in tangential stretching mode, namely the D-band at 1340-1390  $\text{cm}^{-1}$ , and a G-band in the range 1550-1600  $\text{cm}^{-1}$ . The D-band is a disorder induced feature arising from double resonance scattering process and its intensity is a measure of defect concentration on the nanotubes. This defect is supposed to be created due various purification reactions, to which the nanotubes are exposed or heteroatom associated at time of growth of nanotubes or disordered carbon. The G band originates from in-plane tangential stretching of the carbon- carbon bonds in graphene sheets.

The D-band in graphite involves scattering from defect which breaks the basic symmetry<sup>134,135</sup> of the graphene sheet. It is observed in  $\text{sp}^2$  carbons containing porous, impurities or other symmetry-breaking defects. Multi-walled carbon nanotubes (MWNT) are made of concentric graphene sheets rolled in a cylindrical form with diameters of tens of nanometers<sup>136</sup> and because of this large diameter of the outer tubes for typical MWNT and because they contain an ensemble of carbon nanotubes with diameters ranging from small to very large, most of the characteristic differences that distinguish the Raman spectra in SWNT from the spectra for graphite are not so evident in MWNT.

The Raman spectra as shown in (Figure 2.3) for pristine and purified CNT's bring out the fact that the  $I_D/I_G$  ratio (Intensity of D band / Intensity of G band) for pristine MWNT's is very high (intensity of D-band being more). This is in accordance with presence of amorphous and carbonaceous impurities, associated with as prepared CNT's, making the surface rough due to defects and disorders. Effective cleaning of the surfaces removes the unwanted materials and thus reducing the intensity of D-band. The  $I_D/I_G$  ratio of pristine nanotubes is 0.6665 which is reduced to 0.2366 in purified nanotubes, thus confirming effecting cleaning.

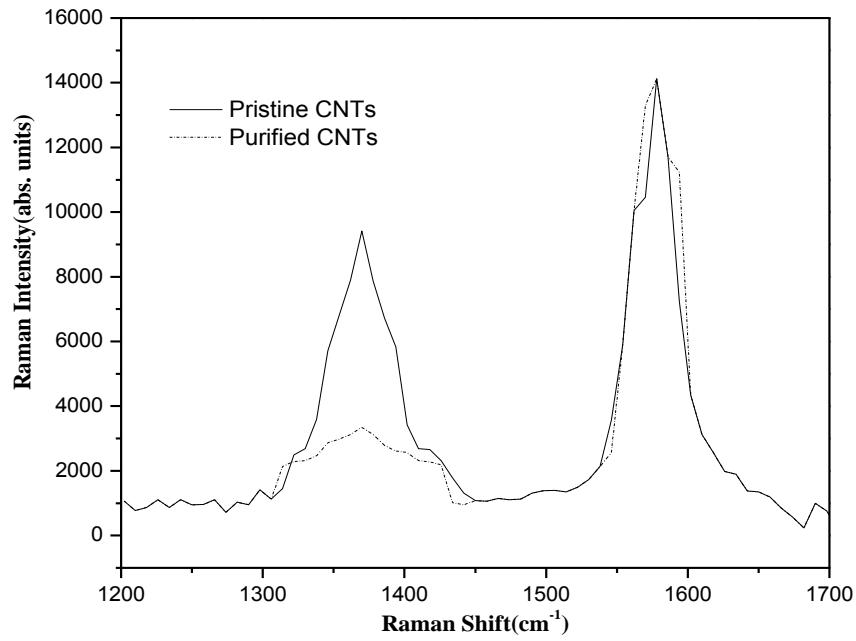


**Figure 2.3** Raman spectra (a) Pristine (b) Purified CNTs.

### 2.5.1.2 Transmission Electron Microscopy

Nanotubes structures with cleaned surfaces and ends are visible in TEM images (Figure 2.4) of functionalized MWNTs. Pristine tubes have amorphous materials associated with them which is removed after cleaning and functionalization. The process ruptures the surface but, this damage is limited to the surface of the nanotube and the internal tubes remain intact. TEM images of cleaned and differently functionalized nanotubes reveal the open tips or ends, and different surface morphologies depending the functionalizing reagent and its strength. Nanotubes appear to have bamboo like structure. There is an outer graphitized layer and the inner tube is subdivided by single or multigraphite layers, which may be caused by surface diffusion of carbon cluster on large catalytic particle across nanotube wall (Li. D.C.; Dai. L. *Chem. Phys. Lett.***2000**, 316, 349).The commercially available nanotubes had an average 5-9 $\mu$  length, which is reduced to 4-6  $\mu$  for some nanotubes as a result of functionalization.

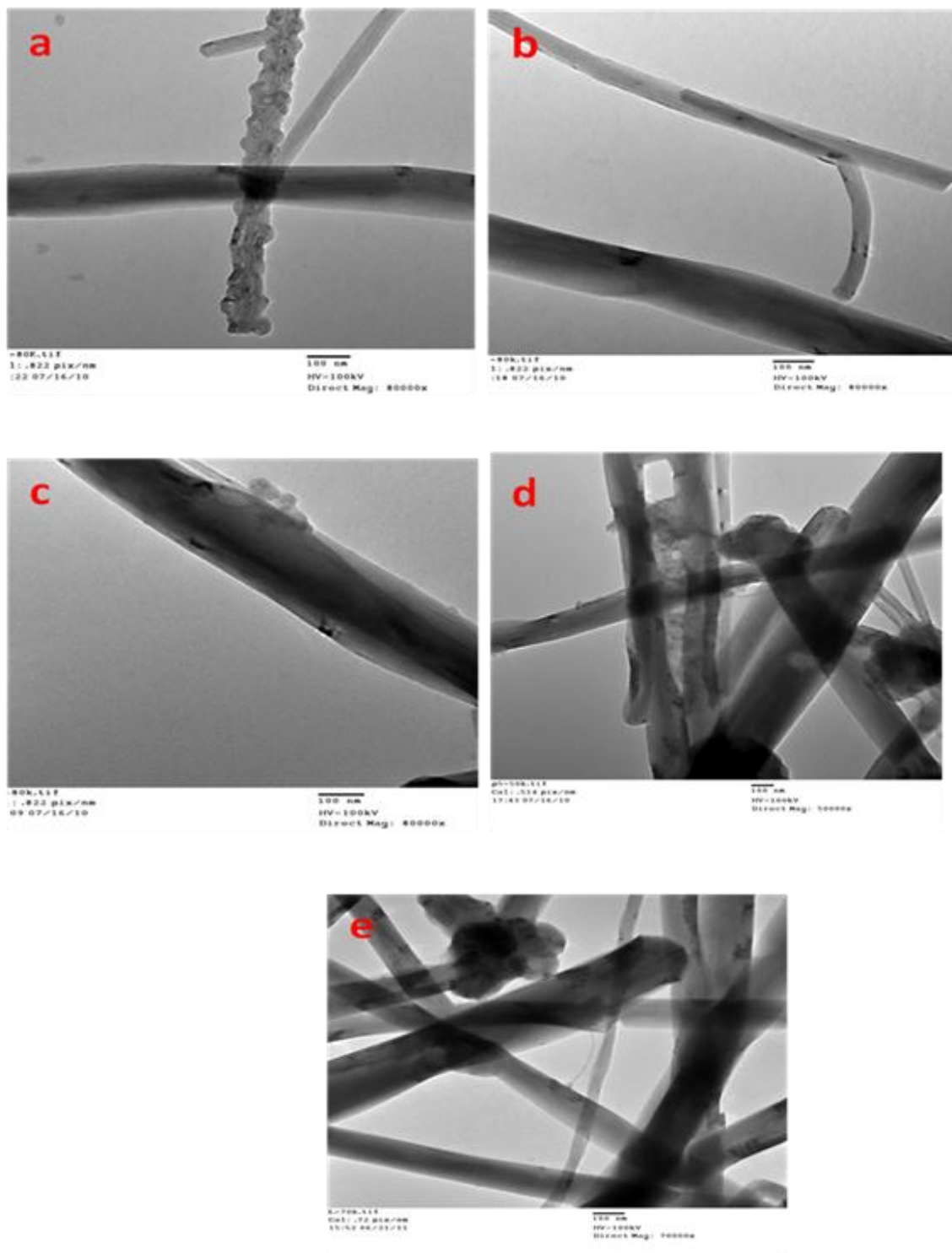


**Figure 2.4** TEM images (a) Pristine (b) Oxidized (c) Acylated (d) Amide (e) Azide functionalized CNTs.

### 2.5.1.3 The FT-IR spectroscopy

The FT-IR spectra (Figure 2.5) of purified MWNTs (a) do not show any significant peaks, whereas the spectra of oxidized MWNT's (b) show a sharp band at  $3500\text{cm}^{-1}$  due to hydroxyl(-OH) group. Band at  $1726\text{cm}^{-1}$  could be due to the presence of C=O stretching of carboxylic group. Similarly the strong peak at  $1618\text{cm}^{-1}$  can be assigned to C-O stretching of carboxylic group. Presence of carboxylate anion can also be confirmed by bands present in the range of  $1460\text{cm}^{-1}$ . FTIR spectra of amide functionalized CNT's showed disappearance of the band at  $1726\text{ cm}^{-1}$  and appearance of a new band at lower wave number ( $1633.41\text{ cm}^{-1}$ ) due to amide carbonyl stretch. In addition, presence of new band at  $1391\text{ cm}^{-1}$ , corresponds to C-N bond stretching . In case of azide functionalized nanotubes, the bands at  $2142\text{ cm}^{-1}$  and  $1566\text{ cm}^{-1}$  corresponds to asymmetric stretching and a weak symmetric stretching of azide functional group, for azide functionalized CNTs. The process thus helped to create sufficient functional groups on nanotubes surfaces (confirmed by titration).

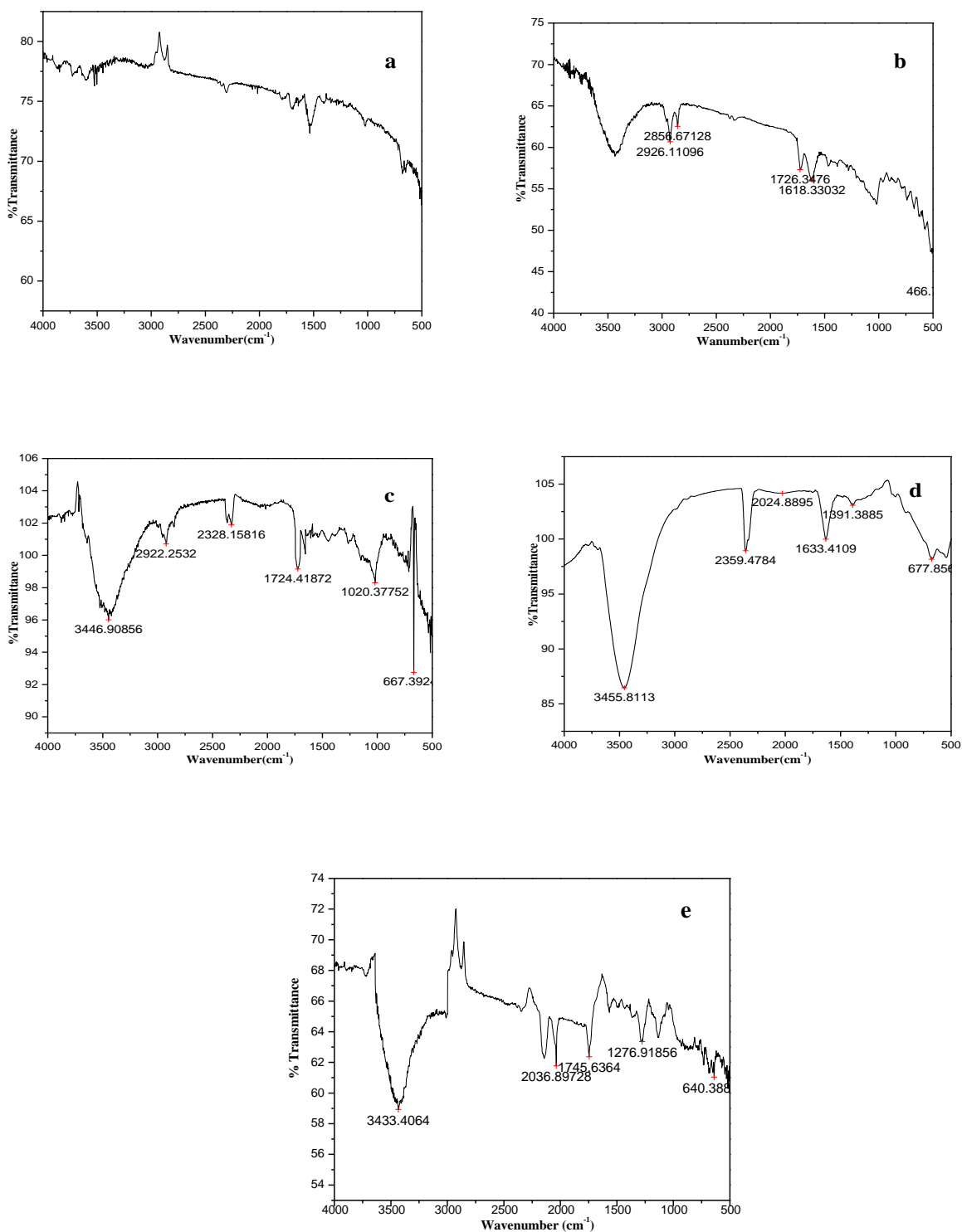


**Figure 2.5** FT-IR spectras (a) Pristine (b) Oxidized (c) Acylated (d) Amide (e) Azide functionalized CNTs.

#### **2.5.1.4 EDS spectral studies**

The EDS spectral studies (Figure 2.6) of CNTs completely reveal the presence of different elements on their surfaces. EDS spectra of pristine CNT (Figure 2.6a) does not show any elemental peak except that of carbon, but elemental peaks of oxygen (Figure 2.6b) and nitrogen (Figure 2.6c) are clearly visible in oxidized and azide functionalized CNTs respectively, which confirm that CNTs have been functionalized by oxygen containing and nitrogen containing groups respectively.

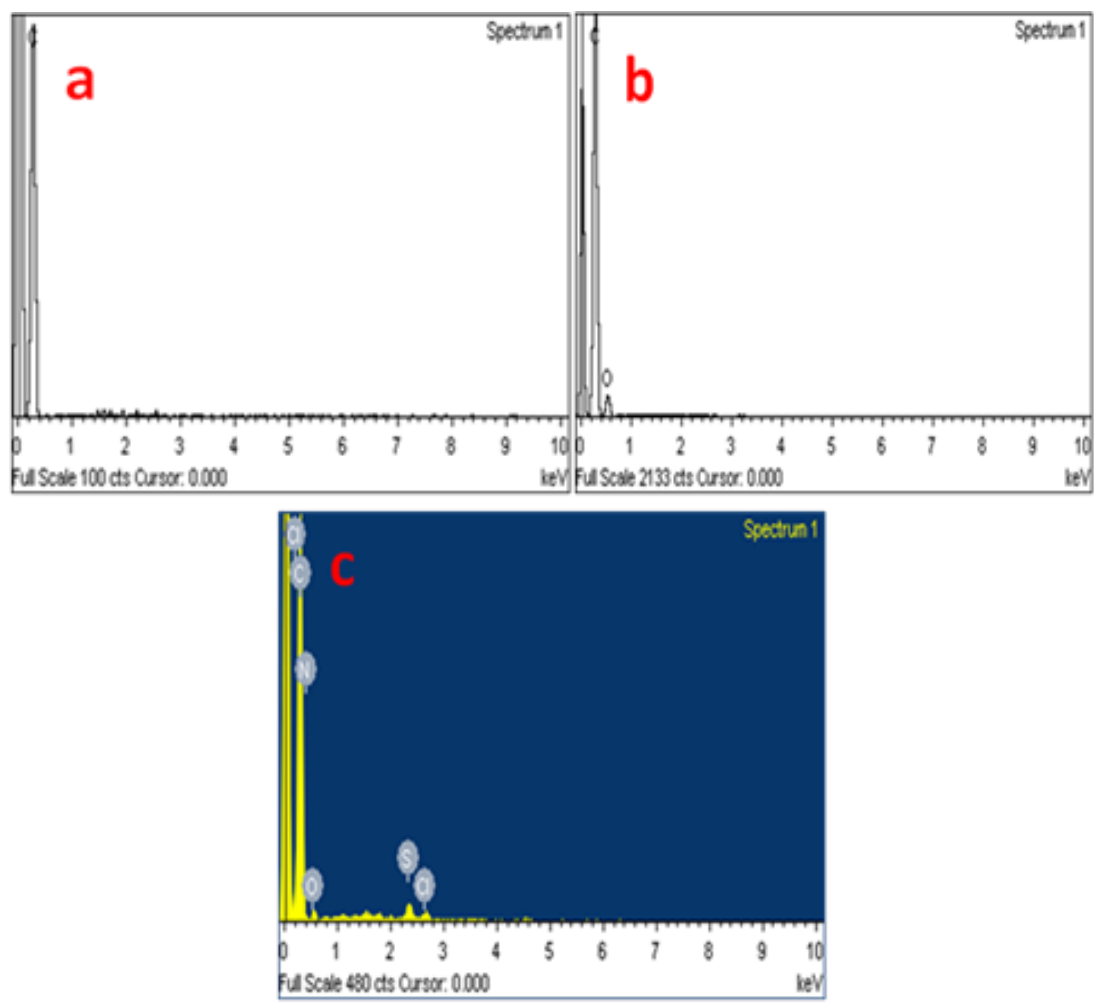


**Figure 2.6** EDS spectras (a) Pristine (b) Oxidized (c) Azide functionalized CNTs.

#### **2.5.1.5 X-Ray Diffraction studies**

Since CNTs are having basic graphitized carbon with  $sp^2$  hybridization, the modification during functionalization may be easily find out by XRD analysis. Figure 2.7 represents comparative XRD patterns for oxidized and amide functionalized CNTs. It is observed clearly that a well crystalline graphitized structure with 002, 100 and 004 planes is present in both materials. This indicates that the crystalline nature of CNT remained unaffected during different steps of functionalization process and proves the presence of CNTs in their actual form after functionalization.

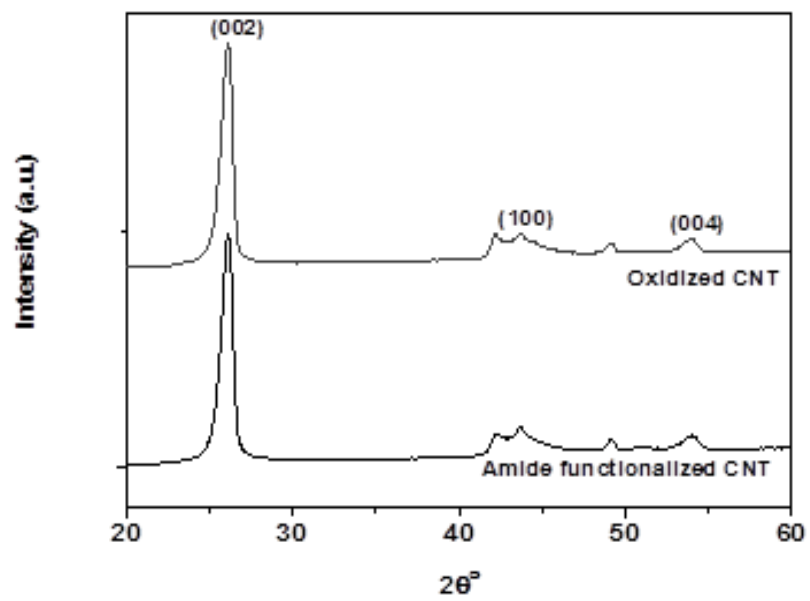


**Figure 2.7** XRD spectra of oxidized and functionalized CNTs.

#### **2.5.1.6 Thermo-gravimetric studies**

Thermogravimetric studies reveal that functionalization of nanotubes disturbs the regular arrangement and geometry of hexagonal and pentagonal rings on the nanotube surface. The requirement of treatment with various reagents breaks the nanotube surface at various sites and thus reducing the thermal stability of nanotube structure. For purified nanotubes the disintegration occurs above 650°C, while disintegration temperature it is much lower for other functionalized CNT's (Figure 2.8).

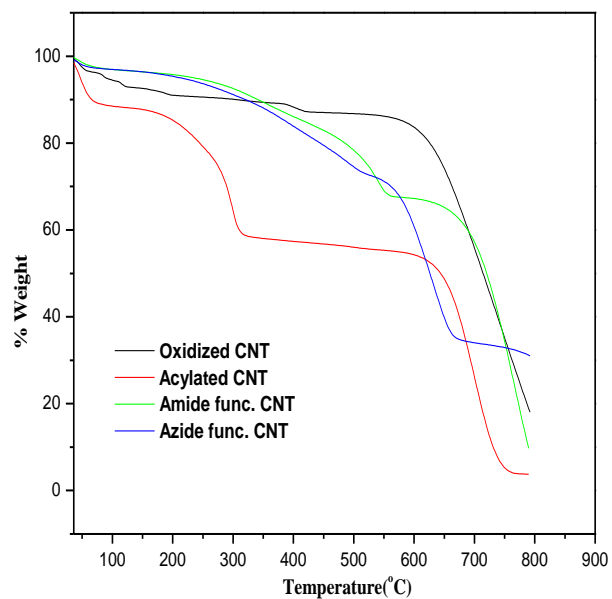
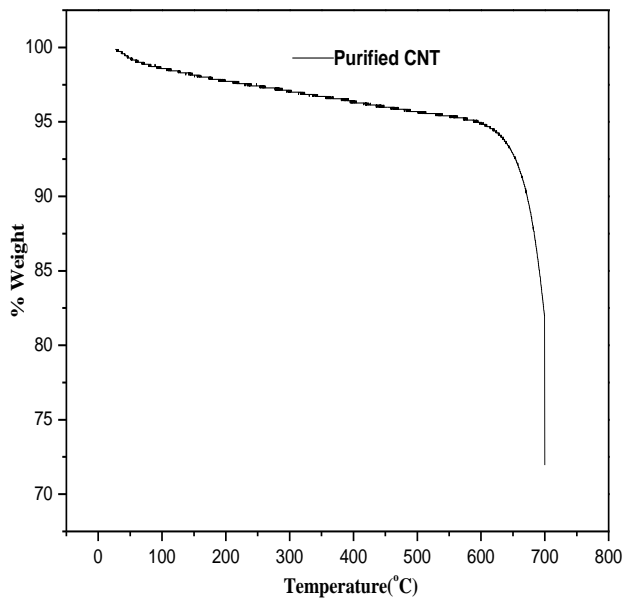


**Figure 2.8** Thermo-gravimetric studies of Purified CNT's and various functionalized CNT's.

## **2.5.2 Adsorption kinetics**

Heavy metal rejection studies were carried out for different metal ions. 1ppm solutions of  $\text{Cr}^{+6}$ ,  $\text{Pb}^{+2}$ ,  $\text{Cu}^{+2}$ ,  $\text{Cd}^{+2}$ ,  $\text{As}^{+3}$  and  $\text{Ni}^{+2}$  were prepared and batch experiments were carried out by putting 10mg each of differently functionalized CNT (oxidized, acylated, amide and azide functionalities) in 10 ml of metal ion solution in ordinary mixing conditions and stirred at speed of 120 rpm. The samples were taken after every 0.5h and filtered through Whatman's filter paper. Concentrations of metal ions in filtrates were determined by AAS.

### **2.5.2.1 Effect of time**

Maximum adsorption and thus percentage removal is observed for Chromium (Figure 2.9a, 2.10a, 2.11a & 2.12a, Table 2.1-2.4) followed by that of Lead, for all types of functionalized CNTs. The percentage uptake of all metal ion increases with increase in contact time. Increase in adsorption with time is greater for initial two hours, but then increase reduces and finally reaches a plateau. This point is equilibrium point where rate of adsorption is equal to rate of desorption from the surface. In all the cases equilibrium is reached at 3.5h where after no increase in uptake occurs with time of contact. At equilibrium the adsorption process becomes steady and does not increase with increase in contact period. The percentage rejections due to adsorption at surface of functionalized nanotubes were found to be much greater as compared to that by unfunctionalized stuff. Furthermore azide and amide functionalized CNTs proved more effective than the oxidized nanotubes (Table 2.5). This is explained by greater complexation tendency of azide and amide group with metal ion due to presence of hetero atoms nitrogen along with oxygen. The retained metal ions in form of complexes are also supported by adsorptive properties of CNTs, as the metal ions are retained on the surface due to two factors (a) chelate complex formation (b) strong adsorptive forces between metal ions and CNT surface, and the obtained water as filtrate from Whatman's filter paper is 40-90% free of hazardous heavy metal ions.

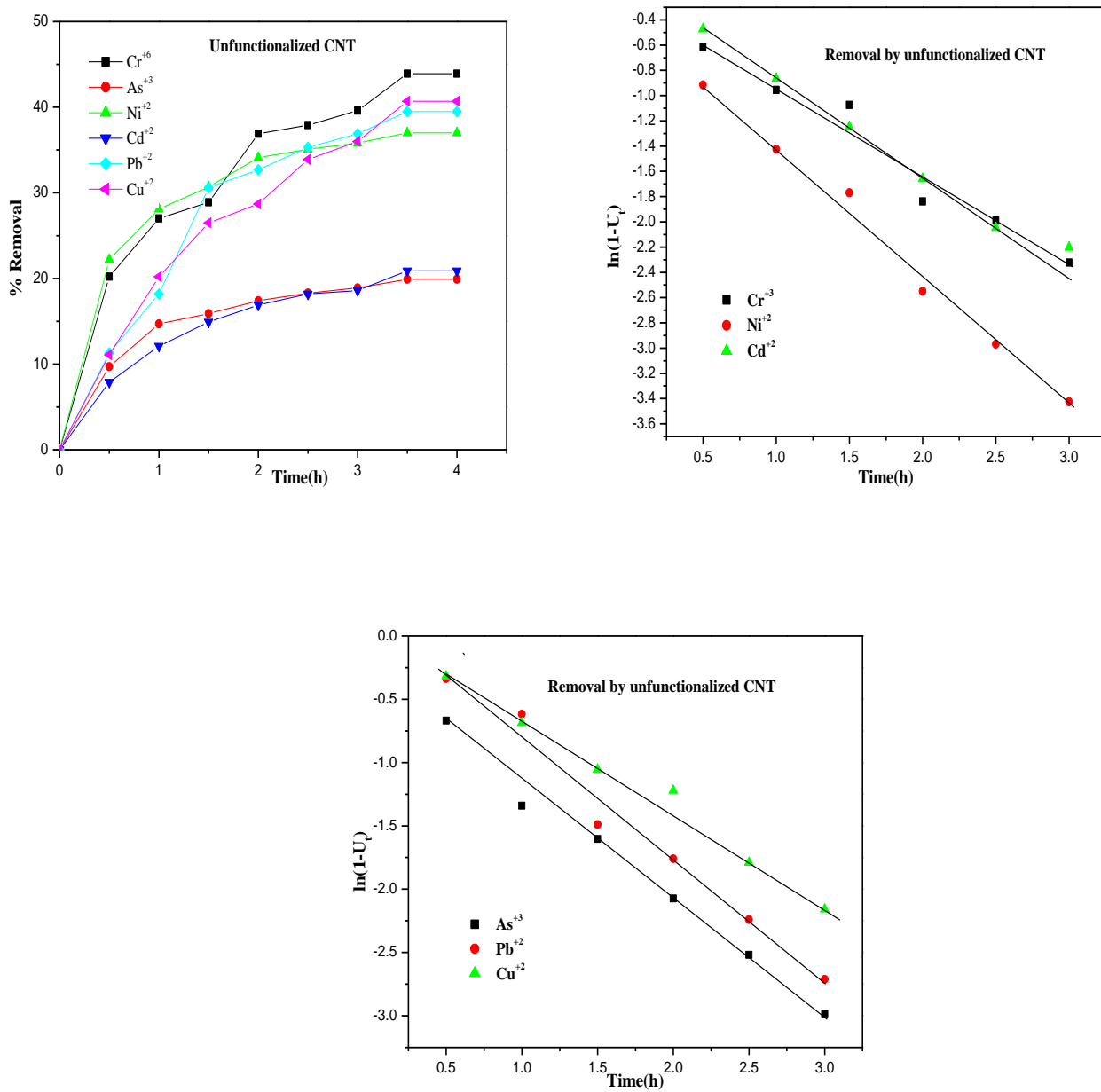


**Figure 2.9** Plots of (a) % Removal of metal ions v/s time (b,c)  $\ln(1-U)$  v/s Time(h) for removal of heavy metals by unfunctionalized CNTs.

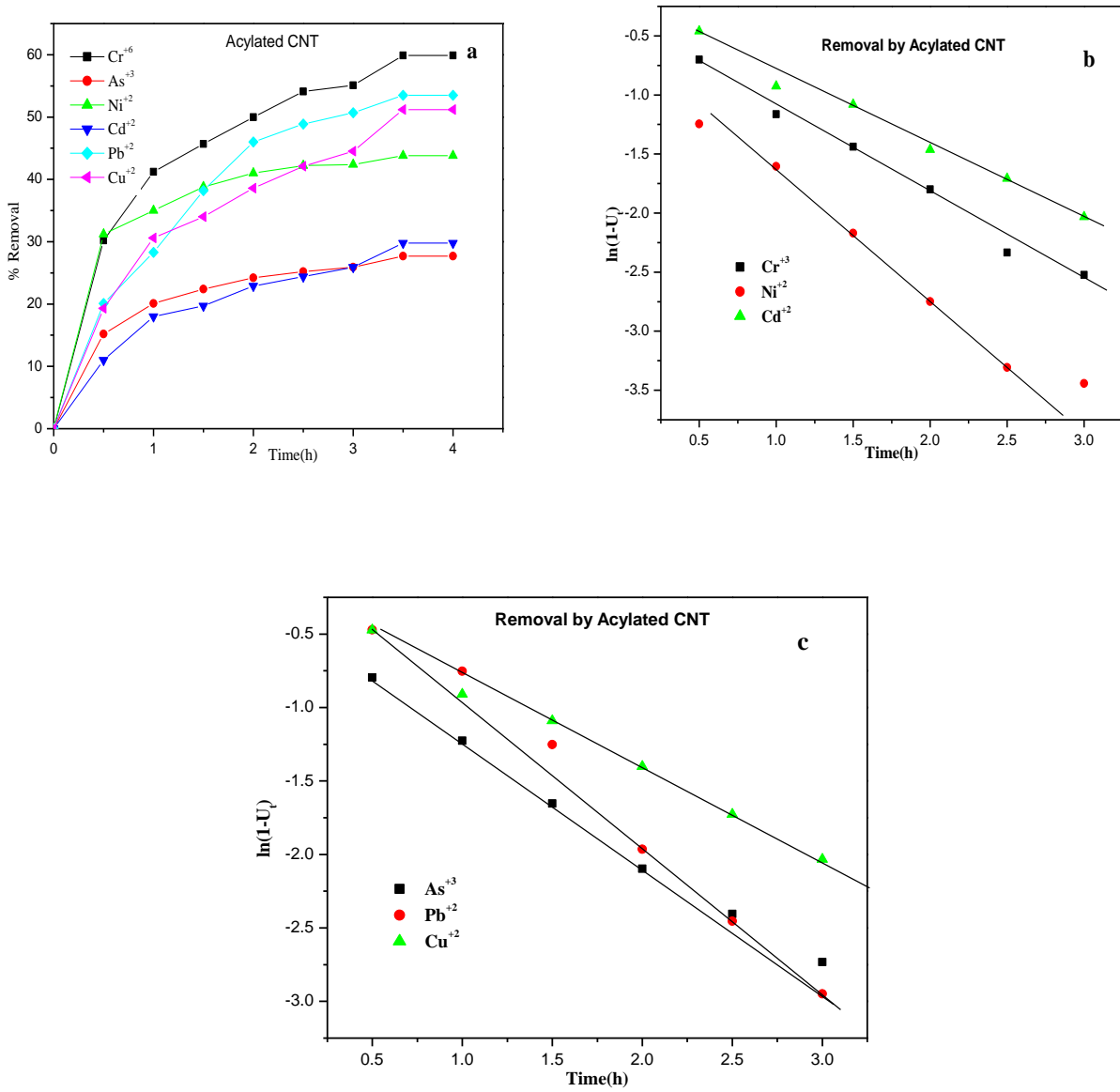


**Figure 2.10** Plots of (a) % Removal of metal ions v/s time (b,c)  $\ln(1-U_t)$  v/s Time(h) for removal of heavy metals by acylated CNTs.

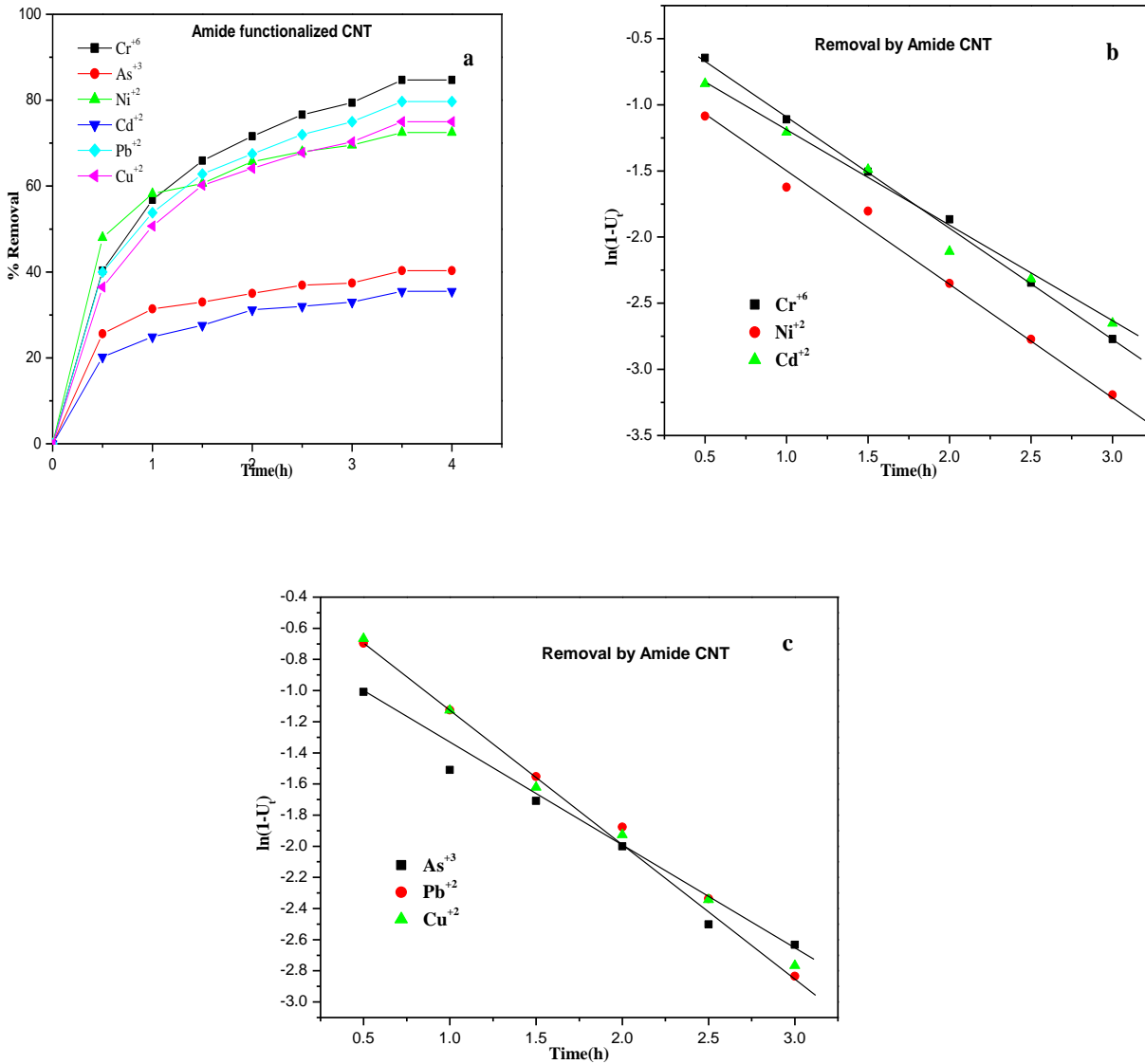


**Figure 2.11** Plots of (a) % Removal of metal ions v/s time (b,c)  $\ln(1-U)$  v/s Time(h) for removal of heavy metals by amide functionalized CNTs.

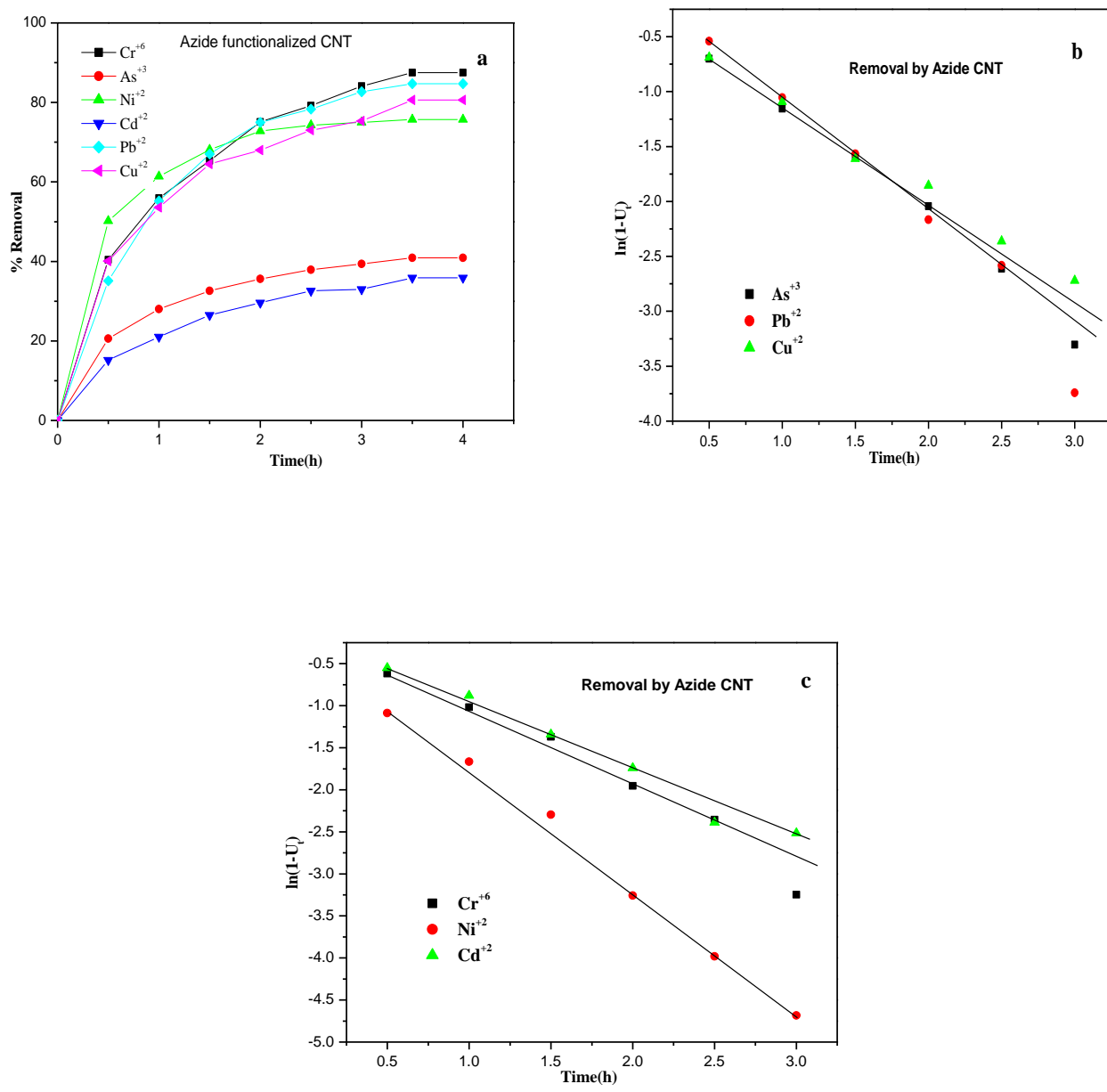


**Figure 2.12** Plots of (a) % Removal of metal ions v/s time (b,c)  $\ln(1-U_t)$  v/s Time(h) for removal of heavy metals by azide functionalized CNTs.

**Table 2.1** % removal of metal ions with time for unfunctionalized nanotubes.

S.No.	Time (Hrs.)	Removal capacity (%) by unfunctionalized CNT					
		Cr (VI)	As (III)	Ni (II)	Cd (II)	Pb (II)	Cu (II)
1	0.5	20.2	9.7	22.2	7.9	11.3	11.1
2	1.0	27.0	14.7	28.1	12.1	18.2	20.2
3	1.5	28.9	15.9	30.7	14.9	30.6	26.5
4	2.0	36.9	17.4	34.1	16.9	32.7	28.7
5	2.5	37.9	18.3	35.1	18.2	35.3	33.9
6	3.0	39.6	18.9	35.8	18.6	36.9	36.0
7	3.5	43.9	19.9	37.0	20.9	39.5	40.7
8	4.0	43.9	19.9	37.0	20.9	39.5	40.7

**Table 2.2** % removal of metal ions with time for acylated nanotubes.

S.No.	Time (Hrs.)	Removal capacity (%) for acylated CNT's					
		Cr (VI)	As (III)	Ni (II)	Cd (II)	Pb (II)	Cu (II)
1	0.5	30.2	15.2	31.2	11.0	20.1	19.3
2	1.0	41.2	20.1	35.0	18.0	28.3	30.6
3	1.5	45.7	22.4	38.8	19.7	38.2	34.0
4	2.0	50.0	24.2	41.0	22.9	46.0	38.6
5	2.5	54.1	25.2	42.2	24.4	48.9	42.1
6	3.0	55.1	25.9	42.4	25.9	50.7	44.5
7	3.5	59.9	27.7	43.8	29.8	53.5	51.2
8	4.0	59.9	27.7	43.8	29.8	53.5	51.2

**Table 2.3** % removal of metal ions with time for amide functionalized nanotubes.

S.No.	Time (Hrs.)	Removal capacity (%) for amide functionalized CNT's					
		Cr (VI)	As (III)	Ni (II)	Cd (II)	Pb (II)	Cu (II)
1	0.5	40.3	25.6	48.0	20.2	40.0	36.5
2	1.0	56.8	31.4	58.2	24.9	53.8	50.7
3	1.5	65.9	33.0	60.6	27.6	62.8	60.2
4	2.0	71.6	35.0	65.7	31.2	67.5	64.1
5	2.5	76.6	36.9	68.0	32.0	72.0	67.8
6	3.0	79.4	37.4	69.5	33.0	75.0	70.3
7	3.5	84.7	40.3	72.5	35.5	79.7	75.0
8	4.0	84.7	40.3	72.5	35.5	79.7	75.0

**Table 2.4** % removal of metal ions with time for azide functionalized nanotubes.

S.No.	Time (Hrs.)	Removal capacity (%) for azide functionalized CNT's					
		Cr (VI)	As (III)	Ni (II)	Cd (II)	Pb (II)	Cu (II)
1	0.5	40.4	20.6	50.2	15.2	35.1	40.1
2	1.0	55.9	28.0	61.4	21.0	55.2	53.6
3	1.5	65.3	32.6	68.1	26.5	67.0	64.5
4	2.0	75.1	35.6	72.8	29.6	75.0	68.0
5	2.5	79.2	37.9	74.3	32.6	78.3	73.0
6	3.0	84.1	39.4	75	33.0	82.7	75.3
7	3.5	87.5	40.9	75.7	35.9	84.7	80.6
8	4.0	87.5	40.9	75.7	35.9	84.7	80.6

**Table 2.5** Comparative study of different MWNTs.

S.No.	Time	Removal capacity (%)					
	(Hrs.)	Cr (VI)	As (III)	Ni (II)	Cd (II)	Pb (II)	Cu (II)
Without func. CNT	3.5	43.9	19.9	37.0	20.9	39.5	40.7
Oxidized CNT		59.6	25.2	41.9	27.3	52.5	45.8
Acylated CNT		59.9	27.7	43.8	29.8	53.5	51.2
Amide func. CNT		84.7	40.3	72.5	35.5	79.7	75.0
Azide func. CNT		87.5	40.9	75.7	35.9	84.7	80.6

Sorption process is greatly dependent on time of contact, pH and metal ion concentration, whose adsorption on an adsorbent has to be studied. Effect of pH and metal ion concentration, will be shortly studied later in this section. Adsorption of ions in an aqueous system follows reversible first order kinetics, when a single species is considered on a heterogeneous surface. The sorption of metal ion from solution phase onto adsorbent surface is a reversible reaction with forward rate constant  $k_1$ , backward rate constant  $k_2$  and overall rate constant  $k$  ( $k = k_1 + k_2$ ).

Taking 'a' as the initial concentration of metal ion and x is the amount adsorbed at time t, the reaction rate will be:

$$dx/dt = -d(a-x)/dt = k(a-x) = k_1(a-x) - k_2x \quad (1)$$

Putting the value  $X_e$  as the concentration of metal adsorbed at equilibrium and  $K_c$  as the equilibrium constant, the equation at equilibrium ( $dx/dt = 0$ ):

$$K_c = X_e/a - X_e = k_1/k_2 \quad (2)$$

Solving the above equation and using  $U_t = x/X_e$ , ( $U_t$ =fractional attainment of equilibrium) we get :

$$\ln (1-U_t) = -(k_1+k_2)t = -kt \quad (3)$$

.Equation 3 states that, if a graph plotted between  $\ln (1-U_t)$  and Time t gives a straight line with slope k, then the system follows first order kinetics.

The graphs plotted between  $\ln (1-U_t)$  and Time t gave straight lines with negative slopes for all sets (Figure 2.9(b&c)-2.12(b&c)) from Tables 2.6-2.9, thus confirming the adsorption process to follow first order kinetics, for all functionalized or unfunctionalized CNTs. The slopes of the graphs gave rate constants values ranging between 0.5848 and 1.4452 (Table 2.10).

**Table 2.6** Values of  $\ln(1-U_t)$  for unfunctionalized nanotubes at various times.

S.No.	Time (Hrs.)	$\ln(1-U_t)$ for unfunctionalized nanotubes					
		Cr (VI)	As (III)	Ni (II)	Cd (II)	Pb (II)	Cu (II)
1	0.5	-0.6163	-0.6682	-0.9162	-0.4732	-0.3368	-0.3184
2	1.0	-0.9545	-1.3412	-1.4246	-0.8648	-0.6174	-0.6857
3	1.5	-1.0738	-1.6039	-1.7701	-1.2472	-1.4898	-1.0529
4	2.0	-1.8393	-2.0732	-2.5492	-1.6592	-1.7599	-1.2211
5	2.5	-1.9899	-2.5194	-2.9681	-2.0463	-2.2408	-1.7891
6	3.0	-2.3227	-2.9897	-3.4262	-2.2032	-2.7118	-2.1584

**Table 2.7** Values of  $\ln(1-U_t)$  for acylated nanotubes at various times.

S.No.	Time (Hrs.)	$\ln(1-U_t)$ for acylated nanotubes					
		Cr (VI)	As (III)	Ni (II)	Cd (II)	Pb (II)	Cu (II)
1	0.5	-0.7013	-0.7956	-1.2458	-0.4606	-0.4711	-0.4730
2	1.0	-1.1641	-1.2266	-1.6044	-0.9263	-0.7526	-0.9103
3	1.5	-1.4392	-1.6533	-2.1698	-1.0817	-1.2517	-1.0906
4	2.0	-1.7999	-2.0971	-2.7488	-1.4627	-1.9646	-1.4020
5	2.5	-2.3340	-2.4046	-3.3077	-1.7076	-2.4534	-1.7270
6	3.0	-2.5232	-2.7333	-3.4420	-2.0333	-2.9488	-2.0333

**Table 2.8** Values of  $\ln(1-U_t)$  for amide functionalized nanotubes at various times.

S.No.	Time (Hrs.)	$\ln(1-U_t)$ for amide functionalized nanotubes					
		Cr (VI)	As (III)	Ni (II)	Cd (II)	Pb (II)	Cu (II)
1	0.5	-0.6456	-1.0084	-1.08470	-0.8416	-0.6967	-0.6667
2	1.0	-1.1106	-1.5100	-1.6231	-1.2086	-1.1244	-1.1270
3	1.5	-1.5056	-1.7081	-1.8035	-1.4898	-1.5521	-1.6225
4	2.0	-1.8663	-2.0005	-2.3501	-2.1100	-1.8766	-1.9264
5	2.5	-2.3456	-2.5016	-2.7719	-2.3166	-2.3361	-2.3433
6	3.0	-2.7709	-2.6327	-3.1937	-2.6526	-2.8352	-2.7662

**Table 2.9** Values of  $\ln(1-U_t)$  for azide functionalized nanotubes at various times.

S.No.	Time (Hrs.)	$\ln(1-U_t)$ for azide functionalized nanotubes					
		Cr (VI)	As (III)	Ni (II)	Cd (II)	Pb (II)	Cu (II)
1	0.5	-0.6193	-0.7003	-1.0881	-0.5504	-0.5411	-0.6881
2	1.0	-1.0183	-1.1539	-1.6665	-0.8792	-1.0546	-1.0936
3	1.5	-1.3712	-1.5945	-2.2968	-1.3415	-1.5654	-1.6104
4	2.0	-1.9533	-2.0433	-3.2586	-1.7401	-2.1663	-1.8553
5	2.5	-2.3549	-2.6118	-3.9812	-2.3891	-2.5823	-2.3618
6	3.0	-3.2467	-3.3039	-4.6834	-2.5158	-3.7422	-2.7211

**Table 2.10** Comparative study of different MWNTs.

<b>Rate Constant values( Slope of <math>\ln(1-U_t)</math> v/s Time)</b>				
<b>Metal ions</b>	<b>Unfunctionalized CNT</b>	<b>Oxidized CNT</b>	<b>Amide functionalized CNT</b>	<b>Azide functionalized CNT</b>
Cr <sup>+6</sup>	0.6764	0.7214	0.9300	0.8032
As <sup>+3</sup>	0.9406	0.8620	0.5848	0.8812
Ni <sup>+2</sup>	1.0168	1.1580	0.8436	1.4452
Cd <sup>+2</sup>	0.7832	0.6514	0.7340	0.7972
Pb <sup>+2</sup>	0.9420	0.9776	0.8554	1.0216
Cu <sup>+2</sup>	0.7386	0.6500	0.9206	0.8110

### 2.5.2.2 Effect of pH

Rejection experiments were also carried out at different pH. Different metal ion solutions of concentration 1ppm were prepared and their pH was adjusted by addition of 0.1N NaOH. Batch experiments were carried out at three pH -3.5, 7.2, 9.5 for  $\text{Cr}^{+6}$  and at pH -3.5, 7.2 for other metal ions, as other metal ions get precipitated out in form of hydroxides at basic pH. The observed results (Figure 2.13) confirmed that more adsorption was found at pH 3.5 (acidic), which could be explained as high complexation tendency of surface active sites of the nanotubes with the metal ions, under acidic conditions.

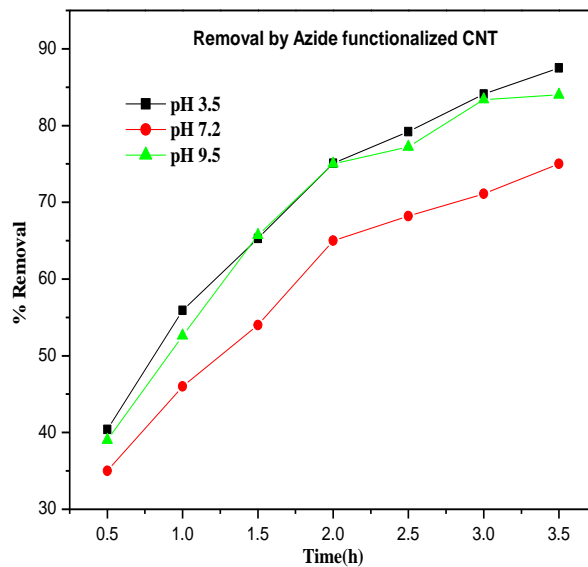
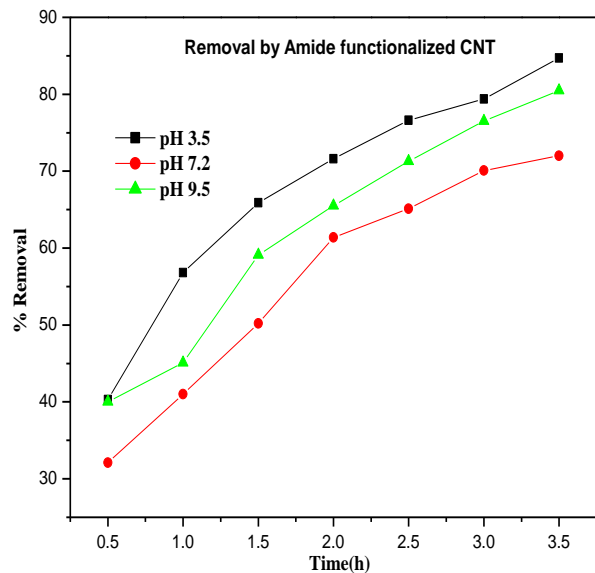


**Figure 2.13** Removal of  $\text{Cr}^{+6}$  ions at diff. pH by (a) amide and (b) azide functionalized CNTs.

### **2.5.2.3 Effect of dosage**

Role of adsorbent dose is also an important factor, which can affect the adsorption reaction. The studies were also directed towards determining the role of functionalized carbon nanotubes dose on metal removal from their aqueous solutions. Percent removal verses FCNTs is shown in Table 2.11. It can be easily observed that adsorption increases with increase in adsorbent dose up to a certain extent after which it is independent and no further increase in removal can be achieved. It was 10mg at which maximum adsorption was observed, and followed a plateau after that where no further increase was found on increasing the dosage.

**Table 2.11** % Removal of metal ions with dosage of functionalized nanotubes.

S.No.	Dosage mg/10 ml	Removal capacity (%) of CNTs							
		Cr (VI)		Pb (II)		As (III)		Cd (II)	
		AmNT	AzNT	AmNT	AzNT	AmNT	AzNT	AmNT	AzNT
1.	1.0	60.7	62.3	58.1	59.8	24.2	25.3	22.7	24.6
2.	2.0	66.5	68.1	64.3	66.4	28.0	29.2	26.5	27.0
3.	2.5	71.5	72.3	66.7	68.5	30.2	31.9	27.0	28.3
4.	3.0	76.8	78.6	69.4	73.2	32.5	34.3	29.2	30.6
5.	5.0	80.6	83.7	76.8	81.0	35.7	38.2	31.8	35.4
6.	10.0	84.7	87.5	79.7	84.7	40.3	40.9	35.5	35.9
7.	12.0	84.8	87.5	79.7	84.7	40.4	40.9	35.5	35.9
8.	15.0	84.8	87.5	79.8	84.7	40.4	40.9	35.5	35.9
9.	20.0	84.9	87.5	79.8	84.7	40.4	41.0	35.5	35.9

\* AmNT: Amide functionalized CNT's & AzNT: Azide functionalized CNT's

### 2.5.3 Adsorption isotherm studies with batch method

Batch adsorption isotherm experiments were conducted by using five concentrations (900, 1000, 1500, 1750 and 2500 µg/L) at pH 3.5. After treatment of a series of 10 mL of chromium solutions of different concentrations with 10 mg of the amide and azide functionalized CNTs, separately for 3.5h(time of reaching equilibrium), the concentration of the filtrates were analyzed by AAS. The amount of metal ion adsorbed by functionalized CNTs per gram ( $Q_e$  mg/g) was calculated, for all sets of both functionalized CNTs according to the following equation:

$$Q_e = (C_i - C_e) \times V/m$$

Where  $C_i$  and  $C_e$  are initial and equilibrium concentration (mg/L), respectively.  $V$  (L) and  $m$  (g) are volume of the sample solution and mass of the functionalized CNT's. The observed adsorption data were fitted in Langmuir<sup>137,138</sup> and Freundlich<sup>139</sup> models.

The amount of  $Cr^{+6}$  adsorbed onto amide and azide functionalized CNTs (Table 2.12, 2.13) from aqueous solutions show that the adsorption capacity of  $Cr^{+6}$  onto per gram functionalized carbon nanotubes increases with increasing the initial  $Cr^{+6}$  concentration, and continues up to 2500 µg/L and level off thereafter, in both cases. Langmuir and Freundlich models are employed to describe the adsorption process. These isotherm relate metal uptake per unit weight of adsorbent  $Q_e$  to the equilibrium adsorbate concentration in the bulk fluid phase  $C_e$ . The Langmuir model represents one of the first theoretical treatments of non-linear sorption. The Langmuir isotherm is given by :

$$Q_e = \frac{Q^0 b C_e}{1 + b C_e} \quad (1)$$

Where  $Q^0$  and  $b$  are Langmuir constants related to maximum adsorption capacity and energy of adsorption respectively. Eq. 1 is generally linearised by inversion to get the following form:

$$1/Q_e = 1/Q^0 + 1/bQ^0 * 1/C_e \quad (2)$$

**Table 2.12** Showing  $X_e$ ,  $Q_e$ ,  $C_e$ ,  $1/X_e$ ,  $1/Q_e$ ,  $1/C_e$ ,  $\text{Log } Q_e$ ,  $\text{Log } C_e$  for different initial concentrations of  $\text{Cr}^{+6}$  solution when their adsorption was studied onto amide CNTs, to study Langmuir and Freundlich isotherms.

<b>Initial conc. (<math>\mu\text{g}</math>)</b>	<b>% Removal at equili. by amide CNT</b>	<b>Cr mg/L</b>	<b>Ce mg/L</b>	<b>Qe mg/g</b>	<b>1/Qe g/mg</b>	<b>1/Ce L/mg</b>	<b>Log Qe</b>	<b>Log Ce</b>
900	86.11	0.775	0.125	0.775	1.290	8	-0.110	-0.903
1000	84.7	0.847	0.153	0.847	1.180	6.535	-0.072	-0.815
1150	80	0.920	0.230	0.920	1.086	4.347	-0.036	-0.638
1750	64.3	1.126	0.624	1.126	0.888	1.602	0.051	-0.204
2500	51.6	1.29	1.210	1.29	0.775	0.826	0.110	0.082

**Table 2.13** Showing  $X_e$ ,  $Q_e$ ,  $C_e$ ,  $1/X_e$ ,  $1/Q_e$ ,  $1/C_e$ ,  $\text{Log } Q_e$ ,  $\text{Log } C_e$  for different initial concentrations of  $\text{Cr}^{+6}$  solution when their adsorption was studied onto azide CNTs, to study Langmuir and Freundlich isotherms.

<b>Initial conc. (<math>\mu\text{g}</math>)</b>	<b>% Removal at equili. by azide CNT</b>	<b>Cr mg/L</b>	<b>Ce mg/L</b>	<b>Qe mg/g</b>	<b>1/Qe g/mg</b>	<b>1/Ce L/mg</b>	<b>Log Qe</b>	<b>Log Ce</b>
900	87.6	0.789	0.111	0.789	1.267	9.003	-0.102	-0.954
1000	87.5	0.875	0.125	0.875	1.142	8	-0.058	-0.903
1150	83.1	0.956	0.196	0.956	1.046	5.123	-0.01	-0.707
1750	68.5	1.200	0.550	1.200	0.83	1.783	0.08	-0.259
2500	56.8	1.421	1.079	1.421	0.703	0.926	0.1525	0.033

Equation 2 is generally used to analyze batch equilibrium data by plotting  $1/Q_e$  versus  $1/C_e$ , which yields a linear plot if the data conform to the Langmuir isotherm. The linear plot of  $1/Q_e$  versus  $1/C_e$  gives the intercept and slope corresponding to  $1/Q^0$  and  $1/(Q^0b)$  respectively, from which both  $Q^0$  and  $b$  are derived.

The Freundlich isotherm is the most widely used non linear sorption model and is given by the general form:

$$\log Q_e = \log K_F + 1/n \log C_e \quad (3)$$

Where  $K_F$  relates to sorption capacity and  $1/n$  to sorption intensity. The above logarithmic form is generally used to fit data from batch equilibrium studies. A plot of  $\log Q_e$  vs  $\log C_e$  should yield a straight line if the Freundlich equation is obeyed by the adsorption equilibrium. The plot of  $\log Q_e$  against  $\log C_e$  gives the intercept and slope corresponding to  $\log K_F$  and  $1/n$ , respectively, from which both  $K_F$  and  $n$  are obtained. Values of  $1/Q_e$ ,  $1/C_e$ ,  $\log Q_e$ ,  $\log C_e$  were calculated using reports from AAS analysis as in Table 2.12, 2.13. Graphs were plotted between  $1/Q_e$  and  $1/C_e$ , and  $\log Q_e$  and  $\log C_e$  to get Langmuir and Freundlich isotherms (Figure 2.14, Figure 2.15).

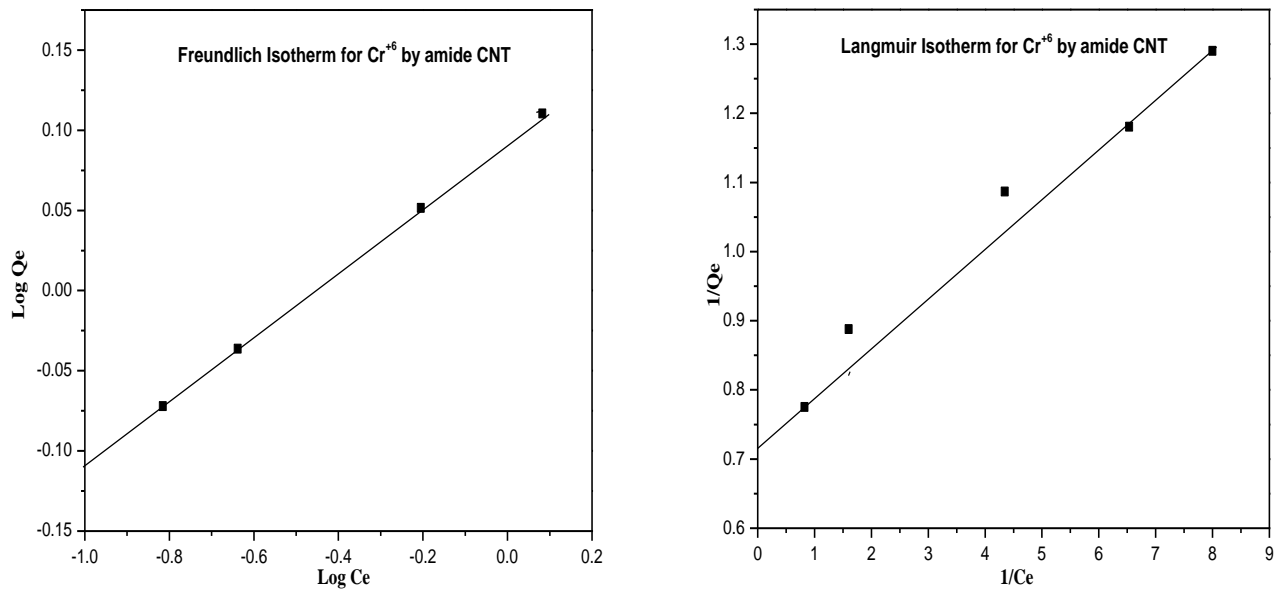


**Figure 2.14** Freundlich and Langmuir adsorption isotherm of Chromium onto amide functionalized CNTs.

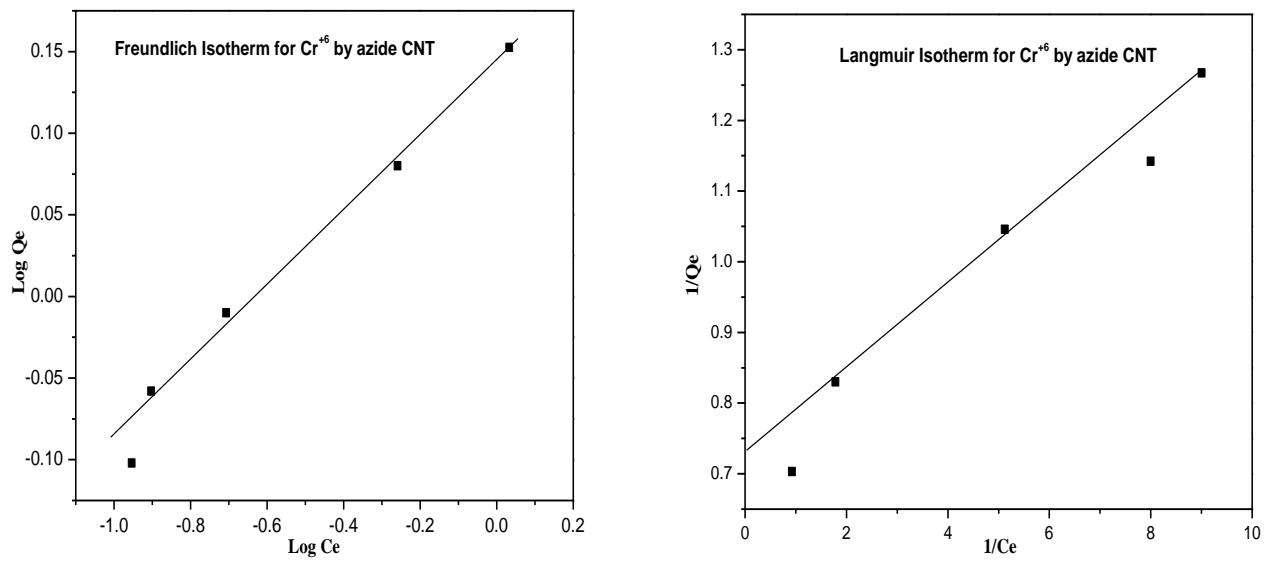


**Figure 2.15** Freundlich and Langmuir adsorption isotherm of Chromium onto azide functionalized CNTs.

The parameters  $Q^0$ ,  $K$ ,  $R^2$  and  $1/n$  as calculated (Table 2.14) from Figure 2.14 & Figure 2.15 suggest that the Freundlich model is more suitable to fit the adsorption data than Langmuir model since the correlation coefficients ( $R^2$ ) are higher 0.9878, 0.9967 for adsorption of heavy metal ions onto functionalized CNTs. The value  $Q^0$  gives maximum adsorption capacity of the carbon nanotubes, which comes out to be 1.386 mg/g. The numerical value of  $1/n < 1$  indicates that adsorption of metal ions onto functionalized CNTs is multilayer adsorption process.

**Table 2.14** The regression equations parameters  $Q^0$ ,  $K$ ,  $R^2$  and  $1/n$  for functionalized CNTs.

	<b>Langmuir Model</b>			<b>Freundlich Model</b>		
	$Q^0$ (mg/g)	$b$ (L/mg)	$R^2$	$K_F$	$1/n$	$R^2$
<b>Amide CNT</b>	1.386	9.63	0.9389	0.762	0.2024	0.9967
<b>Azide CNT</b>	1.386	11.933	0.9301	0.754	0.2436	0.9878

## 2.6 Conclusion

% Removal is a function of time and continuously increases with time of contact, upto a point where equilibrium is reached. At equilibrium the adsorption process becomes steady and does not increase with increase in contact period.

Maximum adsorption and thus percentage removal is observed for Chromium followed by that of Lead. In all the cases equilibrium is reached at 3.5h. The  $\ln(1-U_t)$  is plotted against time  $t$ , for different metal ions, and straight line was obtained. This suggested that adsorption process followed first order kinetics. The slope of the plot gives overall rate constant. The removal capacity of azide and amide functionalized CNT is found to be greater than unfunctionalized, oxidized or acylated CNTs due to greater chelation capacity.

The adsorption isotherms of metal ions adsorbed onto functionalized CNTs from aqueous solution show that their adsorption onto per gram functionalized carbon nanotubes increases with increasing the initial  $\text{Cr}^{+6}$  concentration and continued up to 2500  $\mu\text{g/L}$  and level off thereafter. Better rejection is found at acidic pH due to greater complexation tendency.

The regression equations parameters  $Q^0$ ,  $K$  and  $1/n$  and the correlation coefficient were calculated. It is seen that the Freundlich model is more suitable to fit the adsorption data than Langmuir model since the correlation coefficients are higher than 0.9800. The numerical value of  $1/n < 1$  indicates that adsorption of metal ions onto functionalized CNTs is best fitted by Freundlich model and multilayer adsorption occurs on the surface following first order kinetics.

## **Chapter 3 Comparative study of surface cleaning and modification of MWNT's using various oxidizing agents**

### ***3.1 Introduction***

The effects of acid and/or air oxidation at high temperature on CNT surface morphology have been well studied and proved to create defect sites along with effective removal of amorphous carbon and graphitic platelets. This treatment is also supposed to remove the metal catalyst (Co, Fe, Ni) that come to associate with the nanotubes at time of growth of nanotubes. Studies by Hu et al. and Martinez et al.<sup>140</sup> have found that during this treatment, intercalation process of nitric acid molecules into the CNT bundle structure takes place, which is accompanied by bundle exfoliation and etching of the carbonaceous material. This process leads to the formation of additional amorphous carbon nanoparticles covering the remaining smaller bundles of CNT<sup>141,142</sup>. Sufficient carboxylic and hydroxyl groups are generated, but at the same time quantified cutting of the nanotubes and surface destruction was found.

Concerning the oxidation reaction of sulphuric acid/hydrogen peroxide mixture (piranha) with CNTs, Ziegler et al.<sup>143</sup> have shown that the one-dimensional nanostructures can be cut in a controlled manner under specific conditions. At high temperatures, piranha was found to attack existing damage sites, generating vacancies in the graphene sidewall, and consume the oxidized vacancies to yield shorter nanotubes. Increased reaction time results in increasingly shorter tubes.

However, significant sidewall damage also occurs along with selective etching of the smaller diameter nanotubes. On the other hand, room-temperature piranha treatments showed the capability of attacking existing damage sites with minimal carbon loss, slow etch rates, and little sidewall damage.

Experiments were also carried out by V. Datsyuk and co-workers<sup>144</sup> where acid and base treatments were given for a prolonged time at high temperatures. The acid oxidation was successful with a high degree of functionalization but nanotubes were shortened to 700nm and greatly disordered. On the other hand base oxidation showed non-damaged walls with negligible oxidation.

In the present study, a systematic study of the chemical oxidation of MWNT's treated by various reagents that possess different degrees of oxidation power was carried out. The as obtained HiPCO MWNT were effectively cleaned using Brij-98 surfactant, followed by HCl washing to remove the associated carbonaceous and amorphous materials. The cleaned graphitic surfaces were subjected to various oxidation processes, such as treatment with acid mixture ( $\text{H}_2\text{SO}_4$ ,  $\text{HNO}_3$ ), acid piranha ( $\text{H}_2\text{SO}_4$ ,  $\text{H}_2\text{O}_2$ ), base piranha ( $\text{NH}_4\text{OH}$ ,  $\text{H}_2\text{O}_2$ ) and  $\text{KMnO}_4$ ,  $\text{CH}_3\text{COOH}$  in presence of a phase transfer catalyst. All the reactions were performed at room temperature for 1-2h. Effective functionalization was observed with very less cutting of lengths and damage of sidewalls, the degree and type of functionalization being different. Basic oxidation also showed significant oxidation with quantitative functional groups on non-damaged sidewalls. The variations in the surface morphology as compared to pristine CNT's were recorded by SEM (scanning electron microscopy). The defect concentration and concentration of functional groups were determined by Raman spectroscopy and acid-base titrations.

### **3.2 Materials**

The multi-walled nanotubes (90+% diameter 110-170 nm and length 5-9  $\mu\text{m}$ ), and Brij-98 were purchased from Sigma Aldrich. Conc.  $\text{H}_2\text{SO}_4$  (98%), conc.  $\text{HNO}_3$  GR (69%), ammonia solution GR (25%), conc. HCl (35%),  $\text{H}_2\text{O}_2$  (30%),  $\text{KMnO}_4$  AR, glacial acetic acid (99%) were purchased from Merck.

### **3.3 Experiment**

Various conventional methods of cleaning the surfaces of nanotubes to remove the amorphous and carbonaceous materials associated with heavy metal traces have been reported such as high temperature annealing, SDS washing, air oxidation etc. The harsh cleaning methods damage the reactive sites on surface of nanotubes and mild SDS washing does not effectively clean the surface. In the present study MWNTs were dispersed in 1% Brij 98 solution by sonication for 1h and then stirred for another 1h. It was allowed to stand overnight. Next day the mother liquor was decanted into another beaker separating it from the soot. The mother liquor was centrifuged for 10 minutes at 3000rpm. The supernatant liquid contained nanoparticles and the settled residue was taken as nanotubes. The nanotubes were washed with distilled water two times and then kept in 50% HCl solution for 6 hours. They were again washed with distilled water several times and then dried. This systematic washing gave 100 times better cleaning as compared to conventional methods. The obtained nanotubes do not get attracted (Figure 3.1b) to the magnetic needle showing that the nanotubes are free from traces of heavy metal ions. This is shown in Figure 3.1. Now these washed and dried nanotubes were used to treat with various oxidizing agents.

#### **3.3.1 Treatment with acid piranha solution**

Acid piranha is a mixture of conc.  $\text{H}_2\text{SO}_4$  and conc.  $\text{H}_2\text{O}_2$  in the ratio of 3:1. It is a strong oxidizing agent, highly corrosive and potentially explosive. Acid piranha solution was prepared by slow addition of 6ml of  $\text{H}_2\text{SO}_4$ (98%) to 2ml of  $\text{H}_2\text{O}_2$ (30%) and heating to  $60^\circ\text{C}$  for about 15 minutes. 38 mg of purified nanotubes were taken and added to it. The mixture was stirred for 1h at room temperature. It was then diluted and given several washings with distilled water till the pH was neutral and then dried.

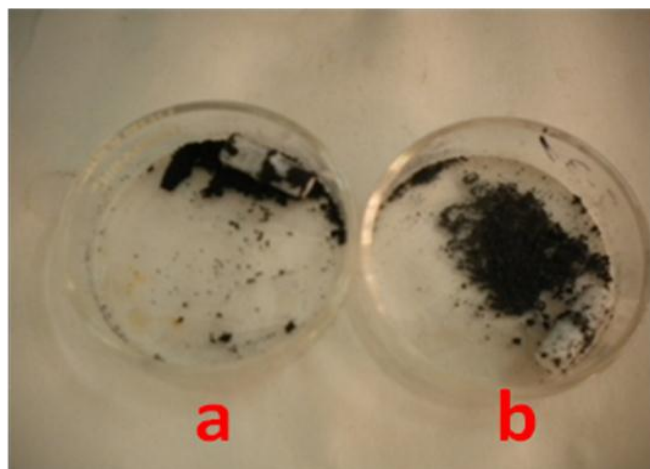


**Figure 3.1** Effect of washing on the behavior of nanotubes towards magnetic needle.

### **3.3.2 Treatment with HNO<sub>3</sub>+H<sub>2</sub>SO<sub>4</sub> Mixture**

To 9ml of conc.H<sub>2</sub>SO<sub>4</sub> taken in a round-bottomed flask, 3ml of conc.HNO<sub>3</sub> was slowly added. To this mixture 100 mg of nanotubes were added and stirred for 24 h at room temperature. It was diluted and washed with distilled water till the pH was neutral and then dried.

### **3.3.3 Treatment with base Piranha**

Base piranha solution is a mixture of NH<sub>4</sub>OH and H<sub>2</sub>O<sub>2</sub> in the ratio of 3:1.About 100 mg of nanotubes were taken and stirred with 12 ml of base piranha for 1h at room temperature. After that it was diluted and washed with distilled water till the pH was neutral. It was then dried.

### **3.3.4 Treatment with KMnO<sub>4</sub> + CH<sub>3</sub>COOH in presence of phase transfer catalyst**

KMnO<sub>4</sub> solution was prepared by dissolving 125 mg of KMnO<sub>4</sub> in 5 ml of distilled water. 100mg of purified nanotubes were taken in a round-bottomed flask and 5ml of KMnO<sub>4</sub> solution, 5ml of glacial acetic acid, and 5mg of tertiary butyl ammonium bromide (phase transfer catalyst) were added to it. It was heated at100°C and stirred for 24h. The functionalized product was washed with toluene and dried.

### **3.3.5 Titration analysis of functionalized CNT's**

The modified CNT was quantitatively analyzed by titration to determine the COOH concentrations on the surface of the treated CNTs. The oxidized CNTs were added into a 20-ml 0.05 N NaOH solution, sonicated for 2h and stirred for 24h to stabilize the functionalized CNT material in the NaOH solution. The homogenous solution was then titrated with a 0.05 N HCl solution to determine the degree of functionalization (concentration of the carboxylates) on CNTs.

## **3.4 Characterization**

The dispersions of the MWCNTs in dimethylformamide were casted on carbon grids. FT-IR was carried out on Perkin-Elmer spectrophotometer at 20 scans using the KBr pellet method and Scanning

electron microscopy(SEM) on JEOL JSM-5610 model No. 6587 LV instrument for clean surfaces and attached functional groups. The TGA data were obtained in nitrogen atmosphere on Mettler Teledo Star SW 7.01 thermogravimetric analyzer with 7.4640mg of the specimen at heating rate of 10°C/minute. Raman spectra were recorded using microscope equipped triple monochromator combined with a peltier cooled charge couple device detector system. The spectra were acquired in the back-scattering geometry, while for excitation the 785 nm line of an Ar<sup>+</sup> laser was focused on the sample by means of an 80X objective at a power of 2mW, measured directly before the sample. The phonon frequencies were obtained by fitting Lorentzian line shapes to the experimental peaks after background subtraction.

### **3.5 Results**

#### **3.5.1 Electron microscopy**

Scanning electron microscopy documented the severity of different oxidation processes on the fullerene cap and side wall of nanotube. It was observed that reflux with acid mixture H<sub>2</sub>SO<sub>4</sub>/HNO<sub>3</sub> for 24h gave clean surfaces, but at the same time defect concentration was very high, with some cutting of the tubes. The SEM images show clear nanotube surfaces with open tips, but the nanotubes have been selectively cut down to an average length of 2-3μ. The tube surface was damaged, creating kinks and cuts where either carboxylic or hydroxyl groups would grow. Concerning the basic oxidative treatment (ammonium hydroxide/hydrogen peroxide mixture), perfectly clean and smooth surfaces without any cuts or damaged surface were observed (Figure 3.2). The effect of acid piranha was appreciable but less effective than either the acid mixture or base piranha. The nanotubes were cut and average size was 4-5μm while base piranha treated nanotubes had an average of 8-10μ. This fact shows that basic oxidation cleans the surface effectively generating open caps for successful

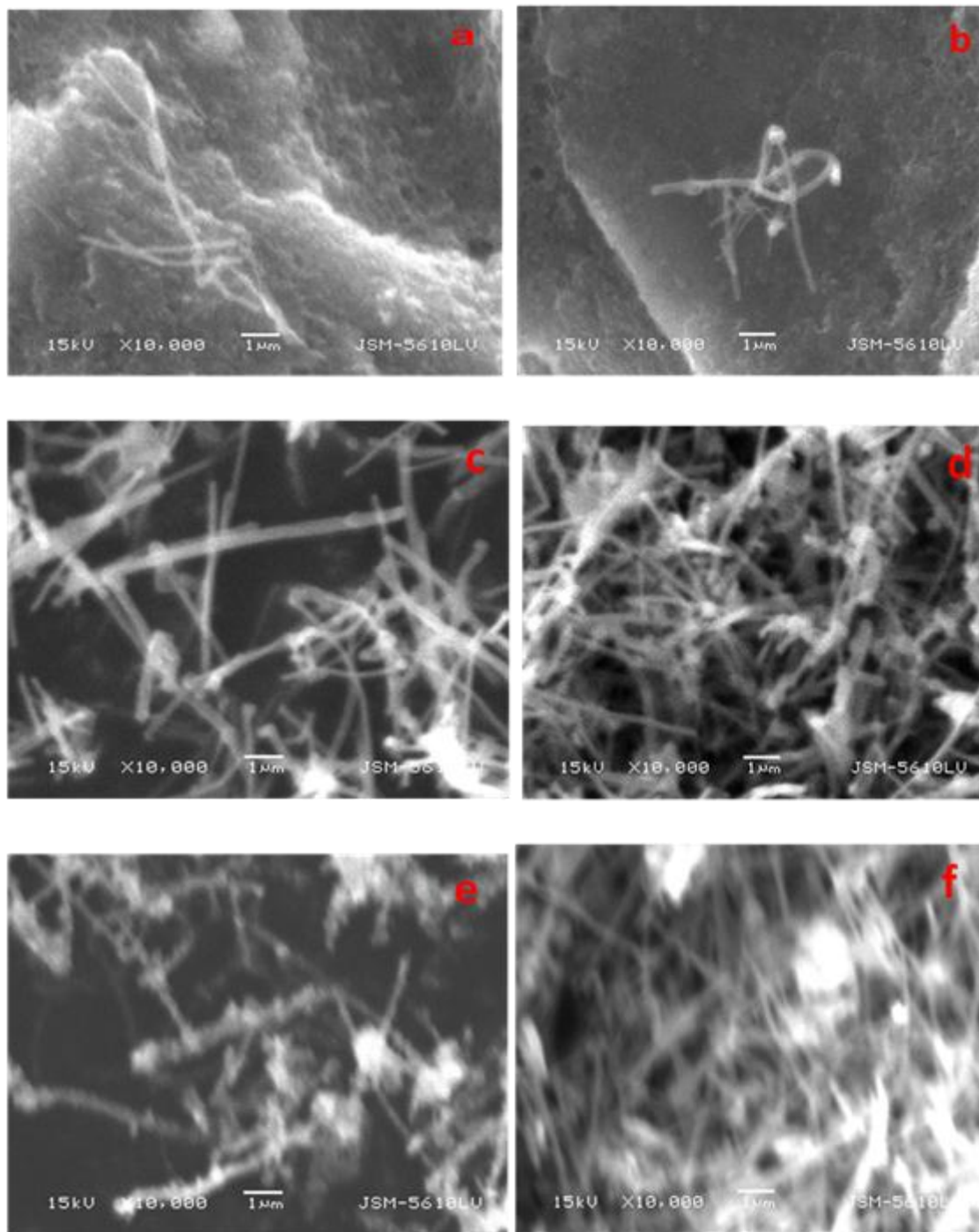


**Figure 3.2** SEM images of MWNT's (a) pristine (b) H<sub>2</sub>SO<sub>4</sub>/HNO<sub>3</sub> treated (c) Base piranha treated (d) Acid piranha treated (e) KMnO<sub>4</sub>/CH<sub>3</sub>COOH treated in absence of PTC (f) KMnO<sub>4</sub> /CH<sub>3</sub>COOH treated in presence of PTC.

functionalization, while the acidic treatments are harsh enough for spoiling the nanotube texture and thus less effective.

The treatment of  $\text{KMnO}_4$  and  $\text{CH}_3\text{COOH}$  in little  $\text{HCl}$  showed no desirable effects. The carbonaceous and amorphous carbon could not be removed. Instead when tertiary butyl ammonium bromide was used as phase transfer catalyst (PTC), the associated soot and other carbon residues, heavy metal traces could be separated, without cutting the lengths or damaging the surfaces of the nanotubes. This is a clear indication that the basic treatment is not destructive for the tubes, and at the same time, highly purified material is produced. After oxidation with strong oxidants such as nitric acid and piranha, some bundles appear exfoliated and curled in Figure 3.2b,3.2d. In addition, a major alteration of the structural integrity of CNTs is observed.

The above observations are in full agreement with the Raman spectroscopic results. The presence of a large amount of oxygen-containing functionalities at the defect sites support the colloidal stability of the acid-treated material in polar media (Figure 3.3).

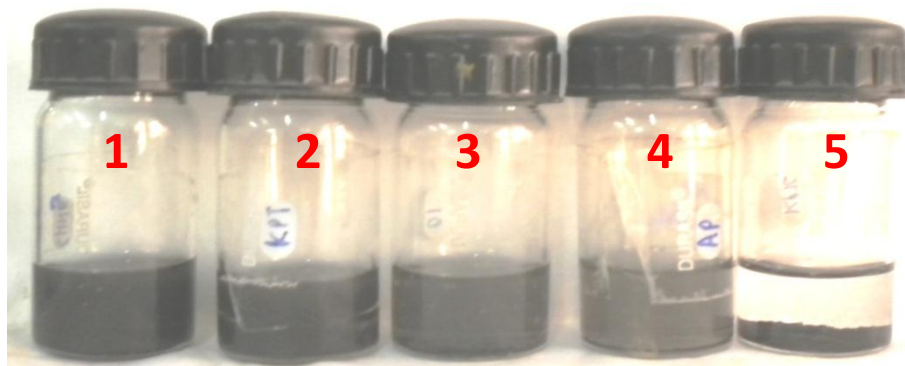


**Figure 3.3** Pictures of the dispersion of the MWCNTs (10 mg) in water (10 ml). 1- $\text{H}_2\text{SO}_4/\text{HNO}_3$ -treated MWCNTs; 2- $\text{KMnO}_4$ -PTC treated MWCNTs; 3-base piranha treated MWCNTs; 4-acid piranha treated MWCNTs; 5-Pristine MWNT's. Samples were kept for 100 days. MWCNTs were dispersed in water by sonication for 1h.

### 3.5.2 FT-IR

In the IR spectra for H<sub>2</sub>SO<sub>4</sub>/HNO<sub>3</sub>oxidized MWNT's (Figure 3.4b) a sharp band at 3500cm<sup>-1</sup> due to hydroxyl(-OH) group is seen. The band at 1720cm<sup>-1</sup> is due to presence of C=O stretching of carboxylic group. A strong peak at 1068cm<sup>-1</sup> is due to C-O stretching of carboxylic group. Presence of carboxylate anion can also be confirmed by bands present in the range of 1540, 1510 and 1460cm<sup>-1</sup>. Less intense spectral peaks corresponding to carboxylate ion and C=O stretching could also be observed in spectra for acid piranha treated MWNT's, which confirm the growth of some of carboxylic groups, but does not support the growth of enough hydroxyl groups.

In the IR spectra of base piranha (Figure 3.4c) treated carbon nanotubes, clear peaks at 3478cm<sup>-1</sup> and 1720cm<sup>-1</sup> can be correlated to the presence of hydroxyl as well as carboxyl group, while in KMnO<sub>4</sub>treated nanotubes (Figure 3.4e) only hydroxyl groups are produced and there is no evidence of formation of carboxyl group. The FT-IR of acid piranha (Figure 3.4d), the intensity of carboxylic and hydroxyl group peak is very less.

Thus it was concluded that degree of functionalization followed the trend H<sub>2</sub>SO<sub>4</sub>/HNO<sub>3</sub>> Base piranha >Acid Piranha >KMnO<sub>4</sub>. These results coincide with the defect concentrations recorded by Raman spectroscopy.

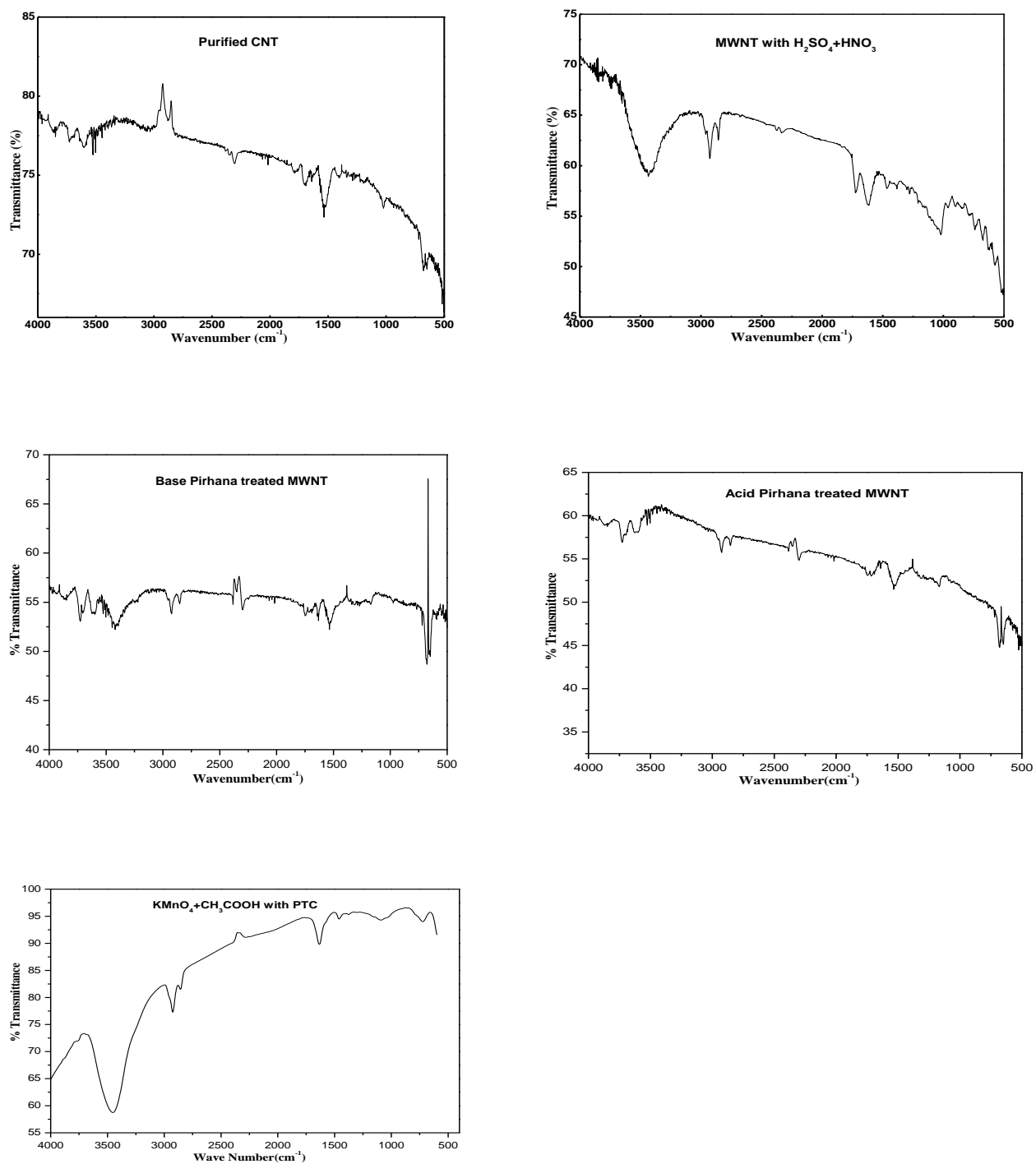


**Figure 3.4** FT-IR spectra of MWNT's (a) Purified (b) H<sub>2</sub>SO<sub>4</sub>/HNO<sub>3</sub> treated (c) Base Piranha treated (d) Acid Piranha treated (e) KMnO<sub>4</sub> /CH<sub>3</sub>COOH treated in presence of PTC.

### 3.5.3 Thermo-gravimetric analysis

Thermo gravimetric analysis gives valuable information on thermal stability of functional groups and elemental species, over a wide temperature range. Oxidative treatment of CNT's produces disordered or amorphous carbon surface. This ruptured surface has large number of active sites over a large surface area. Such distorted carbon shows complete oxidation at around 550°C<sup>145</sup>, because of their lower activation energies for oxidation. Well graphitized structure like graphene sheet or its cylindrical form oxidizes at higher temperatures between 600 and 700°C<sup>146,147</sup>.

The thermogravimetric (TGA) analysis reports of as received and oxidized MWCNT samples are presented in Figure 3.5. The thermal degradation of MWCNTs is a multistage process. The TGA curve for acid mixture H<sub>2</sub>SO<sub>4</sub>/HNO<sub>3</sub> treated sample shows strong degradation at about 100°C owing to loss of adsorbed water and then subsequent removal of carboxylic and hydroxyl groups attached during functionalization. Appreciable weight loss occurs in the region 150-350°C and also from 350-500°C for base piranha treated nanotubes which corresponds to elimination of carboxyl and hydroxyl functionalities respectively. Thus various TGA curves with different degradation points account for the presence variation in degree and type of functionalization.

No significant difference is observed in TGA curve of acid piranha and KMnO<sub>4</sub> treated nanotubes. These graphs confirm acid piranha treated CNTs to have some carboxyl groups, but not enough hydroxyl groups, while it is reverse for KMnO<sub>4</sub> treated nanotubes. This finding is in agreement with the Raman spectra and we could conclude that this specific treatment is the most effective for purification of the tubes and base piranha oxidation (mild oxidation) is the best method to get greater degree of functionalization with least disruption of CNT surface.

### 3.5.4 Raman Spectroscopy

Raman spectroscopy is a reliable technique for the characterization of carbon-based nanostructures. It points at the various radial breathing and tangential stretching modes of vibrations. The vibrations

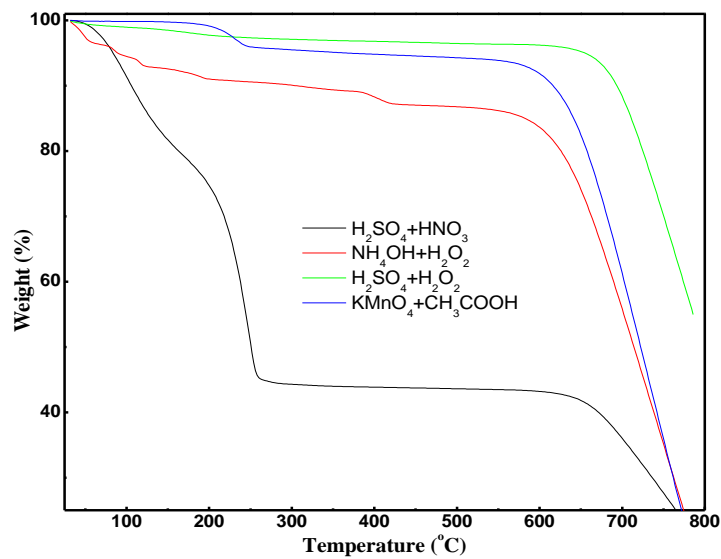


**Figure 3.5** TGA curves of the MWCNT samples: (a) MWCNT- $\text{HNO}_3$ , (b) MWCNT- $\text{NH}_4\text{OH}/\text{H}_2\text{O}_2$ , (c) MWCNT- $\text{H}_2\text{SO}_4/\text{H}_2\text{O}_2$ , (d) MWCNT- $\text{KMnO}_4$ -PTC.

corresponding to radial breathing mode at 785nm laser wavelength are very weak and not significant. The Raman spectra of MWNTs excited with this laser line show two characteristic bands in tangential stretching mode, namely the D-band at 1340-1390  $\text{cm}^{-1}$ , and a G-band in the range 1550-1600  $\text{cm}^{-1}$ . The D-band is a disorder induced feature arising from double resonance scattering process and its intensity is a measure of defect concentration on the nanotubes. This defect is supposed to be created due various functionalization reactions, to which the nanotubes are exposed or heteroatom associated at time of growth of nanotubes or disordered carbon. The G band originates from in-plane tangential stretching of the carbon- carbon bonds in graphene sheets.

The D-band in graphite involves scattering from defect which breaks the basic symmetry<sup>148,149</sup> of the graphene sheet. It is observed in  $\text{sp}^2$  carbons containing porous, impurities or other symmetry-breaking defects. Multi-walled carbon nanotubes (MWNT) are made of concentric graphene sheets rolled in a cylindrical form with diameters of tens of nanometers<sup>150</sup> and because of this large diameter of the outer tubes for typical MWNT and because they contain an ensemble of carbon nanotubes with diameters ranging from small to very large, most of the characteristic differences that distinguish the Raman spectra in SWNT from the spectra for graphite are not so evident in MWNT.

The Raman spectra as shown in Figure 3.6, 3.7 and in Table 3.1 for pristine and other oxidized CNT's bring out the fact that the  $I_D/I_G$  ratio for pristine MWNT 's is the highest (intensity of D-band being the maximum). This is in accordance with presence of amorphous and carbonaceous impurities, associated with as prepared CNT's, making the surface rough due to defects and disorders. Raman spectra for  $\text{H}_2\text{SO}_4/\text{HNO}_3$  treated sample shows decrease in value of  $I_D/I_G$  ratio, as compared to that of pristine CNT's due to efficient cleaning of the surface. At the same time effective functionalization (maximum  $I_D/I_G$  for all oxidized CNT's) breaks down the symmetry of the surface of the CNT's, generating functional groups (-COOH,-OH) and thus creating defects on the surface. The base piranha

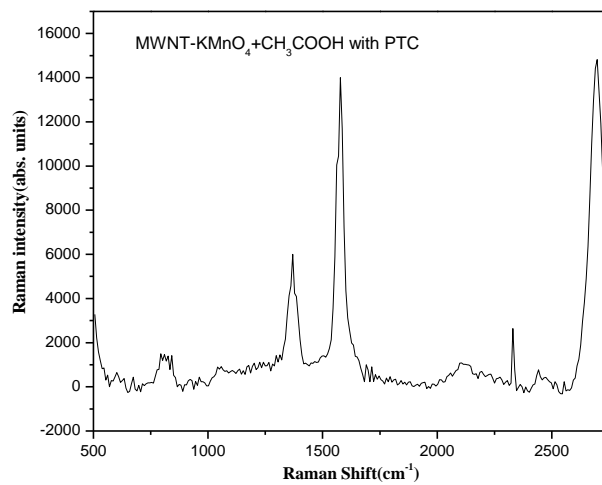
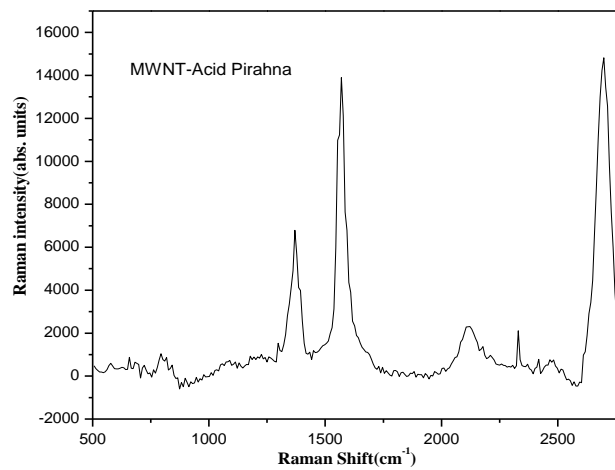
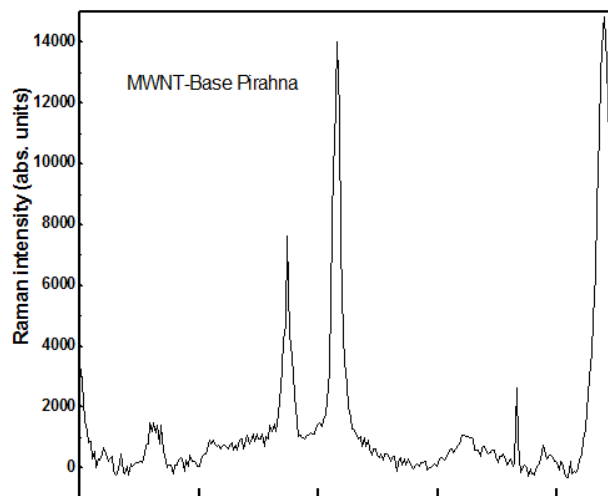
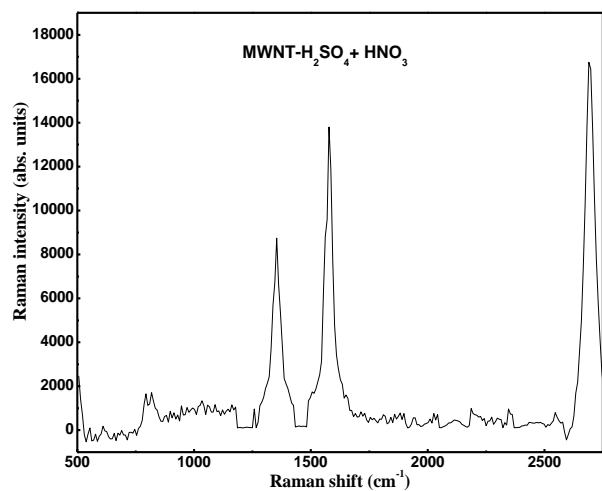


**Figure 3.6** Raman spectra of the MWCNT samples: (a) MWCNT–HNO<sub>3</sub>, (b) MWCNT–NH<sub>4</sub>OH/H<sub>2</sub>O<sub>2</sub>, (c) MWCNT–H<sub>2</sub>SO<sub>4</sub>/H<sub>2</sub>O<sub>2</sub>, (d) MWCNT–KMnO<sub>4</sub>-PTC.

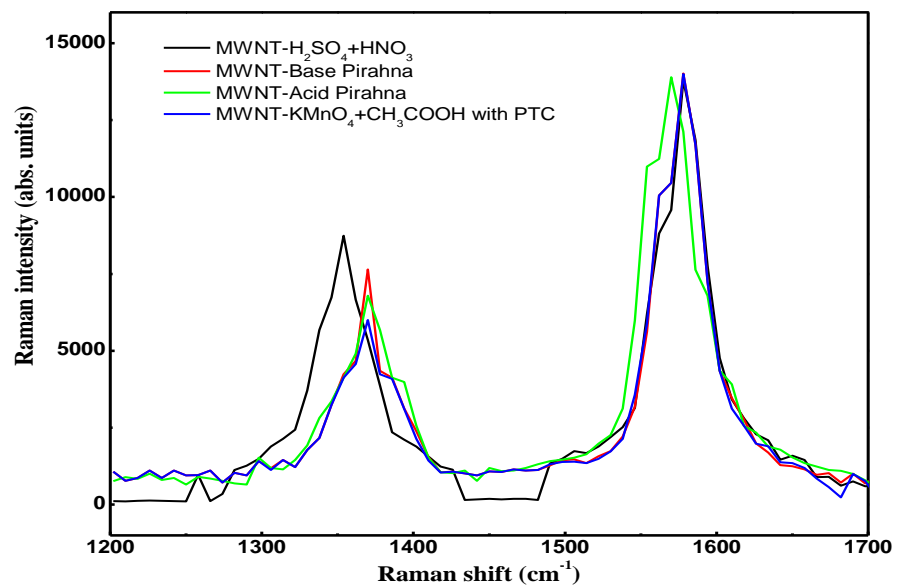


**Figure 3.7** Raman spectra of differently oxidized MWCNT samples.

**Table 3.1**  $I_D/I_G$  ratios for differently oxidized MWNT's samples.

Sample	$I_D$ (Intensity of D line)	$I_G$ (Intensity of G line)	Ratio $I_D/I_G$
H <sub>2</sub> SO <sub>4</sub> /HNO <sub>3</sub> treated MWNT	8743	13798	0.6336
Base Piranha treated MWNT	7643	14011	0.5454
Acid Piranha treated MWNT	6789	13895	0.4885
KMnO <sub>4</sub> treated MWNT	5998	13997	0.4285
Purified MWNT	3342	14121	0.2366
Pristine MWNT	9413	14122	0.6665

treatment gave absolutely clean surfaces, without cutting the nanotubes. At the same time  $\text{NH}_4\text{OH}/\text{H}_2\text{O}_2$  mixture effectively created  $-\text{OH}$  groups the nanotube surface. The  $I_D/I_G$  value for acid piranha treated nanotubes was 0.4885, which is significantly less than base piranha treatment where the ratio is 0.5454. Acid piranha treatment cuts some of the nanotubes and generates  $-\text{COOH}$ ,  $-\text{OH}$  functional groups on the surface. The concentration of these functional groups is less than that for the  $\text{H}_2\text{SO}_4/\text{HNO}_3$  or  $\text{NH}_4\text{OH}/\text{H}_2\text{O}_2$  treatment. All these results are in accordance with SEM, FT-IR results. There is minimum concentration of (only  $-\text{OH}$ ) functional groups in case of  $\text{KMnO}_4$  treated nanotubes.

### 3.5.5 Volumetric titration

Titration results (Table 3.2) reveal the fact that following maximum cutting and defect generation, highest carbonyl group concentration was found for  $\text{H}_2\text{SO}_4/\text{HNO}_3$  treated MWNTs. The maximum  $I_D/I_G$  ratio for pristine nanotubes is subjected to presence of amorphous carbon and metal oxide impurities, which is removed by Brij-98 and HCl treatment. Thus presence of defect in pristine nanotubes does not relate to presence of carbonyl group. Though some amorphous carbon may be present in oxidized form due to atmospheric oxygen. The carbonyl functionality concentration on the CNTs follows the trend  $\text{H}_2\text{SO}_4/\text{HNO}_3 > \text{Base piranha} > \text{Acid Piranha} > \text{KMnO}_4$  which is confirmed by FT-IR and Raman spectroscopy results.

**Table 3.2** Carbonyl group concentration for differently oxidized MWNT's samples.

MWNTs	H <sub>2</sub> SO <sub>4</sub> /HNO <sub>3</sub> treated	Base Piranha treated	Acid Piranha treated	KMnO <sub>4</sub> -PTC treated	Pristine
Concentration of carbonyl group in mol/g	4.1 x 10 <sup>-3</sup>	2.8 x 10 <sup>-3</sup>	1.5 x 10 <sup>-3</sup>	1.1 x 10 <sup>-3</sup>	0.45 x 10 <sup>-3</sup>

### 3.6 Conclusions

Extent of functionalization and surface etching of different oxidizing agents were studied on MWCNTs. The action of Brij-98 followed by centrifugation, sedimentation and HCl washing results in highly cleaned surfaces as compared to SDS washing and other conventional methods. The cleaned nanotubes were subjected to oxidation by  $\text{H}_2\text{SO}_4/\text{HNO}_3$  acid mixture, mixture of ammonium hydroxide/hydrogen peroxide (base piranha), a acid piranha ( $\text{H}_2\text{SO}_4/\text{H}_2\text{O}_2$ ) solution and  $\text{KMnO}_4$ -PTC mixture. The degree of functionalization i.e. the density of carboxyl and hydroxyl functional groups on the graphitic network, was quantified by means of titration measurements. Oxidation with  $\text{H}_2\text{SO}_4/\text{HNO}_3$  under extreme conditions (reflux) increases the defect formation, shortens the length and gives highest degree of functionalization as verified by SEM, FT-IR, Raman spectroscopy and confirmed by titration measurements. The degree of defect formation and functionalization followed the trend  $\text{H}_2\text{SO}_4/\text{HNO}_3 > \text{Base piranha} > \text{Acid piranha} > \text{KMnO}_4$ . Use of non-acidic treatments such as the mixture of  $\text{NH}_4\text{OH}$  and  $\text{H}_2\text{O}_2$ , facilitates the complete removal of carbonaceous materials and gives good number of functional groups, though less as compared to treatment with acid mixture but better as compared to acid piranha. All the results were confirmed by Raman spectroscopy and thermogravimetric analysis.

## **Chapter 4 Preparation of MWNT/PSf composite membranes and its effect on metal removal**

### ***4.1 Introduction***

In present study we report the synthesis of functionalized multi-walled carbon nanotube/polysulfone (MWNT/PSf) composite membranes by the phase inversion method using DMF as solvent and water with isopropanol as coagulant. Carbon nanotubes have proved to be the most promising materials for the design of functional thin films, including those for catalytic membranes, actuation, mechanical thin film applications, and now as nanocomposite membranes with polymer structures.

It has been shown that pristine single walled nanotubes as membranes can be used for efficient gas separation<sup>151</sup>. Controlling the architecture of CNT thin films at the nanometer and micrometer-scale is critical to tailoring film properties and functionality; therefore attempts have been made to incorporate the nanotubes into polymer matrices. For example, carbon nanotube/polymer nanocomposite membranes have been fabricated and reported for high flux gas transport<sup>152</sup>. High water vapour permeability has been achieved by using poly(ether urethane) filled with isophorone diisocyanate-grafted carbon nanotubes<sup>153</sup>. It has been reported that enhanced rejection of solutes of brilliant blue R and safranin O from methanol and aqueous solutions can be done using polyamide/functionalized CNT's nanocomposite membranes prepared by interfacial polymerization<sup>154</sup>. Similarly CNT/polycarbonate matrix composite membranes have been found to have good hydrogen separation properties<sup>155</sup>. Unmodified MWCNT/polysulfone microporous conductive membranes have also been prepared by sonication technique<sup>156</sup>.

The continued attention of membrane scientists for polysulfone (PSf) is due to its excellent characteristics such as solubility in a large range of aprotic polar solvents (dimethylformamide,

dimethylacetamide, dimethylsulfoxide), high thermal resistance (150-170 °C), chemical resistance on the entire pH range, resistance in oxidative medium (hypochlorite, hydrogen peroxide) and also due to the high mechanical resistance of the films (fracture, flexure, torsion). They facilitate the formation of interpenetrating networks with blends while preserving the mechanical and thermal properties. As biocompatible and non-degradable materials, these polymers are utilized in bio-applications such as hemodialysis, ultrafiltration, filtration, and bioreactor technology<sup>157,158</sup>. However, applications of the PSf membrane are often limited because of its hydrophobic nature. Because of its hydrophobic properties, performance of PSf membranes results in low water flux and serious membrane fouling. The thermodynamic, rheological and the adsorption properties have been found to significantly change on its surface modification<sup>159,160</sup>. Enhancement of hydrophilicity is one area that is being studied extensively. Carboxylated or sulfonated polysulfone showed increased hydrophilicity. Thus retention towards proteins like sulfhydryl modified bovine serum albumin (cys-BSA) was found to be effected by degree of functionalization<sup>161,162</sup>. Structural segregation and excessive swelling of chitosan/polysulfone composite membranes has been controlled and geometric stability increased by immersing the polysulfone substrate into hydrophilic binding polymer solution like PVA, PAA before casting of chitosan layer<sup>163,164</sup>. Various hydrophilic modifications such as UV radiations treatment or additives like emeraldine base polyaniline (PANiEB) could be used to increase pore size without effecting retention and thus improve the performance of polysulfone membranes<sup>165,166</sup>. High performance affinity matrix from epoxy functionalized polysulfone have been reported to show high degree of adsorption and separation of amino acids<sup>167</sup>. Several other methods for polymer modification such as DNA immobilization, oxygen plasma treatment, treatment with aminated derivative could be used to serve various purposes<sup>168-170</sup>. Novel nanocomposite membranes containing single walled carbon nanotubes inside a polysulfone matrix have been reported to show high permeability and

diffusiveness for H<sub>2</sub>, O<sub>2</sub>, CH<sub>4</sub> and CO<sub>2</sub><sup>171,172</sup>. An increase of upto 67% selectivity between polar and non polar gases using oxidized nanotubes/polysulfone composite membranes has been reported<sup>173</sup>. Based on density functional theory calculations, it has been shown that different gas adsorption behaviors are introduced via modification by metals or carboxyl functional groups that further influence the gas permeability. Based on both experimental and theoretical results, it has been suggested that gas diffusion takes place through the interface between polymer chains and carbon nanotubes, rather than the CNT channels. Thus tailoring the modification on the external surface of carbon nanotubes could be an effective method for improving gas separation performance of CNT-based nanocomposite membranes<sup>174</sup>. Similarly, modifications on CNT's were also found to enhance the hydrophilicity of the composite membranes of CNT/PSf. However there are conflicting reports on the role of CNTs in the composite membranes. On one hand it is reported that protein fouling behavior of PSf composite membranes by bovine serum albumin and ovalbumin has been drastically reduced due to presence of nanotubes<sup>175</sup> where as on the other hand the modification on the CNT surface with 5-isocyanato-isophthaloyl chloride is reported to enhance protein adsorption on the membrane surface thus resulting in better separation<sup>176</sup>.

Heavy metals are among the most prevalent pollutants in the untreated water and are becoming severe public health problem. Industrialization and globalization is the major cause of various kinds of metal pollutants in water. These heavy metal ions are non-degradable and are toxic even at very low concentrations and can cause hypertension, nephritis, abdominal pain, nausea, vomiting, behavioral changes and development defects. Pb<sup>+2</sup>, Ni<sup>+2</sup>, Hg<sup>+2</sup>, Cr<sup>+6</sup> and Cd<sup>+2</sup> are hazardous heavy metal ions. A wide variety of techniques to remove heavy metals from water are available, such as, ion exchange reverse osmosis and nanofiltration, precipitation, coagulation/co-precipitation and adsorption. present study concentrates at membrane separation of heavy metal ions from drinking water.

Various studies related to flux improvement, pore structure and size control have made polysulfone/CNT composite membranes an interesting field for desalination<sup>177,178</sup>. However, to our knowledge no studies have been done on the metal ion removal from water using CNT/polysulfone composite membranes. The large surface and the nano size diameters of the CNT's could be effectively used in modifying the polysulfone membrane, a step forward in transforming an ultrafiltration membrane to a nanofiltration membrane. This could then be used for metal ion removal in critical applications. In the present study CNT's were modified to enhance the interaction with the polysulfone matrix and thus expecting it to 'bond' well with the matrix resulting in the modification of the composite membrane in both the porosity and hydrophilicity.

## **4.2 Materials**

Polysulfone(PSf) Udel P-3500 was a gift sample from M/s Solvay Speciality Polymers, Vadodara, India and had the following characteristics: tensile strength-70.3MPa, compressive strength-96MPa, thermal conductivity-0.26W/Mk and specific gravity-1.24. Multiwalled Carbon nanotubes (MWNTs, HiPCO supplied by Iljin Nanotech, Korea) whose purity was greater than 90%, were purchased from Sigma Aldrich and were of diameter 110-170 nm and length 5-9 microns. Ethylenediamine (>99%, Sigma Aldrich), Sodium azide (>99%, Sigma Aldrich), isopropanol, Dimethyl formamide(DMF) were used as it is.

## **4.3 Experiments**

### **4.3.1 Purification and functionalization of MWNTs**

#### **4.3.1.1 Surface cleaning and washing of nanotubes**

The >90% pure commercially available MWNTs are still associated with amorphous carbon and traces of metal ions that come to be associated with these nanotubes during preparation and thus were purified. Cleaning the surface of these pristine CNTs with SDS has been previously reported<sup>179</sup>. A modified method for cleaning of surface was adopted and this method helped to remove the amorphous carbon soot and nearly all heavy metals present in the as purchased CNTs. In this process, 2g of these nano tubes were sonicated with 500 ml of 1% Brij 98 (a non-ionic surfactant) for about 2h. The sonicated solution was allowed to stand for about 6h. The sediment was rejected as soot associated with the nanotubes. The nanotubes were collected from the mother liquor by subsequent centrifugation and sedimentation at 3000 rpm for 15 minutes. This process was repeated 2-3 times to obtain clean nanotubes. The surfactant associated with the nanotubes could be easily removed by alternate washing with water and brine solution. Subsequently, some of the heavy metals that may have remained attached to the surface of the CNT's were removed by converting these heavy metals into their soluble metal chlorides using 50% HCl solution. The yield was ~35% of the initial raw CNTs used. The remaining could be considered to be amorphous and other undesired carbonaceous material and heavy metal traces. Significantly, the obtained nanotubes do not get attracted to the magnetic needle unlike the uncleaned pristine CNTs which contain Fe, Co, Ni and other trace metals that get attracted to the magnetic bar. Purification and washing removes the unwanted carbonaceous material and metal ions and these washed and dried nanotubes were used to treat with various functionalizing agents.

#### **4.3.1.2 Oxidation, amide and azide functionalization of carbon nanotubes**

The washed and cleaned CNTs were treated with a 3:1 mixture of concentrated nitric and sulfuric acid (40 mL) for 24 h at 33°C. The oxidized nanotubes were washed with double distilled water five times, to obtain oxidized clean surfaces of MWNT's. Carboxylation is the most favored starting point

because it can be covalently bonded to form ester or amide linkages easily. The sample was then dried in a vacuum oven at 80 °C for 4 h. The oxidized nanotubes were treated with  $\text{SOCl}_2$  to introduce the acyl groups. 200 mg of obtained nanotubes were added to 20 mL of thionyl chloride and 2 mL of DMF (dimethyl formamide) in 100 mL round bottom flask. The system was refluxed for 36 hrs. at 60°C. The product obtained was washed with toluene. The sample was then dried in a vacuum oven at 80 °C for 4 h.

Twenty milligrams of the acylated nanotubes was dispersed by sonication in 10 mL of Ethylenediamine. The sonication was followed by stirring for 16 h at 33°C. The product was then diluted with 200 mL of methanol. The functionalized MWNTs were then dried in a vacuum oven at 80 °C for 4 h. This helped to introduce the amide groups on the CNT's

For azide functionalization, 60 mg of acylated nanotubes were treated with 5mg of  $\text{NaN}_3$  in DMF as solvent for 24h, and precipitated in toluene. The product was dried in an oven at 80°C for 4h. The different functionalization carried out were confirmed from FTIR and shown in Figure 4.1.

#### **4.3.2 Blending of CNT's into polysulfone to form nanocomposite membranes**

Polysulfone resin was first dried for at least 24h in a vacuum oven at temperature about 80°C before being used. N,N-dimethylformamide (DMF) was used as solvent and water containing isopropanol was used as coagulation medium during the phase inversion process. An optimized two component dope solution was used, 18% (w/w) polysulfone; 82% (w/w) DMF. To this solution different percentage of various functionalized CNT's were added to form PSf-CNT nanocomposite solution. The functionalized CNT's (oxidized, amide, azide) were used for the purpose. MWNTs in five different weight percentages (0.0%, 0.1%, 0.2%, 0.5%, 1.0%) were added to polysulfone solution, for

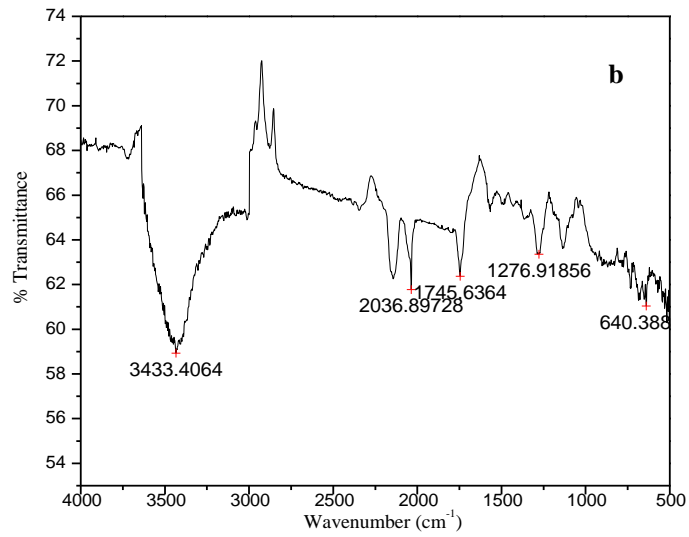
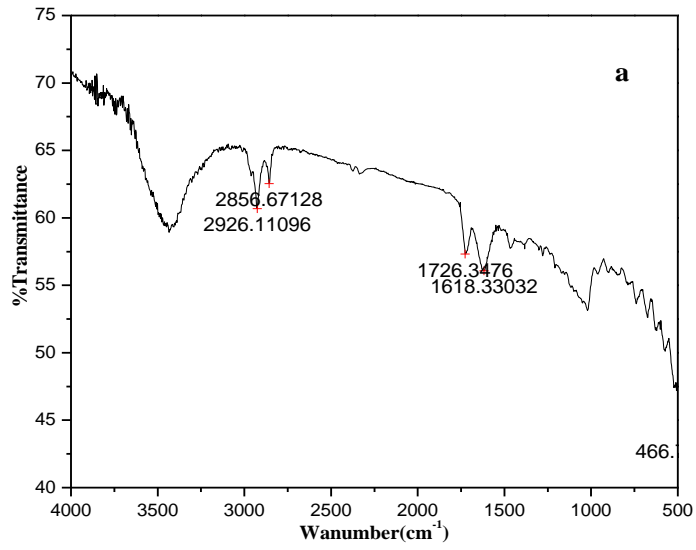


**Figure 4.1** FT-IR scans of MWNTs (a) carboxylated MWNT and (b) azide functionalized MWNTs.

all three different functionalized CNTs. These groups were expected to form hydrogen bonds with sulfone groups of PSf (Figure 4.2). The solutions were mixed in a round bottom reaction vessel and stirred using a magnetic bar and sonicated at 60°C for 72h until the polymeric solution became homogeneous. The homogeneous solution was placed in an ultrasonic water bath to remove the gas bubbles that may exist in the casting solution dope prior to the membrane casting process.

#### **4.3.3 Preparation of asymmetric flat sheet membranes**

Asymmetric flat sheet membranes were prepared according to the dry/wet phase separation process. The polymer solution was cast on a PET base using glass plate as support. The homogenous polymer solution was stretched into a thin film maintaining the thickness of the film. The casting knife consisted of a steel blade, or a glass rod which rested onto two runners, arranged to form a precise gap of 0.5mm between the rod and glass plate. The cast membranes were immediately soaked in a coagulating water bath containing 1% isopropanol, where the solvent-non solvent exchange takes place and membranes of uniform thickness of 5 mil (125  $\mu\text{m}$ ) are prepared. These membranes were then dried at 60°C and kept soaked in deionized water for several days.

#### **4.3.4 Capillary flow porometry**

Pore size analysis of membranes was done by Capillary Flow Porometer (Porous Materials Inc, USA, Model 1500 AEX), considering the pore as a capillary. First, the membrane samples were soaked in a wetting liquid, 'Porewick' having low surface tension ( $\gamma$ ) of 1.6 N/m<sup>2</sup> and has a contact angle zero with the membrane surface i.e., it wets the membrane samples fully and spontaneously fills all the pores in the sample. Then gas was blown through the membrane and the pressure of the gas was gradually increased until the liquid was removed from the pores, forming gas flow through pores, which increases with further increase in pressure<sup>180,181</sup>. At any given pressure, the largest pore is emptied first and the gas flow starts through the membrane, which gives the bubble point pressure.

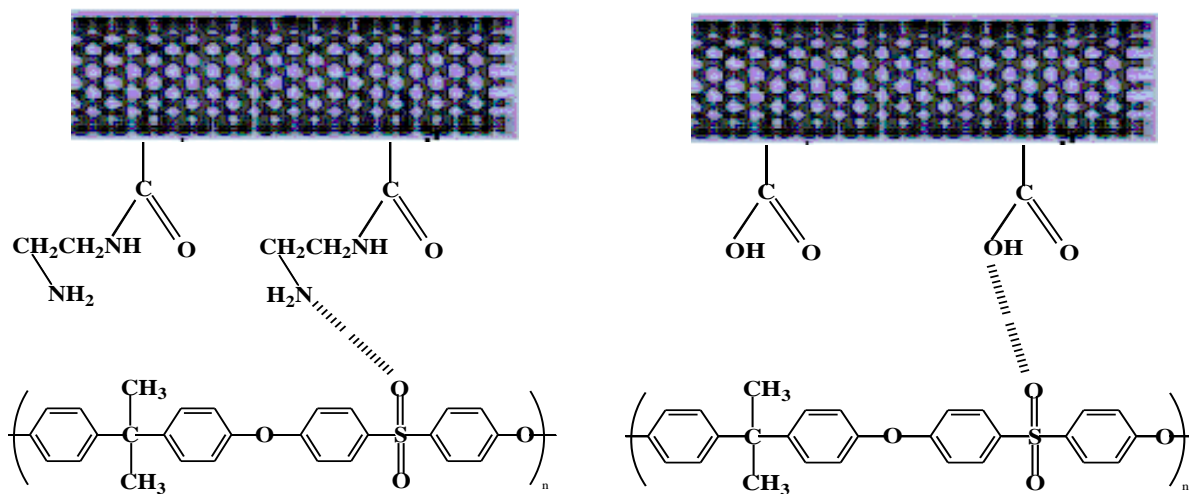


**Figure 4.2** Hydrogen bonding between the possible arrangement of functional groups on nanotubes and polysulfone.

On further increase of the pressure, smaller pores are then emptied and gas flow increases. The flow rate was determined as a function of pressure and used to calculate the desired pore characteristics using the Washburn equation.

$$D = 4 \gamma \cos \theta / p$$

Where D is the diameter of a pore,  $\theta$  is the contact angle, and p is differential pressure. For wetting liquid Porewick which was used,  $\theta = 0^\circ$  and the equation becomes

$$D = 4 \gamma / p$$

From this equation the diameter of pores in the membrane were calculated.

#### **4.3.5 Permeation test**

The common method to characterize the MWNTs/PSf blend membrane was to measure its performance in terms of pure permeability, flux and solute rejection of different feed solutions, using a general UF test cell set-up. The flux was measured by weighing permeates penetrated through the membrane per unit time and solute rejection was calculated from the concentrations of the feed solution and permeate using the following equation.

$$\text{Rejection (\%)} = (C_f - C_p) / C_f \times 100$$

where  $C_f$  and  $C_p$  are the concentrations of metal ions in the feed solution and permeate respectively. The  $C_f$  and  $C_p$  were measured by AAS. The collected filtrate samples were used for quantitative determination of ions using Atomic Absorption Spectrophotometer (Model: Analytikjena Nova-400). The Mercury and Arsenic were measured in graphite furnace mode of AAS and other metal were measured in flame mode of AAS. Control experiments in absence of functionalized CNTs were also carried out in order to correct any adsorption of metal on container surface. These experiments indicated that no adsorption by the container surface were detectable. All atomic absorption

spectrometer (AAS) (Analytik-Jena-Nova-400) measurements were carried out on flame mode/graphite furnace mode with single beam. AAS equipped with 100 mm burner, a cross flow nebulizer 5.0 ml/min and 1.2 mm slit were used throughout the experiments. Each experiment was duplicated under identical conditions using this instrument for concentration determination.

#### **4.3.6 Zeta Potential measurement**

Zeta potential is a scientific term for electrokinetic potential. It is denoted using the Greek letter zeta ( $\zeta$ ), hence  $\zeta$ -potential. The zeta potential is the electric potential in the interfacial double layer (DL) at the location of the slipping plane versus a point in the bulk fluid away from the interface. In other words, zeta potential is the potential difference between the dispersion medium and the stationary layer of fluid attached to the dispersed particle or surface.

Polymeric membranes possess a surface charge due to presence of functional group on their surface. When brought into contact with an aqueous solution, the surface charge is compensated by counter ions in the solution close to the surface, forming the so-called electrical double layer. The vital feature of the electric double layer is that the surface charge is balanced by counter ions, some of which are located very close to the surface, in the so-called Stern layer; the remainder are distributed away from the surface in the diffuse layer (Figure 4.3). An important parameter of the electric double layer is the Stern potential, that is, the potential at the boundary between the Stern and diffuse layers. The Stern potential cannot, however, be measured directly; the electro kinetic (zeta) potential is often considered an adequate substitute. The zeta potential is the potential at the plane of shear between the surface and solution where relative motion occurs between them. Several techniques can be used to determine the zeta potential of surfaces. The streaming potential technique is most suitable for membrane surfaces

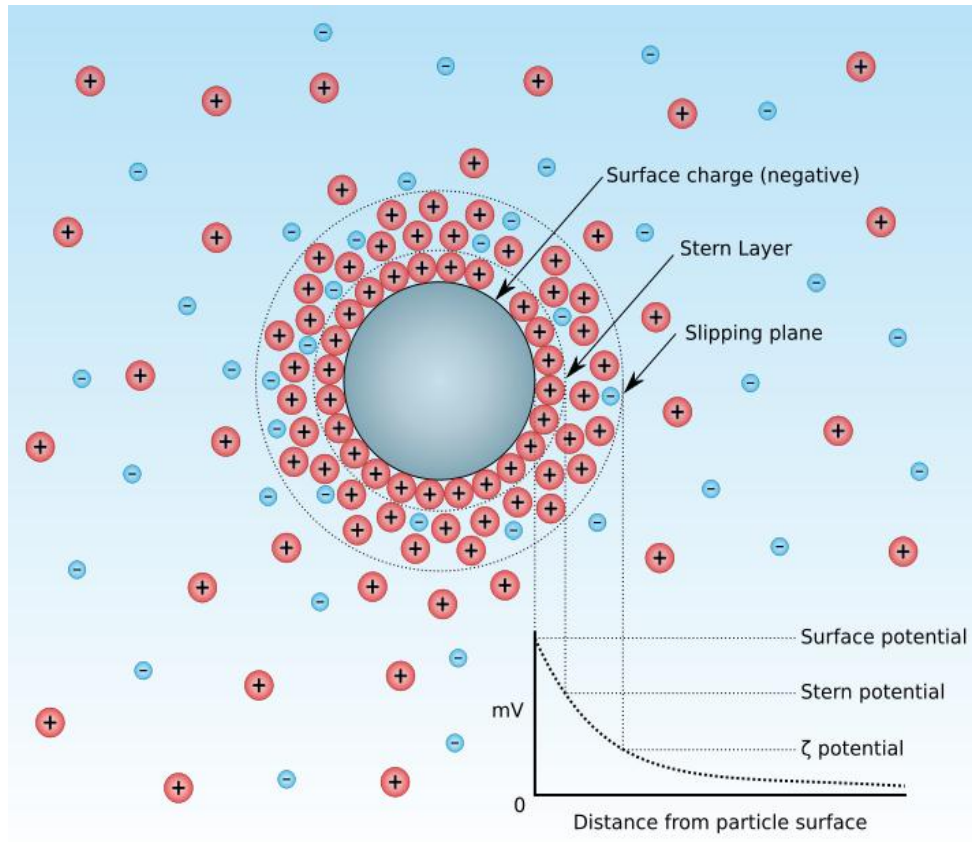


**Figure 4.3** Charge development on surface of membrane or dispersed particle in a dispersion medium.

The introduction of Reverse osmosis and nanofiltration membranes have proved a wonderful advancement in water purification technologies. The major advantage of membrane treatment is the superior quality of the product water. This quality is attained with the addition of fewer chemicals than conventional water treatment. The major obstacle to further incorporation of membrane processes into water treatment plants is membrane fouling. Fouling causes a decrease in the water flux across the membrane, an increase in salt passage through the membrane, and affects both the performance and longevity-of membranes. Membrane foulants can be broadly classified into four categories (1) sparingly soluble salts, (2) biological growth, (3) dissolved organic compounds, and (4) colloidal or particulate matter. The attack of colloidal matter on membrane surfaces is basically due to charge on polymer surfaces. Thus a complete understanding of charges and particle-membrane and particle-retained particle interactions must be considered for more understanding of colloidal fouling. Thus Zeta potential measurement would help in gaining an idea on the value of charges and potential on the surfaces.

#### ***4.4 Characterization***

The prepared blend membranes were characterized by FT-IR (Perkin-Elmer spectro photometer at 20 scans using the KBr pellet method) and scanning electron microscopy (SEM) using JEOL JSM-5610 model No. 6587 LV instrument for clean surfaces and attached functional groups. The TGA data were obtained in nitrogen atmosphere with Mettler-Teledo Star SW 7.01 thermo gravimetric analyzer at 10 °C/min.

#### ***4.5 Results and Discussion***

##### **4.5.1 Membrane casting by phase-inversion process**

The MWNTs/PSf blend membranes were prepared by the immersion phase inversion process, using DMF as solvent and water with isopropanol as a coagulant. This involves solvent/non-solvent

exchange process. Homogeneous solutions of PSf, DMF and functionalized MWNTs were prepared by sonication, and then used for casting blend membranes. By the phase inversion process it was observed that the membranes were uniform without any variation in the concentration of the solution. If the solutions were not homogeneous then the casting would not be uniform and the resulting membrane would have variations in the thickness as well as the porosity would be non uniform.

## **4.5.2 Characterization of composite polysulfone membranes**

### **4.5.2.1 FESEM**

The prepared composite MWNT/PSf membranes had thickness of 5mil (125 $\mu$ m). It is known that polysulfone blend membranes show porous morphology. Addition of MWNTs could help to reduce the pore size, due to nanosize (110-117nm) diameters of MWNTs and this is what can be seen from the FESEM for the membranes in Figure4.4. The functionalization of the surface of the nanotubes helps in formation of physical bonds between the polysulfone and the functionalized nanotube and so this influences the formation of the porous structure. The decrease in pore size of membranes with gradual increase in amount of carbon nanotubes is not very significant, as the arrangement of carbon nanotubes in the membranes is less manageable and controlled. The increase in carbon nanotube makes the surface of the membrane more smooth (Figure4.4b& Figure4.4c) as the solvent-non solvent exchange process becomes slower, owing to increase in viscosity of blend solution. These results are supported by the porometry results which will be discussed later. The largest visible pore size in unblended polysulfone membrane (Figure 4.4a) is 25 $\mu$  while in blend membrane containing 1% nanotubes, it is less than 1 $\mu$ .

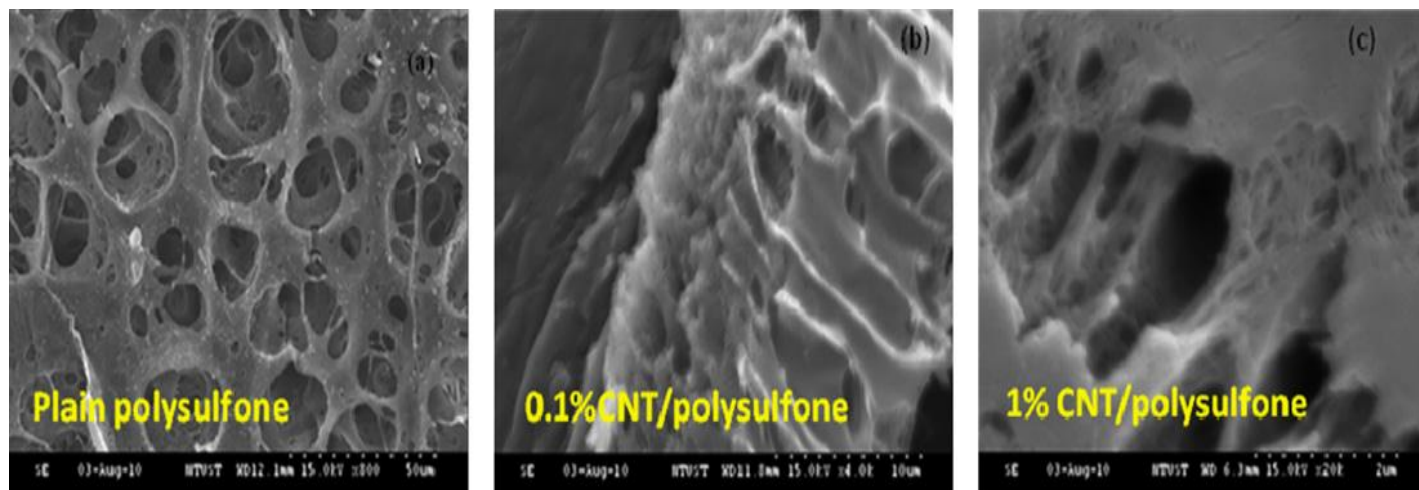


**Figure 4.4** FESEM images of CNT/PSf composite membranes (a) 0.0% (b) 0.1% (c) 1% functionalized MWNTs.

#### 4.5.2.2 Infra red spectroscopy

The FTIR spectra of blend membranes containing oxidized and amide functionalized CNTs show presence of bands at  $1290\text{cm}^{-1}$  corresponding to S=O asymmetric stretching vibration,  $1243.15\text{cm}^{-1}$  corresponding to C-O-C symmetric stretching vibration,  $1134.23\text{cm}^{-1}$  corresponding to S=O symmetric stretching vibration for polysulfone. Presence of oxidized nanotubes gives band at  $3487.56\text{cm}^{-1}$  (Figure 4.5a) corresponding to -OH stretching vibration,  $2850\text{-}3000\text{cm}^{-1}$  corresponding to C-H stretching vibration, and at  $1720\text{-}1730\text{cm}^{-1}$  corresponding to C=O stretching vibration. In Figure 4.5b disappearance of band at  $1720\text{cm}^{-1}$  and presence of a weak band at  $1623\text{cm}^{-1}$  confirm the presence of amide carbonyl stretch in amide functionalized CNTs. Disappearance of broad band at  $3500\text{cm}^{-1}$  and appearance of weak bands at  $3250\text{-}3400\text{cm}^{-1}$  show the possibility of overlap between N-H stretch of primary amine with O-H stretching in some extent. There is a hydrogen bonding between the nanotubes and the polysulfone, and so the functional peaks of the additional components are separately observed. The existence of hydrogen bonding between the carboxylic groups or amide or azide groups of nanotubes and the sulfonic groups of polysulfone membrane has been previously reported<sup>182,183</sup> and is also confirmed from our TEM and FESEM results.

#### 4.5.2.3 Thermo-gravimetric analysis

The TGA data shows the effect of MWNTs in the polysulfone matrix. The blend membranes show a slow and high temperature degradation as compared to polysulfone membrane without MWNTs. MWNTs owing to their high mechanical and heat resistance, offer increased heat tolerance and thus degradation occurs at higher temperatures as the concentration of MWNTs increase from 0-1 wt%. In polysulfone membrane without CNTs, the degradation starts at  $312^{\circ}\text{C}$ , while in blended membranes the degradation temperature increases through 0.1-1.0 wt% MWNT content

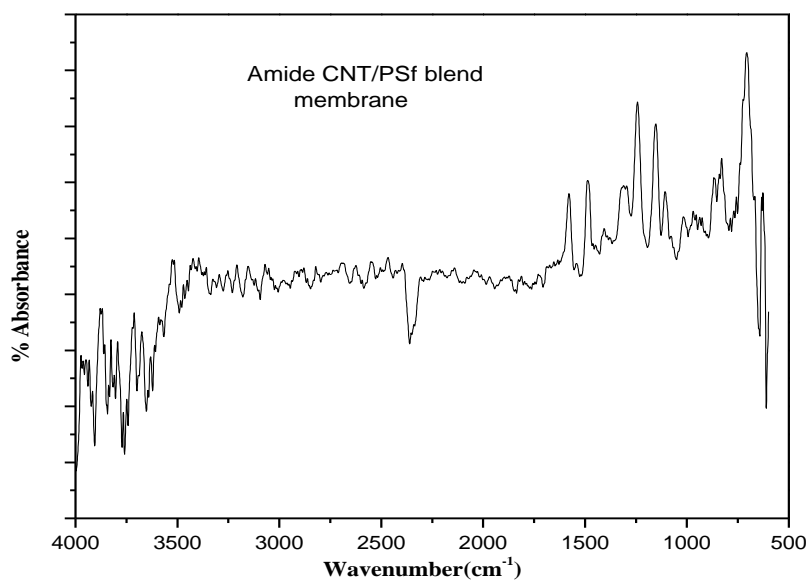
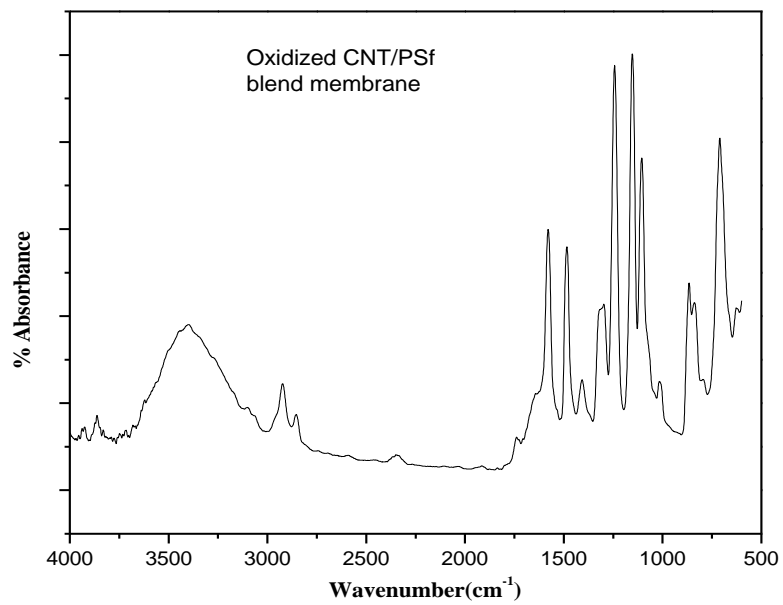


**Figure 4.5** FT-IR of (a) oxidized CNT/PSF (b) amide functionalized CNT/PSF blend membranes.

and is maximum for 1% MWNT /Polysulfone blended membrane i.e. 369°C and 374°C for amide and oxidized MWNTs. Thus it can be said that carbon nanotubes increase thermal stability of polysulfone membranes as the compatibility between the nanotubes and the polysulfone is enhanced by the functionalization of the nanotubes (Figure 4.6).

#### **4.5.2.4 Capillary flow porometry**

The increase in amount is also reflected in form of pore size of membrane and contact angle measurements. When MWNT content is very high (above 1%), the density of MWNTs in membrane is high enough, and steric hindrance and electrostatic interactions between modified MWNTs and aggregate in the membrane during phase-inversion and would make the casting process difficult. Thus composite mixtures containing greater than 1% MWNT were not studied. The high density of MWNTs in the membrane could reduce the porosity. The addition of MWNTs causes an increase in hydrophilicity of the membrane (reduced contact angle) and decrease in pore size. These results can be explained as arising due to the fact that during phase inversion process, hydrophilic MWNTs migrate spontaneously to membrane/liquid interface to reduce interfacial energy. As the amount of MWNTs increases from 0.1-1.0 wt%, the PSf hydrophobic membrane behaves more and more hydrophilic. With increase in MWNTs, there is increase in viscosity of the blend solution and the solvent-non solvent exchange process becomes slower and the surface becomes more smoother, with smaller pore sizes though the pore size variations are not very demarcating on addition of higher

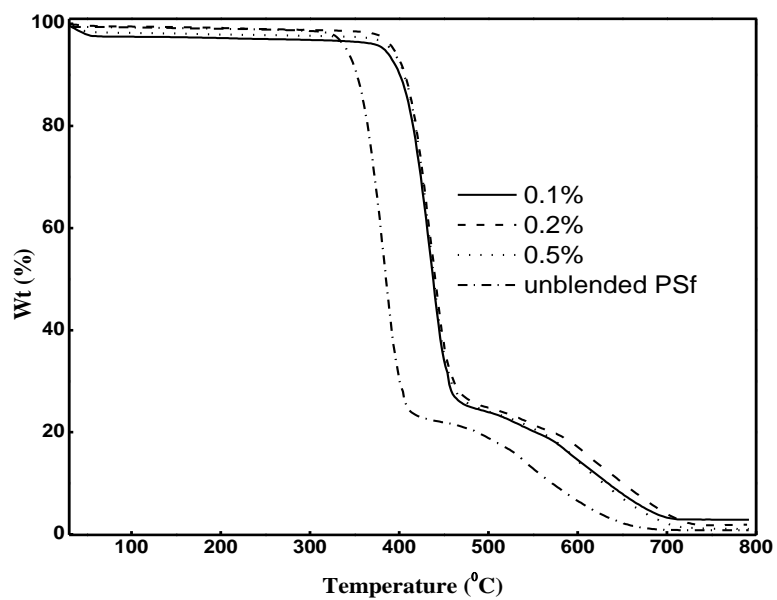


**Figure 4.6** TGA data composite polysulfone membranes with different percentages of amide functionalized MWNTs.

percentage of MWNTs. These results are in accordance with the flux rate measurements. The smallest pore diameter reduces from 0.1079 $\mu$  (~100nm) for pure polysulfone to 0.0257 $\mu$  (~26nm) on addition of nanotubes under similar coagulation bath conditions. This can be seen in Table 4.1.

It is to be noted here that depending on the coagulation bath additives, the pore diameter of the unblended polysulfone can also be controlled. The results are summarized in Table 4.2. In order to determine the pore size distribution of the membrane, the pressure at which the bubble is formed is required. In order to reach bubble point, sufficient gas pressure must be applied to overcome the capillary forces of the pores. Gas pressure is applied on the underside of the membrane, and is gradually increased over time.

A constant flow of rising bubbles on the top side of the membrane indicates that the gas pressure has reached bubble point. It is at this pressure when the largest pore gets emptied first. The smallest pore size can also be calculated by increasing the gas pressure till all pores have been emptied and gas flow through the membrane matches that of a dry membrane. At pressures below the bubble point, gas can only pass through the membrane through diffusion.

#### **4.5.2.5 Zeta Potential studies**

Samples were analyzed for the evaluation of zeta potential from streaming current by streaming electrolyte KCl (0.001 M) in contact with PSf/CNT composite membrane samples. The fundamental equation for evaluating zeta potential from streaming current is Helmholtz Smoluschowski i.e.

$$\zeta = \frac{U_s}{\Delta P} \frac{\mu}{\epsilon \epsilon_0} \frac{L}{A} \frac{1}{R}$$

**Table 4.1** Variation of the pore size with amount of amide functionalized CNT's.

% MWNT	Pore size( $\mu$ )	Contact angle( $\theta$ )
0.0	0.1079	77.7
0.1	0.0286	77.6
0.2	0.0262	77.6
0.5	0.0259	77.5
0.7	0.0259	76.3
1.0	0.0257	26.7

**Table 4.2** Variation of the smallest pore diameter (micron) and required pressure (MPa) with weight % of CNT's.

	Oxidized CNT's (wt %)					Amide CNT's (wt %)				
	0.1	0.2	0.5	0.7	1.0	0.1	0.2	0.5	0.7	1.0
Pore pressure	1.562	1.689	1.740	1.754	262.4	1.600	1.747	1.767	1.767	1.781
Pore diameter	0.029	0.027	0.026	0.026	0.025	0.028	0.026	0.025	0.025	0.025
Mean flow pore pressure	0.465	0.470	0.474	0.479	0.487	0.466	0.471	0.478	0.480	0.489
Mean flow pore diameter	0.098	0.097	0.096	0.095	0.093	0.098	0.097	0.095	0.095	0.093
Bubble point pressure	0.044	0.044	0.045	0.045	0.045	0.044	0.044	0.045	0.045	0.046
Bubble point pore diameter	1.029	1.028	1.027	1.019	1.017	1.029	1.029	1.018	1.014	1.013

$U_s$  : streaming potential,  $\Delta P$  : pressure difference across the channel,  $\mu$  : viscosity of the solution  
 $\epsilon$  : permittivity of the solution,  $L$ ,  $A$ , and  $R$  are the length, cross-sectional area, and electrical resistance of the channel

Zeta potential was measured with change of pH by adding HCl acid (0.05 M) in the electrolyte. The results obtained for measurement of zeta potential have been summarized in Tables 4.3 and 4.4. All membranes display an i.e.p. (iso-electric point) at an acidic pH; the zeta potential is negatively charged at pH values above the i.e.p. and is positively charged at lower pH. Zeta potential measurements reveals the surface chemistry of the coated membrane samples. At lower pH values presence of protonated carboxylic groups in carboxylated CNT /PSf composite membranes give positive zeta potential values. The zeta potential values for carboxylated CNT /PSf composite membranes are more negative at high pH. It is attributed to presence of deprotonated carboxylic groups at surface of composite membranes at high pH. With increase in concentration of carboxylic groups, the potential difference at the interface increase and so zeta potential values increase (more negative). The zeta potential values for amide CNT /PSf composite membranes are comparatively positive due to presence of terminal amine groups which are protonated, and thus gives positive charge to interface. The zeta potential values are negative and move to positive end at low pH values for all types of membranes.

### **4.5.3 Heavy metal removal**

Heavy metal salt solutions were prepared by dissolving the salts in ultrapure water (ElixMillipore) and solutions of 1 ppm concentration were prepared. Stock solutions of chromium and lead of 1000 mg/l concentration were prepared by dissolving, 2.848 g of  $K_2Cr_2O_7$ , 1.598 g of  $Pb(NO_3)_2$ , respectively in 1000 ml of ultrapure water (Elix, Millipore), whereas cadmium solution was prepared by dissolving 1 g of cadmium metal in minimum volume of (1 + 1) HCl and then making it up to 1000 ml with

**Table 4.3** Values of Zeta potential developed at the surface of PSf/ % carboxylated CNT composite membranes when in contact with an electrolyte solution.

<b>Zeta Potential at different pH</b>					
PSf/ 1% carboxylated CNT composite membrane		PSf/ 0.5% carboxylated CNT composite membrane		PSf/ 0.1% carboxylated CNT composite membrane	
<b>pH</b>	<b>ZP(mV)</b>	<b>pH</b>	<b>ZP(mV)</b>	<b>pH</b>	<b>ZP(mV)</b>
5.472	-52.49	5.467	-44.87	5.452	-51.63
5.469	-51.89	5.459	-44.92	5.146	-49.37
5.13	-50.97	4.925	-41.55	4.771	-44.92
4.737	-48.2	4.413	-36.35	4.361	-38.5
4.315	-43.54	4.027	-30.53	4.01	-31.84
3.959	-38.17	3.688	-24.19	3.684	-25.01
3.631	-32.55	3.371	-17.96	3.373	-17.69
3.32	-26.31	3.123	-13.05	3.126	-11.67
3.078	-21.44	2.929	-9.271	2.932	-7.323
2.886	-17.42	2.771	-6.453	2.801	-4.613
		2.641	-4.382	2.683	-2.362

**Table 4.4** Values of Zeta potential developed at the surface of PSf/ % amide functionalized CNT composite membranes when in contact with an electrolyte solution.

<b>Zeta Potential at different pH</b>					
PSf/ 1% amide functionalized CNT composite membrane		PSf/ 0.5% amide functionalized CNT composite membrane		PSf/ 0.1% amide functionalized CNT composite membrane	
<b>pH</b>	<b>ZP(mV)</b>	<b>pH</b>	<b>ZP(mV)</b>	<b>pH</b>	<b>ZP(mV)</b>
5.445	-53.5	5.428	-44.52	5.625	-50.93
5.123	-47.14	5.122	-37.04	5.272	-45.6
4.752	-38.53	4.759	-31.54	4.859	-38.82
4.344	-28.54	4.356	-24.37	4.421	-30.59
3.994	-19.77	4.001	-17.14	4.058	-23.45
3.67	-11.37	3.683	-11.18	3.726	-16.49
3.357	-3.608	3.37	-4.897	3.411	-9.581
3.112	2.158	3.123	-0.151	3.163	-4.276
2.918	6.225	2.928	3.086	2.966	0.071
2.761	9			2.807	3.143

ultrapure water. Standard working solutions of copper and arsenic were prepared from 1000 mg/L standard solution (Merck, Germany) and solutions of varying initial concentrations were prepared from a 1000 mg/L by serial dilution using distilled deionized water. The pH of the solutions were set as 2.6 (acidic medium). The pH of Cr<sup>+6</sup> metal ion solution was further adjusted to 6.8 and 9.5 by the addition of 0.1N solution of NaOH during dilution process. The alkaline and acidic solutions of all other metal ions show hydrolysis and hydroxide formation, and so assumed to be not suitable for metal rejection study by prepared composite membranes. Tests were carried out at different pressures 0.49, 0.686 and 0.882 MPa and at various pH 2.6, 6.8, 9.5 for chromium and at pH 2.6 only for other metal ions. The permeation tests were conducted at 25°C, effective membrane area was 16 cm<sup>2</sup>, and feed flow rate 12ml/min. Before measuring the flux, each membrane was subjected at 0.5MPa for about 2h to avoid the compaction effect of the membrane. Studies were also conducted at different pressures.

#### **4.5.3.1 Effect of pressure**

Nearly no permeate flow rate was observed below 0.49 MPa and was found to increase with increase in applied pressure (Figure 4.7, Table 4.5). Increased pressure would force the test solution to flow at high rates through the membrane. Permeate flow for 0.2% and 0.5% oxidized CNT/PSf composite membranes at 0.49MPa is 6.2 and 5.7ml/min respectively while 10.5 and 9.8 ml/min respectively at 0.88MPa. Similarly permeate flow for 0.2% and 0.5% amide functionalized CNT/PSf composite membranes at 0.49MPa is 5.9 and 5.8ml/min respectively while 9.9 and 9.9ml/min respectively at 0.88MPa. The results for all other membranes can be seen in Table 4.5. At higher pressures increased flow rates would cause less rejection of unwanted ions. The permeate flow for 1% oxidized CNTs/PSF and 1% amide CNTs/PSF blend membranes at optimum pressure of 0.49MPa was 5.4 and 5.6ml/min. respectively, while it was 6.3ml/min. for plain PSf membrane.

**Table 4.5** Permeate flow for different membranes at different pressures.

S.No.	Type of membranes	Feed flow (ml/min)	Permeate flow (ml/min)		
			4.90 bar	6.86 bar	8.82 bar
1.	0.2% Oxidized CNT	12.0	6.2	8.3	10.5
2.	0.5% Oxidized CNT	12.0	5.7	7.6	9.8
3.	1% Oxidized CNT	12.0	5.4	7.3	9.6
4.	0.1% Amide CNT	12.0	6.1	8.3	10.3
5.	0.2% Amide CNT	12.0	5.9	8.0	9.9
6.	0.5% Amide CNT	12.0	5.8	7.9	9.9
7.	0.7% Amide CNT	12.0	5.8	7.9	9.8
8.	1.0 % Amide CNT	12.0	5.6	7.8	9.8
9.	Plain PSf	12.0	6.3	8.7	11.8

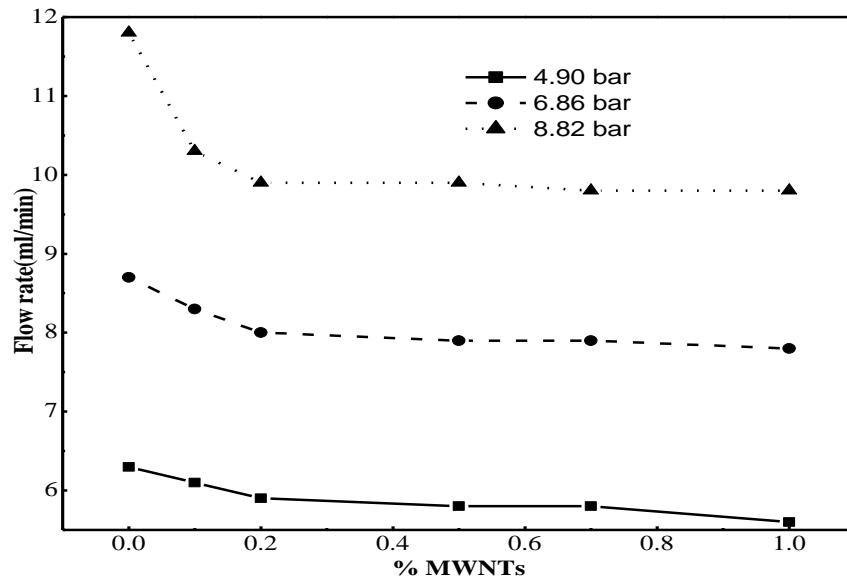


**Figure 4.7** Flow rate at different pressures for different amide MWCNT/PSf membranes at acidic pH 2.6.

This decrease in permeate flow accounts for greater hindrance at the surface of membrane due to decreased pore size and thus supports rejection of ions. Percentage rejection of  $\text{Cr}^{+6}$  at 0.49 MPa and 2.6 pH for composite membranes containing 0.1% and 1% amide functionalized CNT was 80.4 and 94.2 respectively which is reduced to 62.3 and 75.3 respectively, when pressure used is increased to 0.882 MPa and 2.6 pH (Tables 4.6 & 4.7). Under similar conditions % rejection of  $\text{Pb}^{+2}$  at 0.49 MPa for composite membranes containing 0.1% and 1% amide functionalized CNT was 72 and 90.1 respectively which is reduced to 50.2 and 62.0 respectively, when pressure used is increased to 0.882 MPa (Figure 4.8). Percentage rejection of  $\text{Cr}^{+6}$  at 0.49 MPa and 2.6 pH for composite membranes containing 0.1% and 1% azide functionalized CNT was 80.9 and 94.8 respectively which is reduced to 63.9 and 76.1 respectively, when pressure used is increased to 0.882 MPa and 2.6 pH. Percentage rejection of  $\text{Cd}^{+2}$  at 0.49 MPa and 2.6 pH for composite membranes containing 0.1% and 1% amide functionalized CNT was 73.1 and 79.1 respectively which is reduced to 57.1 and 69.9 respectively, when pressure used is increased to 0.882 MPa and 2.6 pH.

**Table 4.6** Removal studies of metal ions at pH 2.6 for amide functionalized MWCNT/PSf. at pressure of 0.49MPa and 0.882MPa.

(%) CNT	Removal Capacity(%) amide					
	Cr (VI)		Pb (II)		Cd (II)	
	0.49	0.882	0.49	0.882	0.49	0.882
0.0	10.2	7.2	10.5	7.4	9.9	9.9
0.1	80.4	62.3	72.0	50.2	72.8	55.3
0.5	90.7	68.6	87.8	54.9	77.4	61.2
0.7	92.8	70.1	88.2	57.6	77.9	61.2
1.0	94.2	75.3	90.1	62.0	78.2	78.2

**Table 4.7** Removal studies of metal ions at pH 2.6 for azide functionalized MWCNT/PSf. at pressure of 0.49MPa and 0.882MPa.

(% ) CNT	Removal Capacity(%) azide					
	Cr (VI)		Pb (II)		Cd (II)	
	0.49	0.882	0.49	0.882	0.49	0.882
0.0	10.2	7.4	10.5	7.9	9.9	7.3
0.1	80.9	63.9	72.6	52.2	73.1	57.1
0.5	91.6	69.8	88.3	55.8	78.2	62.2
0.7	93.1	72.1	89.1	58.6	78.8	66.8
1.0	94.8	76.1	90.8	65.2	79.1	69.9

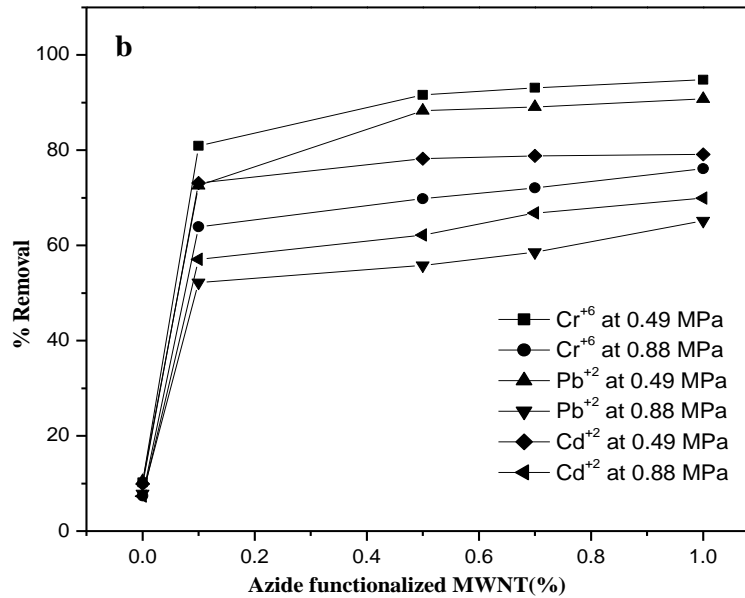
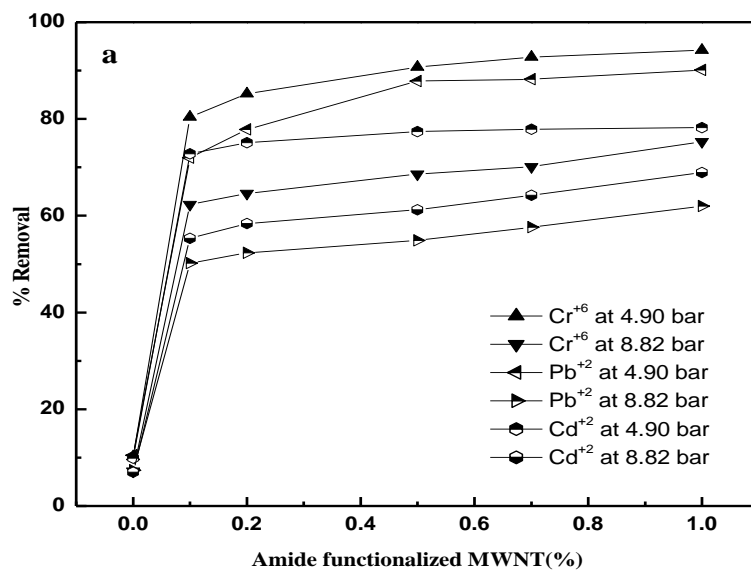


**Figure 4.8** %Removal of metal ions at different pressure (a) %amide CNT/PSf (b) %azide CNT/PSf composite membranes at pH 2.6.

#### 4.5.3.2 Effect of pH

Similar rejection experiments confirmed that maximum rejection for  $\text{Cr}^{+6}$  was found at pH 2.6 (acidic), which could be explained as high complexation tendency of surface active sites of the blend membranes. The modified MWNTs provide sites for complexation with metal ions which are absent in plain polysulfone membranes. The  $-\text{COOH}$ ,  $-\text{OH}$  due to oxidation of membranes surfaces,  $-\text{CONH}$ - and  $-\text{CH}_2\text{NH}_2$  due to amide functionalization and,  $-\text{CON}_3$  due to azide functionalization show complex formation with the heavy metal ions. Apart from these at acidic pH, protons also compete with the heavy metal ions, and thus providing maximum rejection or removal at acidic pH. There is decrease in rejection at pH 6.8, which again increases at basic pH (9.5) due to hydroxide formation of  $\text{Cr}^{+6}$  (Figure 4.9). These hydroxide salts precipitate out of the solution and thus are removed from the solution. Here hydroxide formation on the membrane surface affects or reduces the membrane activity and so is less desired. Thus pressure of 0.49MPa and pH 2.6 could be considered as optimum condition for metal removal studies.

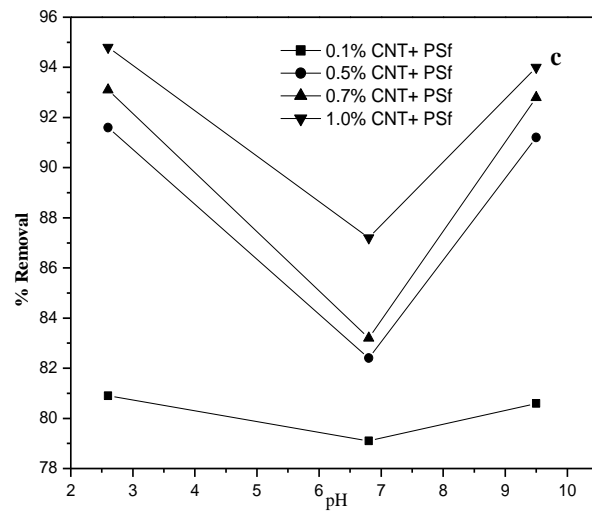
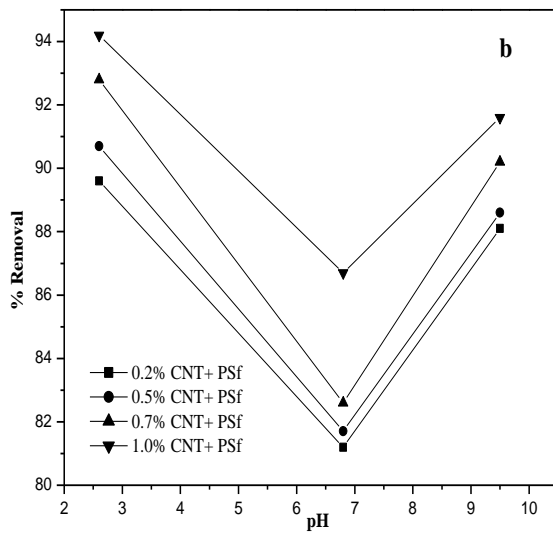
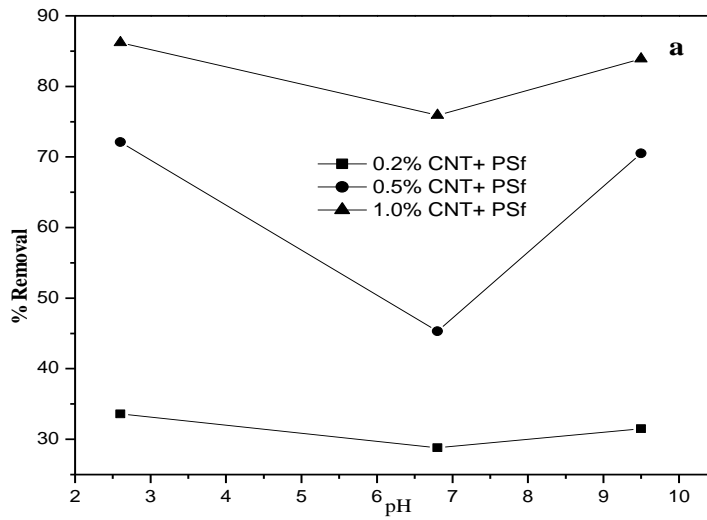


**Figure 4.9** Removal studies of  $\text{Cr}^{+6}$  ions at different pH for (a) oxidized (b) amide (c) azide functionalized MWCNT/PSf. at pressure of 0.49MPa.

Metal removal/rejection studies at set optimum conditions of pH 2.6 and pressure 0.49MPa were done for oxidized, amide functionalized, azide functionalized MWCNT/PSf blend membranes. Metal ions rejection was found to increase with increase in % weight of CNTs added. This may be attributed due to decreased pore size, reduced flow rate and increased number of active sites on CNTs due to functionalization. Appreciable removal was observed for oxidized CNT/PSf composite membranes (Table 4.8). The metal removal was found to be more pronounced in case of membranes containing amide (Table 4.9) and azide (Table 4.10) functionalized CNTs. The presence of amide and azide groups are expected to have better metal binding capacity as compared to carboxylic group, and thus only 33.6% of  $\text{Cr}^{+6}$  and 41.3% of  $\text{As}^{+3}$  is rejected using a oxidized CNT/PSf blend while 80.4% of  $\text{Cr}^{+6}$  and 71.3% of  $\text{As}^{+3}$  is rejected using amide functionalized CNT/PSf .

In case of amide functionalized CNT/PSf membranes, 0.1% amide gave 80.4% rejection of  $\text{Cr}^{+6}$  while 1% amide gave 94.2% rejection. On increasing carbon nanotubes, there is decrease in pore size, which gives reduced flow rate and reduced flux, and thus better removal of heavy metal ions on the surface. On the contrary plain polysulfone membranes (without carbon nanotubes) show very less or negligible rejection. Plain polysulfone membranes gave only 10.2% rejection of  $\text{Cr}^{+6}$ , which is very less as compared to blended membranes.

**Table 4.8** Removal studies of toxic metal ions at pH 2.6 for oxidizedMWCNT/PSf at pressure of 0.49MPa.

(% ) CNT	Removal capacity (%)				
	Cr (VI)	Cu (II)	Pb (II)	Cd (II)	As (III)
0.0	10.2	10.1	10.5	9.9	10.9
0.2	33.6	44.2	26.8	53.2	41.3
0.5	72.1	68.0	39.7	63.5	51.2
1.0	86.2	79.3	41.3	71.6	83.6

**Table 4.9** Removal studies of toxic metal ions at pH 2.6 for amide functionalized MWCNT/PSf at pressure of 0.49MPa.

(% ) CNT	Removal capacity (%)				
	Cr (VI)	Cu (II)	Pb (II)	Cd (II)	As (III)
0.0	10.2	10.1	10.5	9.9	10.9
0.1	80.4	85.6	72.0	72.8	71.3
0.2	89.6	88.2	77.6	74.9	75.3
0.5	90.7	90.6	87.8	77.4	77.9
0.7	92.8	90.9	88.2	77.9	79.2
1.0	94.2	93.1	90.1	78.2	79.4

**Table 4.10** Removal studies of toxic metal ions at pH 2.6 for azide functionalized MWCNT/PSf at pressure of 0.49MPa.

(%) CNT	Removal capacity (%)				
	Cr (VI)	Cu (II)	Pb (II)	Cd (II)	As (III)
0.0	10.2	10.1	10.5	9.9	10.9
0.1	80.9	85.9	72.6	73.1	71.9
0.5	91.6	91.4	88.3	78.2	78.3
0.7	93.1	91.9	89.1	78.8	80.6
1.0	94.8	93.9	90.8	79.1	80.9

#### **4.6 Conclusions**

The polysulfone membranes have an average pore size of 0.05-0.1 $\mu$  (microns). These membranes show high thermal and chemical resistance, but are highly hydrophobic and susceptible to membrane fouling. The large pore size of 0.1 $\mu$  and more give less water flux, and thus only colloids and bacteria are subjected to removal. The MWNTs with clean and active functionalized surfaces, show efficient bonding with the polymeric membrane surfaces. The presence of nanotubes effectively increases the thermal stability of polysulfone, and thermal degradation occurs at comparatively high temperatures. The surface chemistry and charges studied by Zeta potential measurement confirm the presence of active groups and degree of functionalization. The 1% carboxylated CNT /PSf composite membranes have higher value of negative zeta potential, as compared to 0.1% carboxylated CNT /PSf composite membranes. They make the membranes more hydrophilic, impart greater adsorptive nature, and reduced pore size to the range of 20-30nm. The reduced pore sizes and high adsorptivity help the membranes to be efficient enough for metal removal from drinking water. The percent rejection of heavy metal was found to increase with increase in amount of MWNTs. Amide and azide functionalized carbon nanotubes gave better results as compared to oxidized CNTs and best rejection were found at acidic pH 2.6 and pressure 0.49MPa. These encouraging studies can be extended for further investigating the performance of these membranes for more environmentally damaging metal ions.

## Chapter 5 ATRP using functionalized nanotubes /Acetyl Chloride as radical initiators

### 5.1 Introduction

It has been found that recently developed atom transfer radical polymerization (ATRP)<sup>184-188</sup> is one of the most versatile methods to control the structure, chain length, distribution and chain end functionality of polymers. This method of polymerization gives functional and “living “ end groups and helps produce various nanocomposites of immense importance<sup>189,190</sup>. A three-component initiating system for *Atom transfer radical polymerization (ATRP)* contains halide-type true initiator, catalyst – a transition metal salt in the lower oxidation state, and a complexing ligand, based on amine-type or organophosphorus compounds<sup>191,192</sup>. Initiator systems such as alkyl or aryl halides, esters on haloorganic acids, polyhalogenated compounds<sup>193</sup> have been reported. General scheme for CRP method is shown in Figure 5.1.

It involves a reversible redox process whereby a transition metal complex [M<sub>n</sub> –Y/Ligand] catalyses the reaction. After accepting the (pseudo halogen) from the initiator species, the transition metal-ligand complex in its lower oxidation state converts to higher oxidation state. Y is either a ligand or counter ion. This process occurs at a rate constant of activation  $K_{act}$  and deactivation  $K_{deact}$ . Establishing a rapid dynamic equilibration between a very small amount of growing free radicals and a large majority of dormant species (initiators) is the most essential requirement of ATRP for controlled polymerization. Temperature and solvent types also greatly effect the polymer properties.



The rate of polymerization in ATRP increases with increase in temperature due to increase in radical propagation and atom transfer equilibrium constant, but at the same time side reactions also become dominant, which gives high PD. Various initiating systems such as halogenated alkanes, benzylic halides,  $\alpha$ -Haloketones,  $\alpha$ -Haloesters etc. can be used which facilitate the transfer of halogen to catalyst-ligand complex. Atom transfer radical polymerization (ATRP) of methyl methacrylate (MMA) has been reported at room temperature (25 °C) under  $^{60}\text{Co}$   $\gamma$ -irradiation environment. The polymerization proceeded smoothly with high conversion (>90%) within 7 h<sup>194</sup>. Surface initiated ATRP of MMA has been reported at 80°C using modified PANI as macroinitiator<sup>195</sup>. A new ATRP initiator, viz, 2-oxo-1,3-dioxolan-4-yl-(methyl-2-bromo-2-methylpropanoate) (ODMBMP) was used to carry out ATRP reactions of methyl methacrylate (MMA) in the presence of copper chloride/*N,N',N',N''N''*-pentamethyldiethylenetriamine to give low molecular weight cyclic carbonate-terminated poly(methyl methacrylate)s with relatively narrow molecular weight distribution<sup>196</sup>. Various such experiments on ATRP of MMA<sup>197-200</sup> and styrene<sup>201-203</sup> have been reported using various catalyst and ligand systems like 2-pyridinecarbaldehyde imine copper(I) complexes, alkyl pyridylmethanimine, CuI(bpy)<sub>n</sub>Cl or Wilkinson catalyst, but the initiator system had terminal free halide group.

The  $\alpha,\omega$ -dichloro-PMMA prepared by ATRP of MMA using 1,3-bis{1-methyl-1-[(2,2,2-trichloroethoxy)carbonylamino]ethyl}benzene as bifunctional initiator were used as macroinitiators for ATRP of tert-butyl acrylate (t-BuA), giving the corresponding triblock copolymers with narrow MWDs and molecular weights controllable in a wide range<sup>204-206</sup>. Controlled functionalization of multiwalled carbon nanotubes by in Situ ATRP has been performed by generating terminal bromine on CNT by reaction with 2-bromo-2-methylpropionyl bromide. Similar work has been done to

produce polystyrene-*block*-poly(acrylic acid) (PS-*b*-PAA) grafted MWNTs<sup>207</sup>. Construction of polymer brushes on multiwalled carbon nanotubes by in situ reversible addition fragmentation chain transfer polymerization has been done to generate poly(methyl methacrylate)-*block*-polystyrene (PMMA-*b*-PS)<sup>208</sup>.

In present study compounds of the general formula RCO-Cl were used as ATRP initiators, for polymerization of MMA and styrene, in which -R can be a alkyl group of any number of carbon atoms. Use of acetyl chloride groups as initiating systems is a totally as RCO-Cl bond is highly reactive and dissociates readily to form radicals and thus producing halogen radical for further transfer reactions. Apart from various alkanoyl chlorides, acylated nanotubes have also been used as macro initiators.

Free radical polymerization is a method by which a polymer is formed from the successive addition of free radical building blocks. Free radicals can be formed via a number of different mechanisms usually involving separate initiator molecules. Following creation of free radical monomer units, polymer chains grow rapidly with successive addition of building blocks onto free radical sites. Free radical polymerization is a key synthesis route for obtaining a wide variety of different polymers and material composites. The relatively non-specific nature of free radical chemical interactions makes this, one of the most versatile forms of polymerization available and allows facile reactions of polymeric free radical chain ends and other chemicals or substrates.

Poly (methyl methacrylate) and polystyrene were synthesized by emulsion polymerization with Methyl Methacrylate and styrene as monomers respectively, acetyl chloride as initiator in one reaction set and acylated nanotubes as initiator in other set , Brij-98 as the emulsifier and distilled water as a

medium. Similar reactions using pentanoyl chloride and hexanoyl chloride as initiators have also been performed.

PMMA is a versatile material and has been used in a wide range of fields and applications. The German chemist Fittig and Paul discovered in 1877 the polymerization process that turns Methyl Methacrylate into poly Methyl Methacrylate (Lovell 1997). Water born polymerization such as emulsion polymerization are of great importance in industry application as they provide environmental friendly process, remove the reaction heat easily during polymerization and assume the feasible handling of the final product having a low viscosity.

Emulsion polymerization involves the propagation reaction of free radicals with monomer within the monomer-swollen polymer particle dispersed in the hydrophobic particles stabilized by surfactant. Micelles are formed when the level of surfactant is greater than its critical micelles concentration (CMC). Particle nucleation are generated via the capture of radicals by micelles. These absorb monomer to achieve a critical chain length.

## **5.2. Materials**

Methyl methacrylate(>99%, Aldrich), Styrene (Sty, >99%, Aldrich) were passed through alumina in order to remove inhibitor and stored under argon in freezer. CuCl (>99%, Aldrich) was purified by washing with glacial acetic acid, absolute ethanol, and finally with diethyl ether. The ligand 2-2' bipyridyl (>99%, Aldrich) , initiator acetyl chloride (MERCK) ,Carbon nanotubes (multi-walled carbon nanotubes, MWNTs) manufactured by HiPCO , SOCl<sub>2</sub>, methanol(>92%, Aldrich) and chloroform were used as obtained.

## 5.3 *Experimental*

### 5.3.1 Polymerization of MMA

All reagents were nitrogen purged before use. Emulsion of MMA (6.2 mL /5.78 gm, 0.0289mmol) with 28.0 mL of distilled water and 4.6 gm of Brij 98 surfactant was prepared. The solution was stirred for 1.5 h using magnetic stirrer. This emulsion was found to be stable.

In a typical experiment, CuCl (0.0288 g, 0.14 mmol) and a bidentate ligand 2,2'-bipyridyl (0.0872 g,0.28 mmol) were added to a two neck 100 mL round bottom flask, equipped with a magnetic stirring bar. After sealing with a three way stopcock, the flask was degassed and backfilled with argon three times.

To this, emulsion of monomer was transferred by means of cannula using vacuum, keeping flask stirring by use of magnetic stirrer.

After three freeze–thaw–pump cycles *initiator (Acetyl Chloride)* was injected dropwise under nitrogen purging. The reaction mixture was stirred for 20 hours.

(1) at room temperature and

(2) at temperature 60°C.

The reaction was quenched by intensive cooling and diluted with tetrahydrofuran (THF). The formed polymer was recovered by precipitation in acidic methanol/water mixture = 80/20 (v/v) and dried in vacuum at 40°C to constant weight.

For purification it was dissolved in chloroform and reprecipitated it in methanol 3-4 times. Figure 5.2 shows the reaction scheme followed.

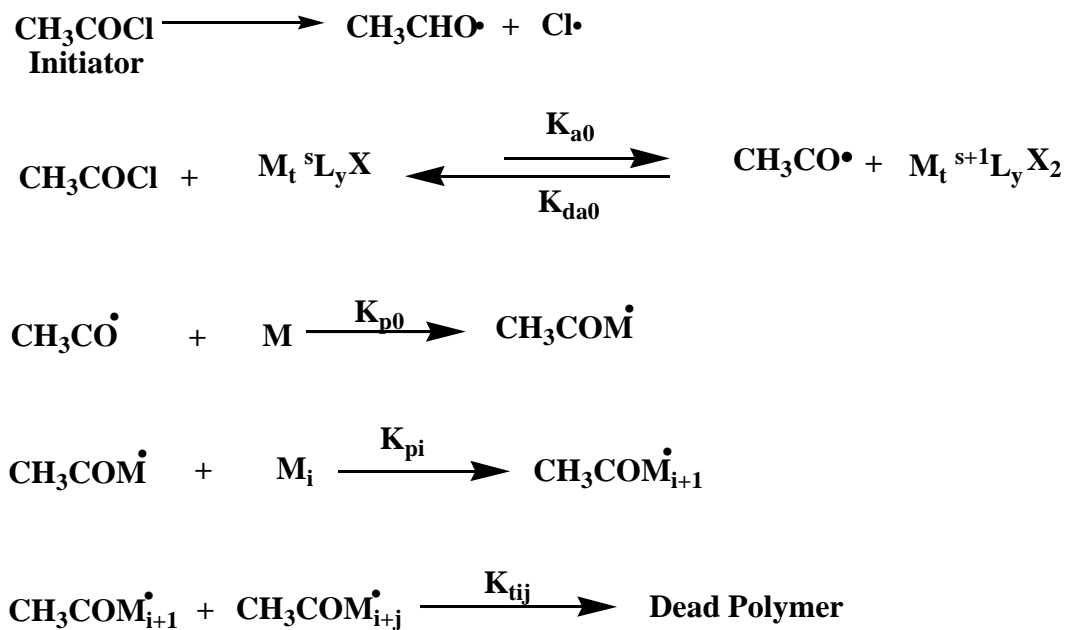


**Figure 5.2** Reaction scheme employed in the process where  $K_a$ ,  $K_p$ ,  $K_t$  are rate coefficients for activation, propagation and termination.

Similar procedures were followed for polymerization of MMA and Styrene using Acylated Nanotubes as initiators. *Acylated nanotubes could be only used as emulsion, due to their insolubility in water.* Acylated nanotubes were prepared by reaction of carboxylated nanotubes with 20 mL of thionyl chloride and 2mL of DMF (dimethyl formamide). The system was properly sealed with grease and teflon, to prevent any moisture contamination and then refluxed for 36 hrs. at 60°C. The product obtained was washed with toluene. The sample was then dried in a vacuum oven at 80 °C for 4 h to get the macro initiator.

For preparation of emulsion of initiator initially distilled water (14.0 ml) was added to 2.3 gm of Brij 98 surfactant and 6 mg of acylated MWCNTs. The solution was sonicated for 1 hr and stirred for 1 hour and 30 minutes using magnetic stirrer. The prepared nanotube emulsion could be used as macro initiator for polymerization process, for either MMA or Styrene. The processes carried out are listed in Table 5.1.

#### **5.4 Characterization**

FT-IR was carried out on Perkin-Elmer spectro photometer at 20 scans using the KBr pellet method. The polymer was confirmed by <sup>13</sup>C NMR. NMR spectra of 10% (w/w) solutions in CDCl<sub>3</sub> were measured at 330K with a Bruker Avance DPX300 spectrometer at 300.13 and 75.45 MHz resonance frequency, respectively. All polymers were characterized by SEC (WATERS) in THF at room temperature at a flow rate of 1 ml/min using a PSS column (5 lm; 103 and 105A °) (PSS, AUSTRIA), equipped with RI detector. Polystyrene standards and the Mark–Houwink constants for the PS/THF system ( $K = 1.17 \times 10^4 \text{ mL g}^{-1}$ ,  $a = 0.717$ ) were used to establish the number average molecular weights ( $M_n$ ) and molecular weight distributions (MWD). The apparent molecular weights ( $M_n$ ) were obtained from here. The TGA data were obtained in Nitrogen atmosphere with mettle Teledo Star SW 7.01 thermo gravimetric analyzer with 7.4640 mg of the specimen at 10 degree centigrade per minute.

**Table 5.1** Various sets performed to obtain polymers.

<b>Monomer</b>	<b>Initiator</b>	<b>Catalyst</b>	<b>Ligand</b>	<b>Temperature</b>
MMA	Acetyl chloride AC	CuCl	2,2' bipyridyl	28 °C
	Acylated nanotubes ANT			60 °C
	Pentanoyl chloride PC			
	Heptanoyl chloride HC			
Styrene	Acetyl chloride AC	CuCl	2,2' bipyridyl	28 °C , 60 °C
	Acylated nanotubes ANT			

## 5.5 *Results and Discussion*

### 5.5.1 **Polymerization of MMA and Styrene**

In a 100 mL round bottom flask, catalyst/ligand complex was nitrogen purged for three times, and to it emulsion of monomer was added under nitrogen atmosphere through cannula, followed by addition of initiator. In present work, a novel initiator, acetyl chloride ( $\text{CH}_3\text{COCl}$ ) and acylated nanotubes were used.

### 5.5.2 **Characterization**

#### 5.5.2.1 **IR Spectra**

In the IR spectra (Figure 5.3a) of the polymer PMMA the peaks corresponding to C=O stretching ( $1737.92\text{ cm}^{-1}$ ), C-O stretching ( $1242\text{ cm}^{-1}$ ), C-H stretching ( $2850\text{-}2960\text{ cm}^{-1}$ ) and C-C stretching ( $1450\text{-}1550\text{ cm}^{-1}$ ) and absence of peak corresponding to C=C stretching at  $1500\text{-}1600\text{ cm}^{-1}$  confirm the formation of polymer. Peak at  $752.26\text{ cm}^{-1}$  corresponds to presence of C-Cl terminal end group in growing (living) polymer chain. In the IR spectra (Figure 5.3b) of the Polystyrene strong bands at  $3021.81\text{ cm}^{-1}/3029.47\text{ cm}^{-1}$  show C-H stretching of aromatic ring and at  $2917.72\text{ cm}^{-1}/2925.03\text{ cm}^{-1}$  showing C-H stretching of aliphatic chain present in polystyrene. The bands shown in from  $1650\text{-}2000\text{ cm}^{-1}$  and near about  $3600\text{ cm}^{-1}$  are overtone and combination bands mainly of aromatic C-H *def* absorption. Overtone bands appear at integer multiples of fundamental vibrations, so that strong absorptions at, say, near  $800\text{ cm}^{-1}$  and  $1750\text{ cm}^{-1}$  will also give rise to weaker absorptions at  $1600\text{ cm}^{-1}$  and  $3500\text{ cm}^{-1}$  respectively. Band between  $1400\text{-}1600\text{ cm}^{-1}$  indicates aromatic C=C bending and between  $860\text{-}680\text{ cm}^{-1}$  indicates aromatic C-H bending.

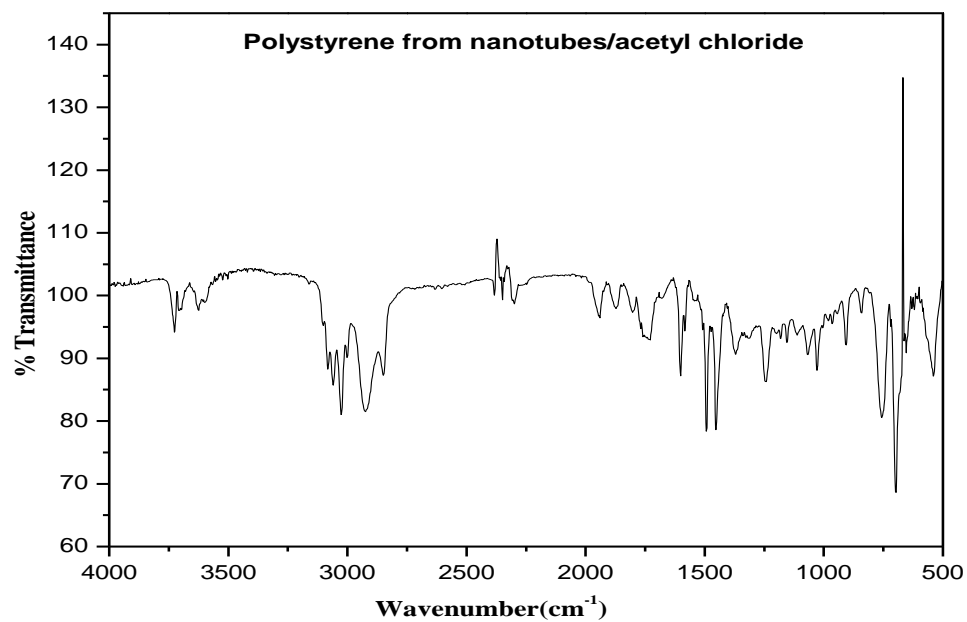
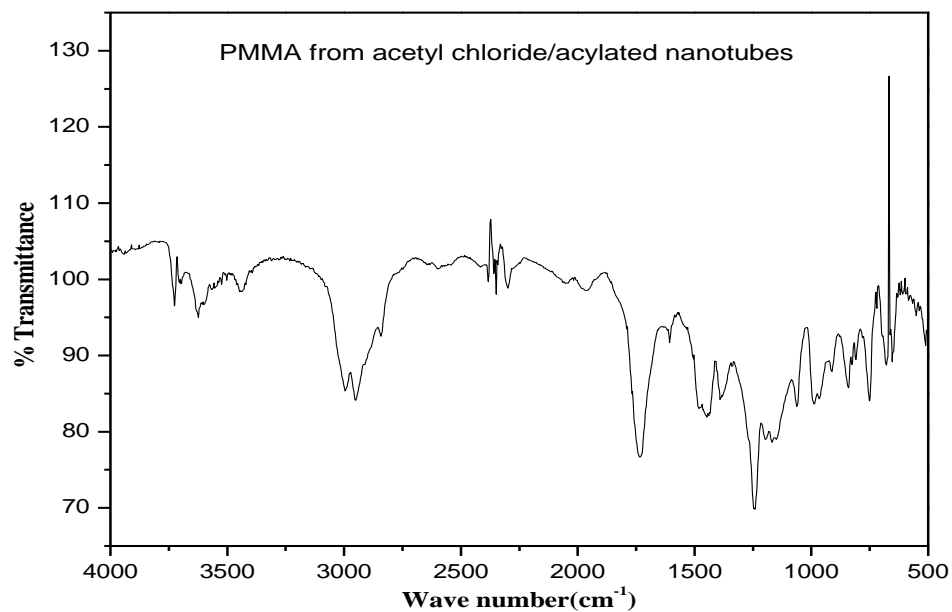


**Figure 5.3** FTIR of (a)PMMA (b) Styrene initiated from acetyl chloride/acetylated nanotubes.

### 5.5.2.2 $^{13}\text{C}$ -NMR

Figure 5.4 shows  $^{13}\text{C}$ -NMR of acetyl initiated PMMA. Peak at 177.938 ppm shows the presence of carbonyl group. Peak at 77.322 ppm shows solvent peak. Peak at 54.479 ppm shows methylene ( $-\text{CH}_2-$ ) group. Peak at 52.174 ppm shows  $-\text{OCH}_3$  group is present. Peak at 44.871 ppm shows quaternary carbon is present. Peak at 19.113 ppm and 16.850 ppm shows two types  $-\text{CH}_3$  groups are present.

The peaks obtained confirm the formation of polymer.

The similar ATRP setup was used with labeled acetyl chloride as initiator. An extra peak (four instead of three) in the range  $170\text{-}190\text{cm}^{-1}$  owing to presence of carbonyl group with labeled carbon ( $^{13}\text{C}=\text{O}$ ) in the end group functionality in NMR spectra of the polymer was obtained (Figure 5.5a). The presence of peaks due to terminal functionalities in the polymer confirms the formation of a living polymer. The results have been verified with standard  $^{13}\text{C}$  NMR PMMA where peaks are matching with the NMR obtained in the study, hereby confirming the formation of polymer using acetyl chloride or acylated nanotubes as initiators (Figure 5.5b).

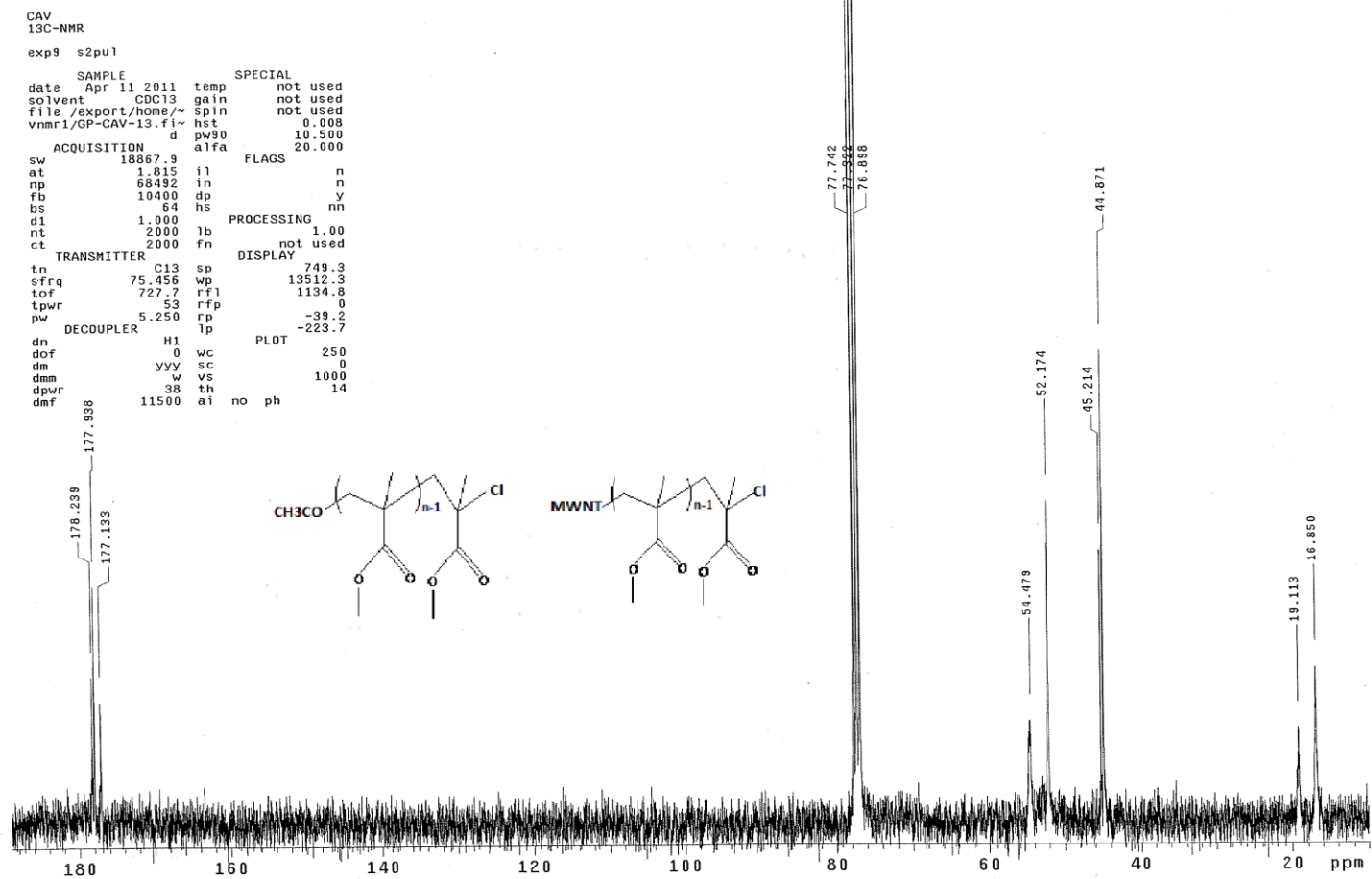


Figure 5.4 NMR of acetylchloride/acetylated nanotubes initiated PMMA.

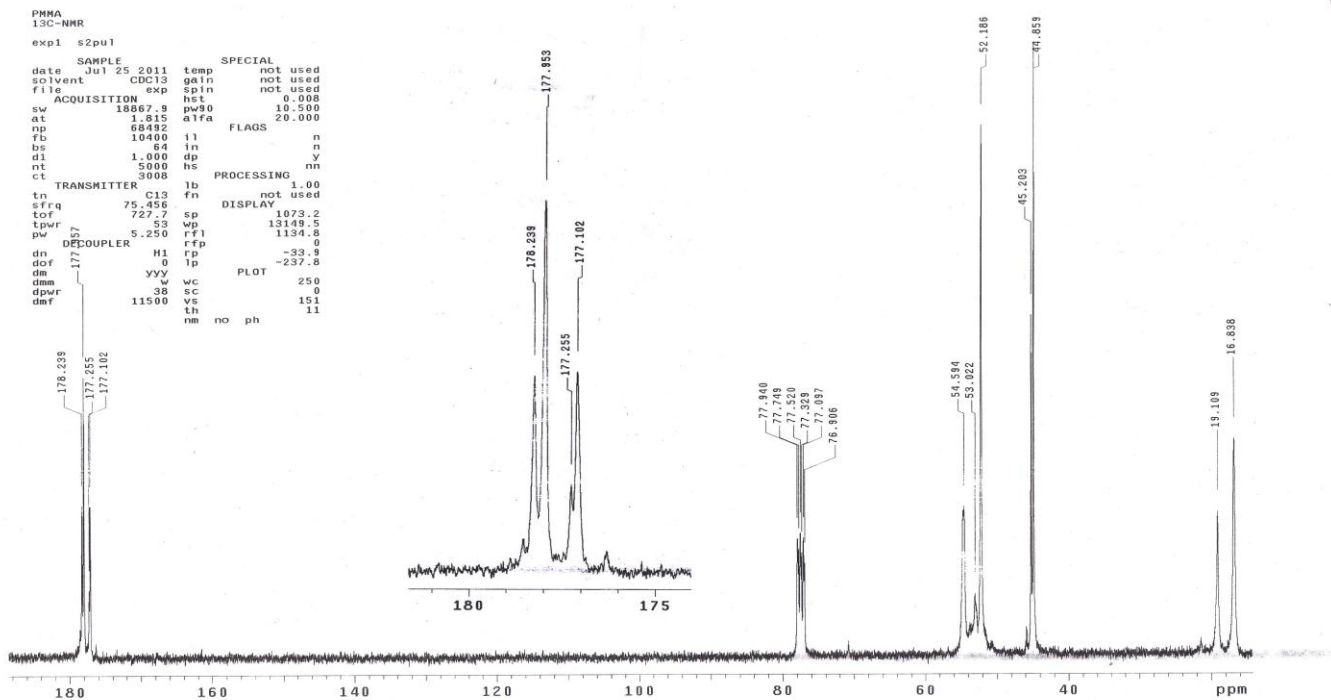


Figure 5.5 (a)  $^{13}\text{C}$  NMR of PMMA obtained from labeled acetyl chloride as initiator

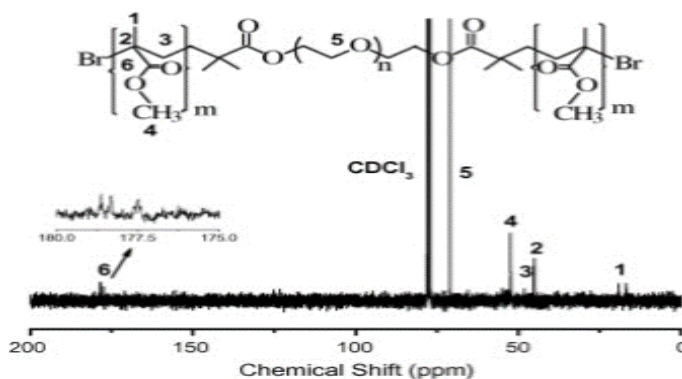
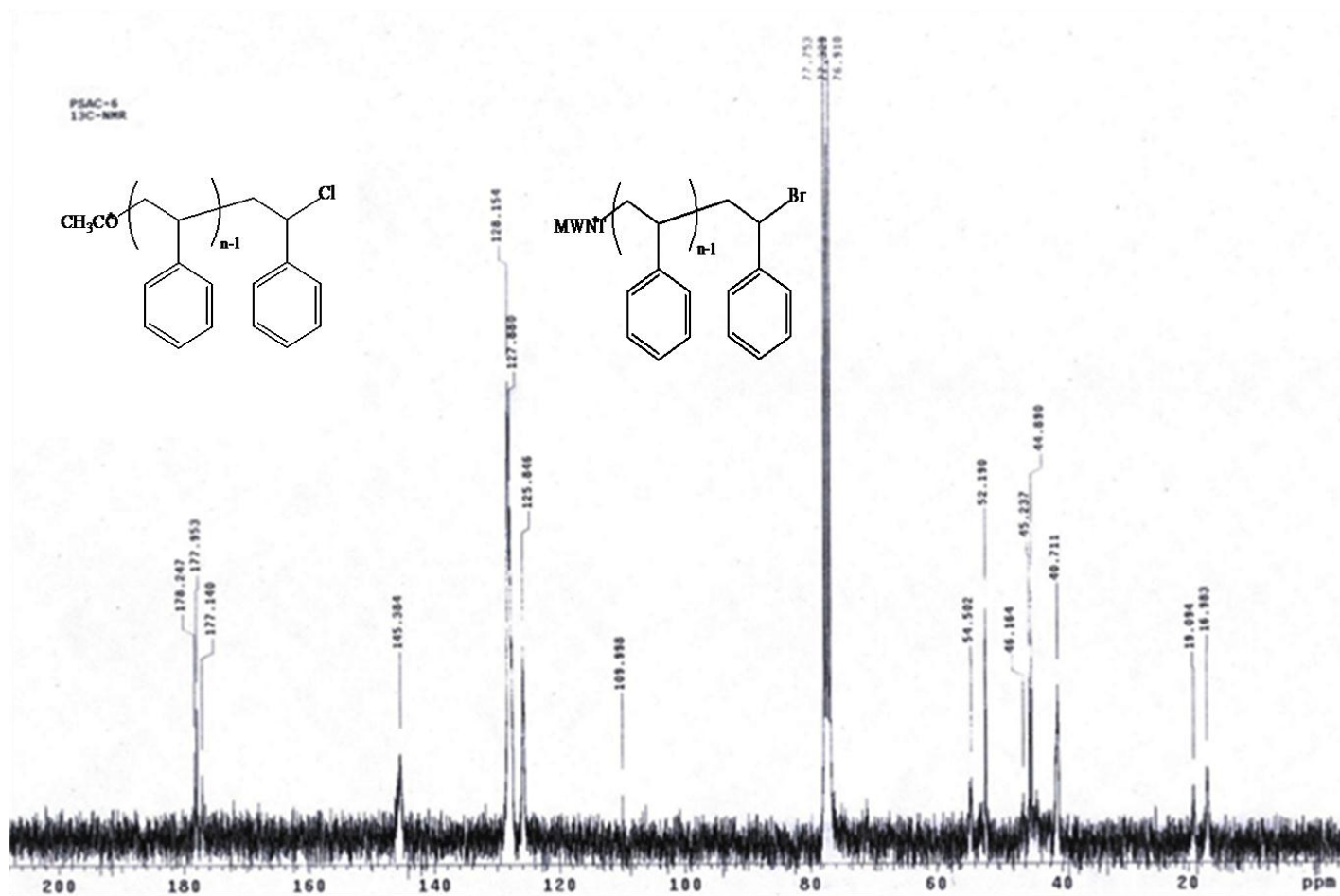


Figure 5.5 (b) Standard PMMA (Dandan Wang et.al *European Polymer Journal* **2007**, 43, 2799-2808)

Presence of  $\text{CH}_3\text{CO-}$  as one of the terminal groups was confirmed by presence of peaks in range 177-178 $\text{cm}^{-1}$  in  $^{13}\text{C}$  NMR of polystyrene prepared by using acetyl chloride as initiator (Figure 5.6). Peak at 128.154/127.880/125.846  $\text{cm}^{-1}$  is obtained due to phenyl ring. Peak at 46.164/45.237/44.890  $\text{cm}^{-1}$  points to presence of Methylene ( $-\text{CH}_2-$ ) group. Peak at 19.094  $\text{cm}^{-1}$  and 16.983  $\text{cm}^{-1}$  indicates the presence of Methyl halide ( $-\text{CH}_2\text{-X}$ ), and Methyl group ( $-\text{CH}_3$ ) groups.

Thus acetyl chloride was confirmed to act as active radical generating initiator molecule both for MMA and Polystyrene.

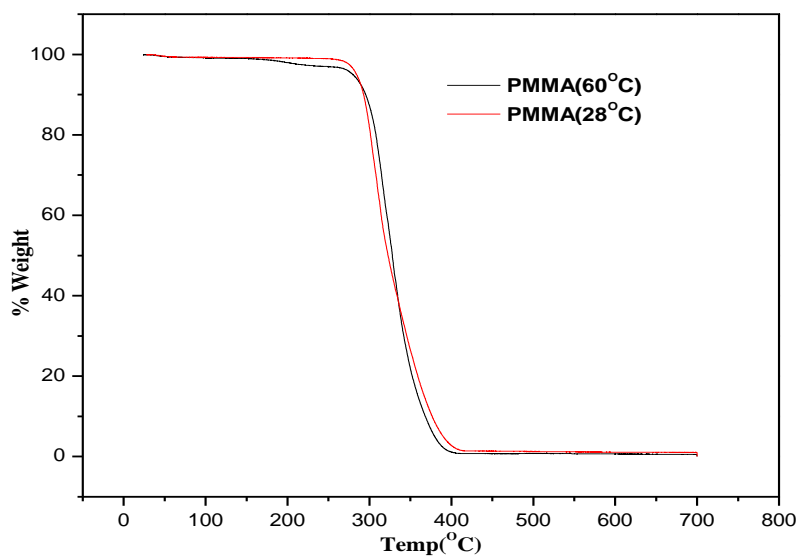
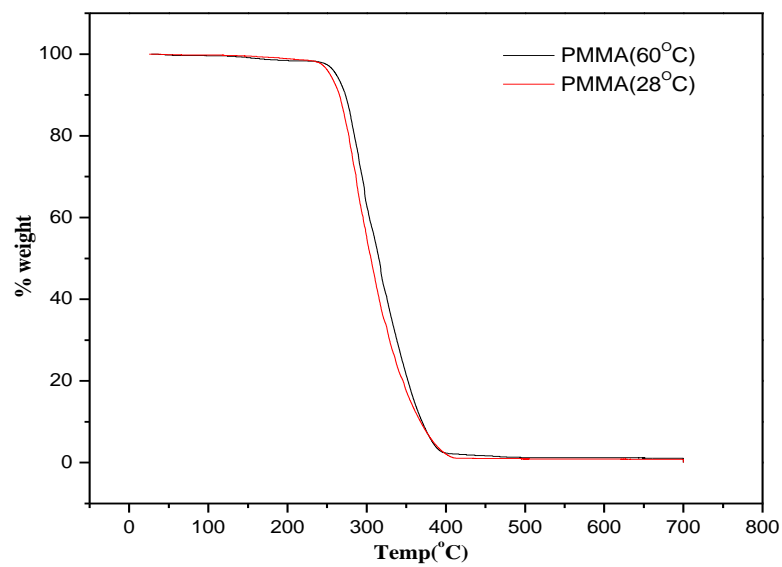


**Figure 5.6** <sup>13</sup>C NMR of Polystyrene obtained from acetyl chloride used as initiator.

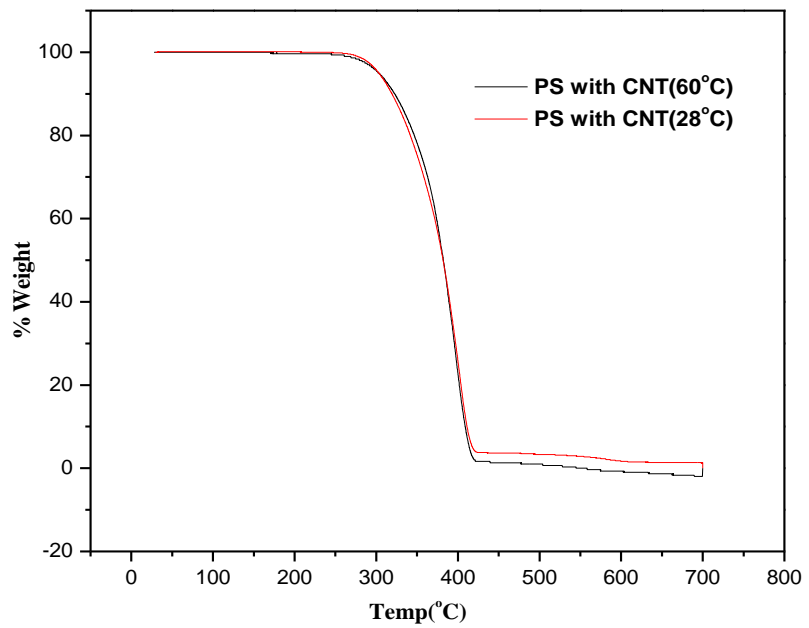
### 5.5.2.3 Thermo-gravimetric analysis

Figure 5.7a shows TGA thermogram of acetyl initiated PMMA polymer. From thermogram it is interpreted that polymer decomposes around 240°C after 22 minutes to around 400°C after 38 minutes. No loss (or decomposition) after around 400°C. The polymer PMMA obtained at 28°C appears to have nearly similar thermal stability as that of the polymer prepared at 60°C. For polymer initiated by acylated nanotubes thermal stability appears to increase as in Figure 5.7b.

From thermogram (Figure 5.8) of polystyrene prepared by acylated nanotubes as initiator, it is seen that polymer decomposition starts at around 308° C to around 421° C. No loss (or decomposition) after 422°C. Polystyrene polymer from conventional methods starts decomposition at around 274° C. From the above results we can say that by using CNTs as an initiator the thermal stability of polymer is increased.



**Figure 5.7** Thermogravimetric analysis of PMMA, obtained by (a) acetyl chloride (b) acylated nanotubes as initiator.



**Figure 5.8** Thermogravimetric analysis of Polystyrene by acylated nanotubes as initiator.

#### 5.5.2.4 DSC :

PMMA can exhibit stereoisomerism tacticity. Changes in tacticity have a significant effect on the glass transition temperature and hence mobility of chain backbone. The  $T_g$  of isotactic polymer is nearly  $48^\circ\text{C}$ , and is significantly lower than that for syndiotactic PMMA ( $T_g=160^\circ\text{C}$ ). Syndiotactic PMMA has been reported to possess lower intramolecular energy, and isotactic PMMA has lower intermolecular energy<sup>209</sup>. The difference in  $T_g$ 's has been attributed to conformational energy difference by MacKnight and Karasz<sup>210</sup>, and to intermolecular interactions by O'Reilly and Mosher<sup>211</sup>. The polymers obtained in present work were observed to possess high glass transition temperature (Figure 5.9 & 5.10)  $T_g=135^\circ\text{C}$  for PMMA and  $T_g=109^\circ\text{C}$  for Polystyrene. This signifies the formation of a highly syndiotactic structure, with high intermolecular and intramolecular interactions and thus effecting the packing structure. As a consequence of these interactions, a fringe micelle structure may be formed with dimensions several times larger than region of specific polymer chain interaction (cross linked structure). This is in accordance with the abnormally high molecular weights obtained by SEC.

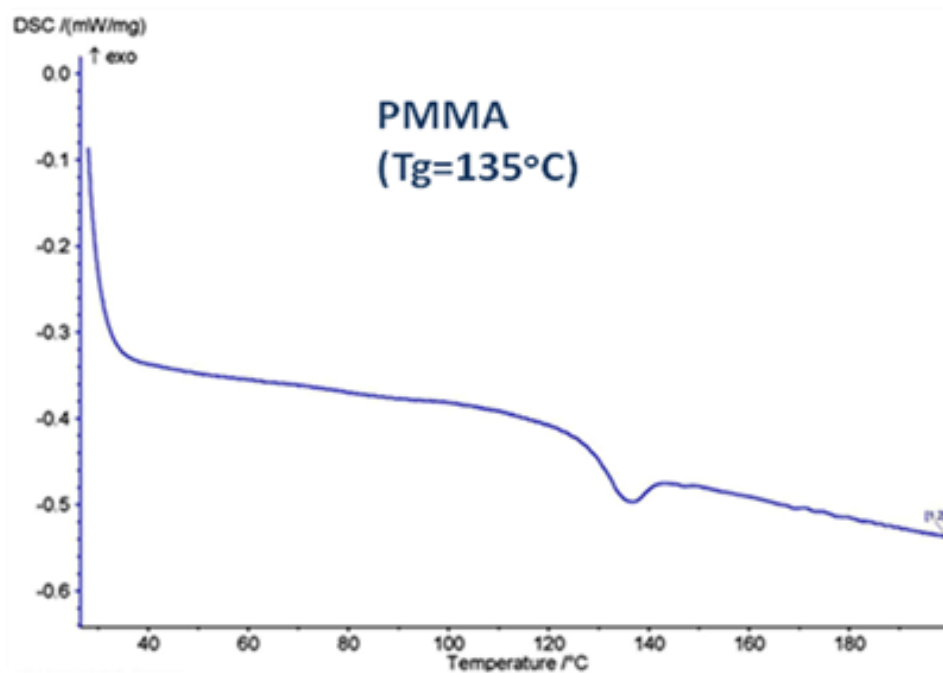


**Figure 5.9** DSC curve for PMMA (glass transition temperature:135°C).

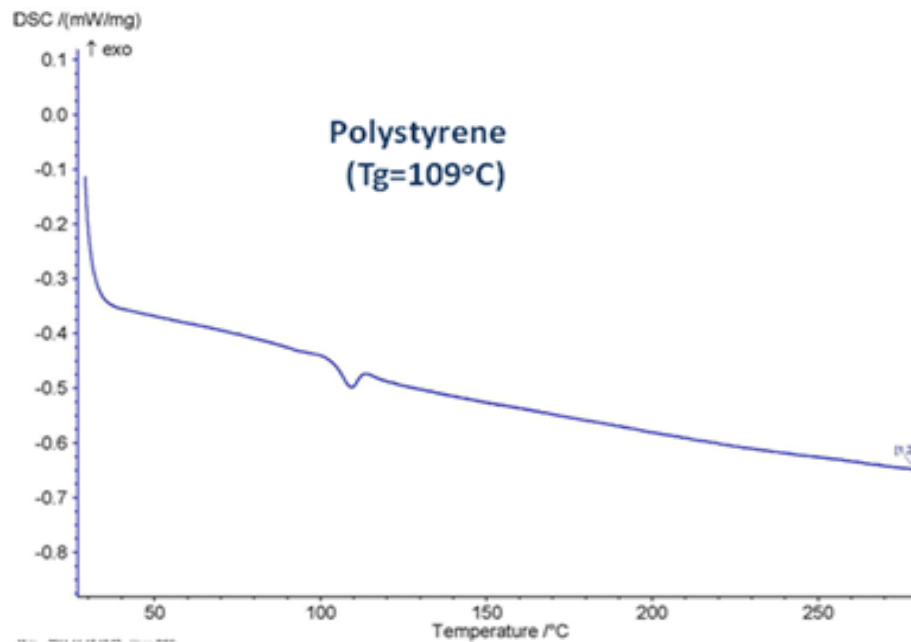


**Figure 5.10** DSC curve for PS (glass transition temperature:109°C).

#### **5.5.2.5 Scanning electron microscopy (SEM)**

Scanning electron microscopy provides information for the shape, morphology and purity of compound. It is also advantageous for investigation of the changes that occurred upon various treatments. SEM photographs (Figure 5.11) of obtained polymer confirm the foamy fibrous texture of polymer. The surfaces are clean and seem to possess no external impurity or traces of side products or unused catalyst/ligand materials.

SEM photographs of PMMA initiated with CNTs clearly show the presence of nanotubes in its texture (Figure 5.12).

SEM photographs of Polystyrene initiated with CNTs have a glassy appearance and a hard texture. The presence of CNT is visible in the SEM images.

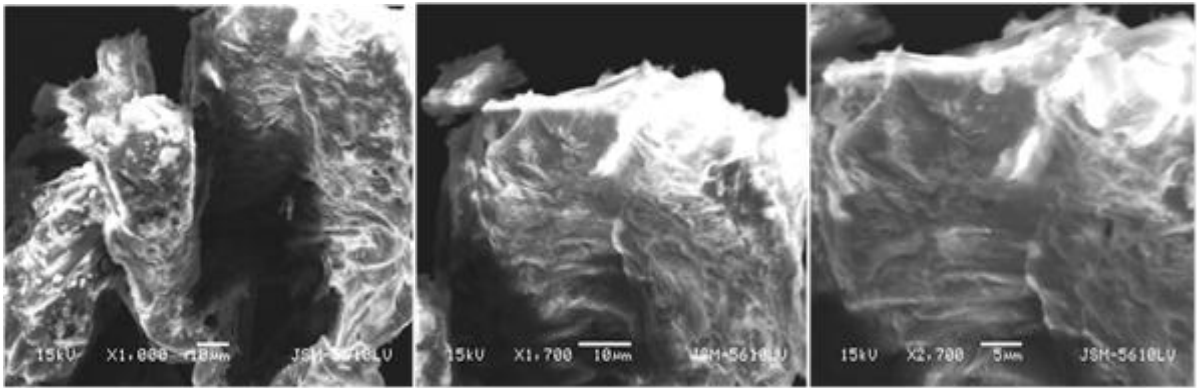


**Figure 5.11** SEM images of polymer PMMA depict the foamy fibrous texture of the polymer.

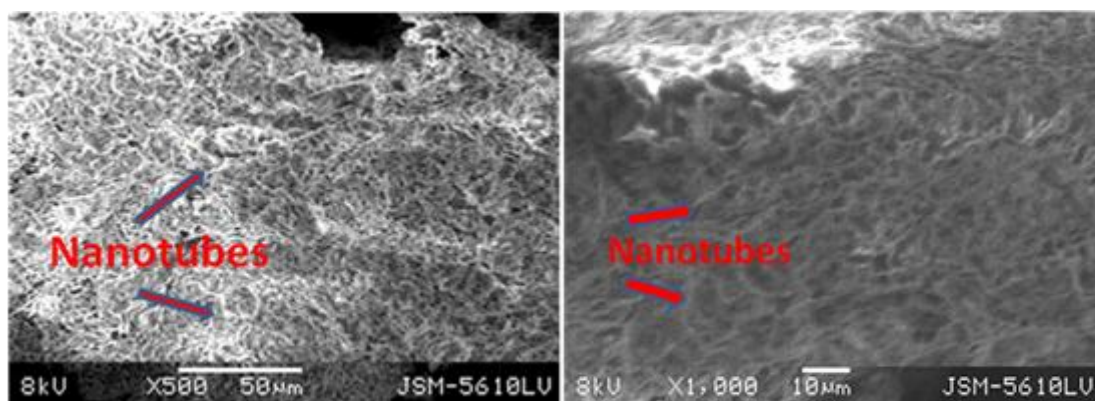


**Figure 5.12** SEM images of polymer PMMA initiated by acylated CNT.

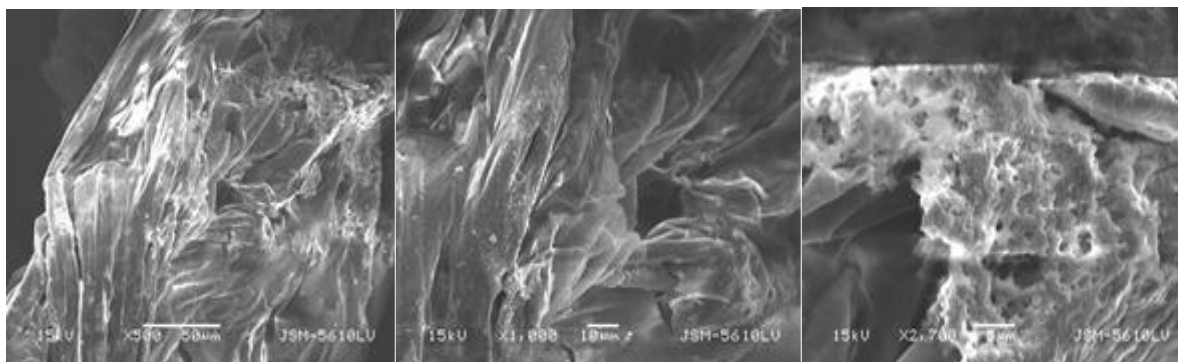


**Figure 5.13** SEM images of PS (polystyrene) initiated by acylated CNT.

### 5.5.2.6 Size exclusion chromatography (SEC)

The number average molecular weights ( $M_n$ ), weight average molecular weights ( $M_w$ ) and polydispersities were determined by GPC.

The GPC results documented the formation of very high molecular weights as compared to  $M_{theo}$

The results obtained in the different sets corresponding to different catalyst/ligand ratio, monomer/initiator ratio, solvent /surfactant ratio in polymerization of MMA by acetyl chloride are as shown in Table 5.2, Figure 5.14, Figure 5.15.

In the first set (S1) ,(catalyst : ligand :: 0.5:1) an emulsion of 4.6 gm of surfactant in 28 ml of distilled water was prepared, and used as solvent for monomer(PMMA). The number average molecular weight ( $M_n$ ) and polydispersities were high as compared to that in ATRP's with other conventionally used ATRP initiators such as alkyl halides.

This can be due to number of reasons, Firstly ATRP itself may result in a broader PDI 1.2-1.7<sup>212</sup> depending on different reaction conditions such as catalyst system, solvent, initiator, temperature etc. Secondly, initiation by acetyl chloride would show a different character as compared to that by conventional methods. High rate of bond dissociation and radical formation tendency in acetyl chloride may disturb the rate of propagation and termination. The  $CH_3CO---Cl$  bond undergoes rapid dissociation and extraction of chloride radical under the effect of catalyst/ligand system.

In the second set (S2) catalyst :ligand ratio was changed to 1:1 ,all other conditions remaining the same. The  $M_n$  was less then ,that in set 1 but polydispersity was more.

In the sets 3,4 (S3,S4)the initiator amount was increased ,but the molecular weights were still higher, though the polydispersities were slightly close to 1.

**Table 5.2** % conversions, weight average molecular weights and polydispersities for different sets.

Sets	Molar ratio M : C : L : I	Surfactant gm/10mL Solvent	Temperature (°C)	Time (h)	% Conv.	M <sub>theo</sub>	Mn 1 x 10 <sup>5</sup>	Mw/Mn
S1	100:0.5:1:0.625	1.64	28	20	92	14798	4.42	1.26
S2	100:1:1:0.625	1.64	28	20	91.3	14686	1.65	1.47
S3	100:0.5:1:1.25	1.64	28	20	94	7598	5.33	1.13
S4	100:1:1:1.25	1.64	28	20	93.5	7558	2.84	1.23
ST	100:0.5:1:0.625	1.64	60	20	92	14798	2.84	1.19
PMLS	100:0.5:1:0.625	0.82	28	20	93	14958	7.22	1.05
PMVLS	100:0.5:1:0.625	0.41	28	20	93	14958	6.55	1.07
PMNS	100:0.5:1:0.625	0.00	28	20	17	2798	1.11	1.10

Monomer(M) = MMA (methyl-methacrylate), Catalyst(C) = CuCl, Ligand(L) = 2,2' bipyridyl,  
Initiator(I) = acetyl chloride, Surfactant= Brij 98, Solvent = water

S1--S5 : PMMA prepared in sets 1-4 at room temperature

ST : PMMA prepared at 60°C

PMLS : PMMA prepared with low surfactant concentration

PMVLS: PMMA prepared with very low surfactant concentration

PMNS: PMMA prepared with no surfactant

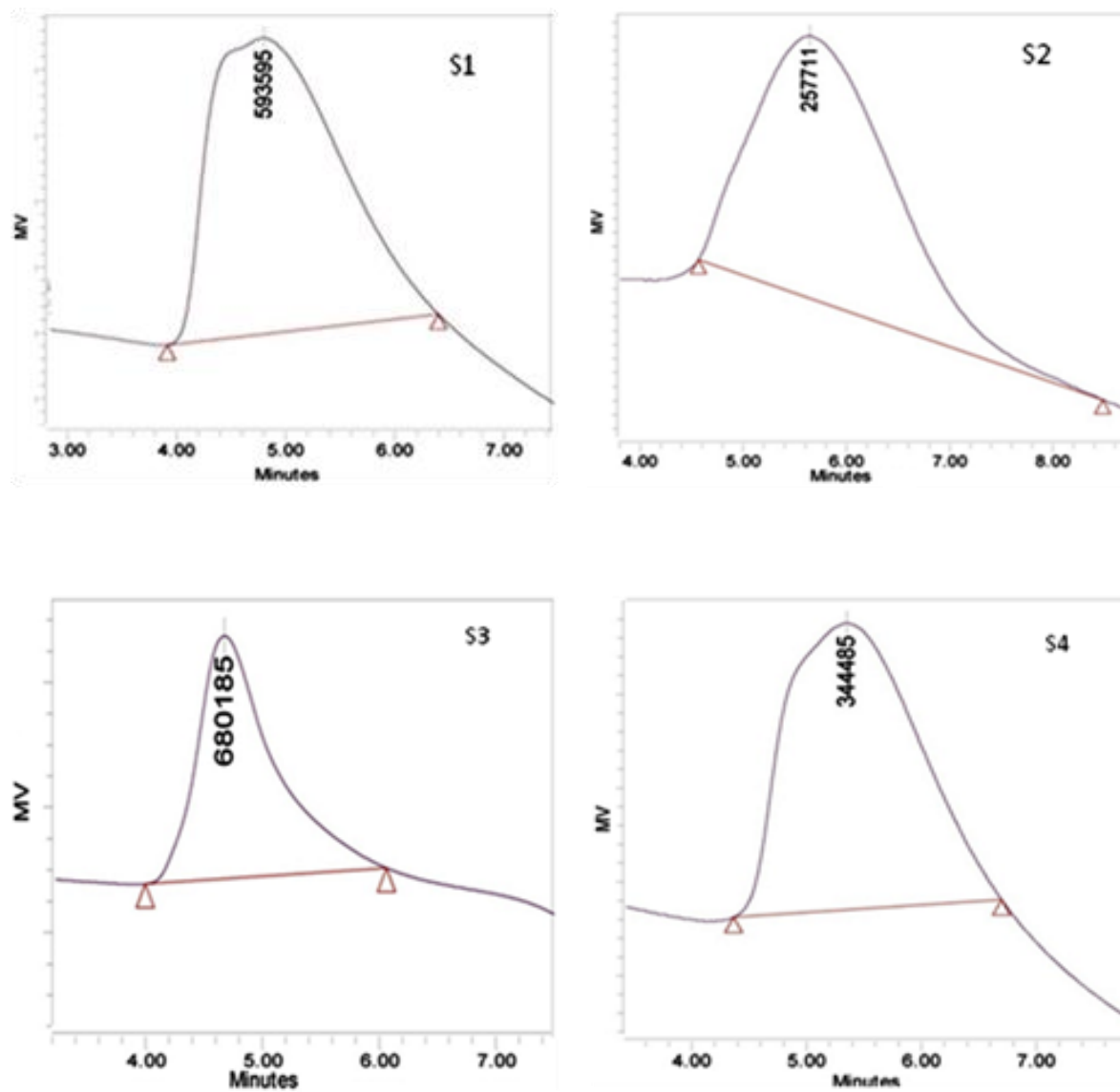


**Figure 5.14** SEC curves for different sets S1, S2, S3, S4 depicting the peak apex and weight average molecular weight.

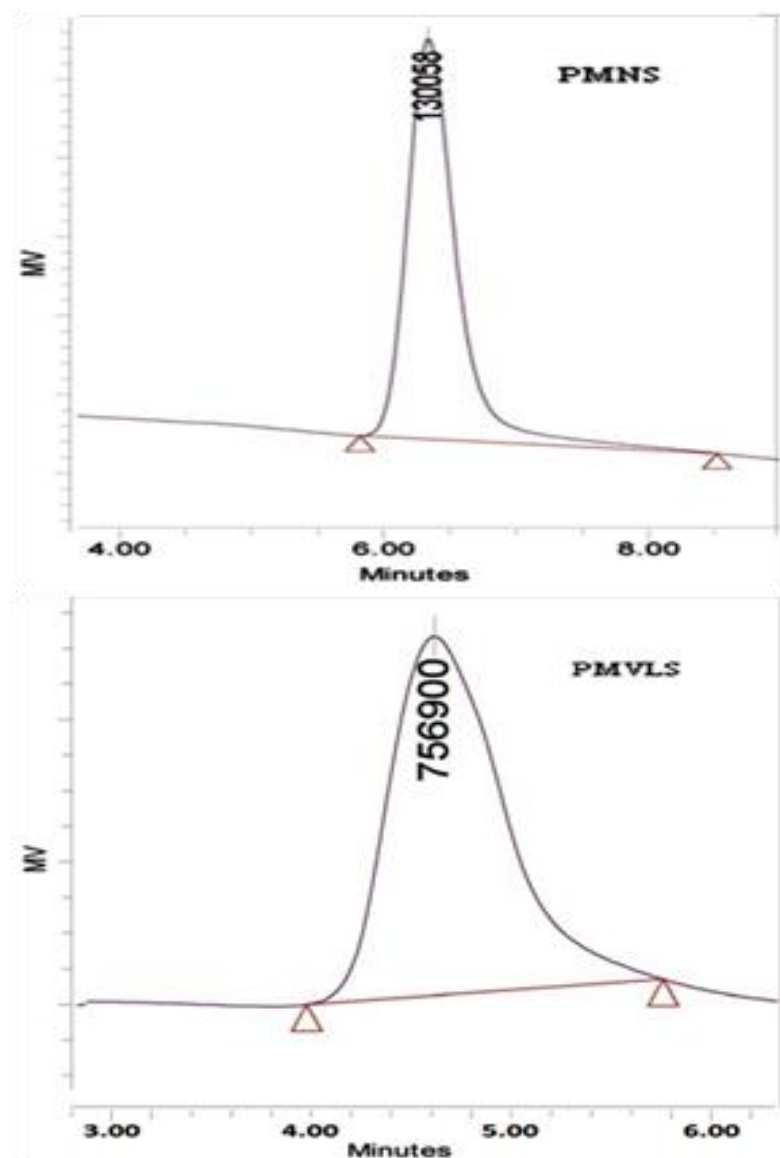


**Figure 5.15** SEC curves for different sets PMNS and PMVLS depicting the peak apex and weight average molecular weight.

In the fifth set (ST) ,all conditions being same as in set 1 ,polymerization was carried out at high temperature (60°C). When the reaction proceeds at high temperature, as a result of higher activation energy for radical propagation than for radical termination, higher  $k_p/k_t$  ratios and better control is observed and thus syndiotactic polymer is dominated by isotactic species and comparatively low MW 's are obtained, but the polydispersities were still higher as compared to Sets(1-4).

When the surfactant amount was reduced, the emulsion was still stable. Set 6 (PMLS) contained 2.3g of Brij-98 where as Set 7 contained 1.15g of the surfactant. Set 8 did not contain any surfactant.

The polydispersities were found to decrease with reducing surfactant amount. The average molecular weights were found to drastically decrease to  $1.11 \times 10^5$  when no surfactant was used in Set 8 (PMNS).

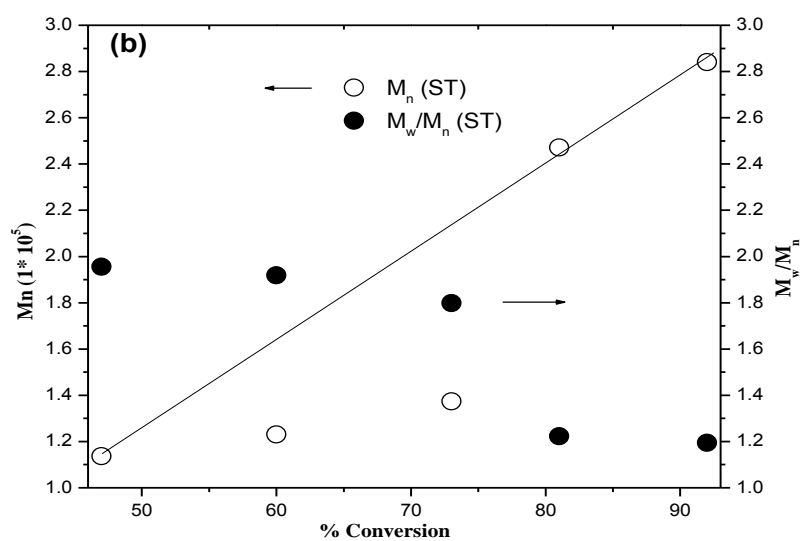
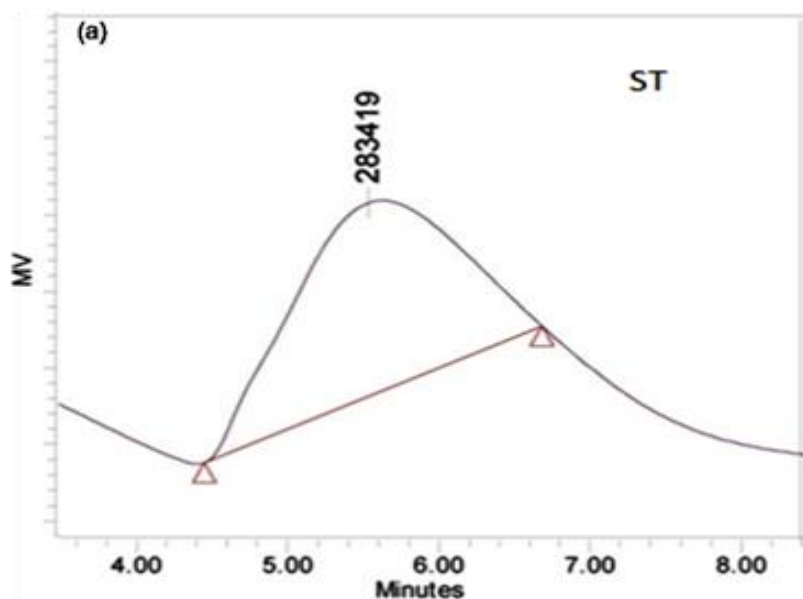
#### **5.5.2.7 Kinectic studies**

Figure 5.16(a,b) and Table 5.3 presents polydispersity (PD) and average number molecular mass ( $M_n$ ) as a function of monomer conversion for ATRP of MMA 60°C. Polymer fractions were obtained at different time intervals by quenching the reaction at different times. At higher monomer conversions PD becomes very low(<1.20). A linear increase of number average molecular weight  $M_n$  (determined by size exclusion chromatography calibrated using polystyrene standards) versus monomer conversions up to 81% was found after 2h and up to 92% after 20h.

The graphs obtained indicate that Acetyl chloride act as efficient initiator. Initially the polydispersities are quite higher but are reduced to nearly one at higher conversions.

**Table 5.3** Kinetic study of ATRP of PMMA at high temperature using acetyl chloride as initiator  
(ST1-ST5)

Sets	Molar ratio M : C : L : I	Temperature (°C)	Time (h)	%Conversion	$M_{theo}$	$M_n$ ( $1 \times 10^5$ )	$M_w/M_n$
ST1	100:0.5:1:0.625	60	0.5	47	7598	1.13	1.95
ST2			1.0	60	9678	1.23	1.91
ST3			1.5	73	11758	1.35	1.79
ST4			2.0	81	13038	2.47	1.22
ST5			20	92	14798	2.84	1.19



**Figure 5.16** (a) SEC curve for acetyl chloride initiated ATRP of MMA depicting  $2.83 \times 10^5$  and  $2.84 \times 10^5$  as peak apex and weight average molecular weight respectively (b) PD and Mn as a function of monomer conversion ; reaction conditions: Temperature =  $60^\circ\text{C}$  and  $[M]_0/[M_t^sX]_0/[L]_0/I_0 = [PMMA]_0/[Cu(1)Br]_0/[2,2' \text{ bipyridyl}]_0/[CH_3COCl]_0 = 100:0.5:1:0.625$  and surfactant (Brij-98) concentration = 1.64gm/10 mL of distilled water.

Similar studies were also performed for set PMLS where the surfactant amount was reduced to 0.82 gm/10ml which was 1.64gm/10mL in earlier sets. Linear relationships of  $M_n$  and PD's with %conversion confirm it to be a efficient ATRP system(Table 5.4, Figure 5.17).A linear plot of  $\ln([M]_0/[M])$  versus polymerization time indicate that the concentration of growing radicals remains constant, and termination is not significant. Both of these results suggest a “living” radical polymerization with negligible number of transfer and termination reactions.

The molecular weights were high as compared to those obtained in other sets, but polydispersities were very close to ideal value (i.e. 1). The reaction showed 89% completion after 2h and conversion was 93% after 20h.

**Table 5.4** Kinetic study of ATRP of PMMA at low surfactant concentration (PMLS) using acetyl chloride as initiator.

Sets	Molar ratio M : C : L : I	Temperature (°C)	Time (h)	%Conversion	M <sub>theo</sub>	Mn 1 x 10 <sup>5</sup>	Mw/Mn
PMLS1	100:0.5:1:0.625	28	0.5	45	7278	1.71	1.075
PMLS2			1.0	64	10318	3.96	1.068
PMLS3			1.5	76	12238	5.27	1.065
PMLS4			2.0	89	14318	6.00	1.060
PMLS5			20	93	14958	7.22	1.056

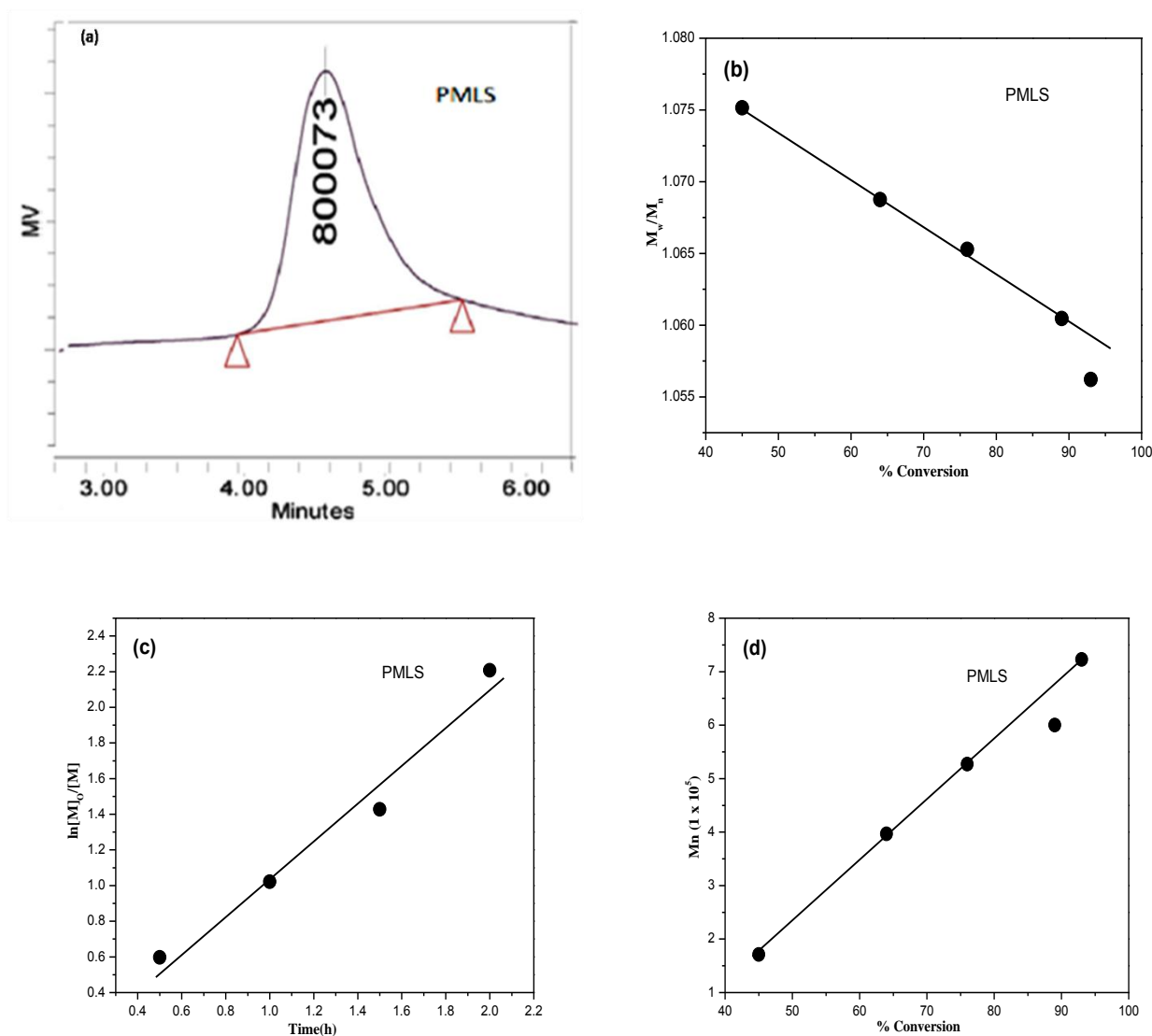


**Figure 5.17** (a) SEC curve for acetyl chloride initiated ATRP of MMA depicting  $8.0 \times 10^5$  and  $7.2 \times 10^5$  as peak apex and weight average molecular weight respectively (b) PD as a function of %Conversion(c)  $\ln[M]_0/[M]$  versus time and (d)  $M_n$  as a function of %Conversion; reaction conditions: Temperature =  $28^\circ\text{C}$  and  $[M]_0/[M]_0^s/[L]_0/I_0 = [\text{PMMA}]_0/[\text{Cu(1)Br}]_0/[2,2'$  bipyridyl] $]_0/[\text{CH}_3\text{COCl}]_0=100:0.5:1:0.625$  and surfactant (Brij-98)concentration =  $0.82\text{gm}/10\text{ mL}$  of distilled water.

Similar results were obtained for Polystyrene polymer, where polymerization was carried out at room temperature as well as at high temperature of 60°C. Kinetics was performed and % conversions were evaluated. High average molecular weights were obtained as compared to theoretical values, but were less as compared to those in PMMA. Linear relationships of Mn and PD's with %conversion and a good linear plot of  $\ln([M]_0/[M])$  versus polymerization time indicate a good efficient ATRP system(Figure 5.18,Table 5.5,5.6).

**Table 5.5** Kinetic study of ATRP of Polystyrene at room temperature (PS1-PS5) using acetyl chloride as initiator.

Sets	Molar ratio M : C : L : I	Temperature (°C)	Time (h)	%Conversion	M <sub>theo</sub>	Mn 1 x 10 <sup>5</sup>	Mw/Mn
PS1	100:0.5:1:0.625	28	0.5	67	11242	1.99	1.50
PS2			1.0	73	12242	2.21	1.42
PS3			1.5	81	13575	2.41	1.35
PS4			2.0	89	14908	2.46	1.34
PS5			20	94	15472	2.99	1.22

**Table 5.6** Kinetic study of ATRP of Polystyrene at 60°C (PST1-PST5) using acetyl chloride.

Sets	Molar ratio M : C : L : I	Temperature (°C)	Time (h)	%Conversion	M <sub>theo</sub>	Mn 1 x 10 <sup>5</sup>	Mw/Mn
PST1	100:0.5:1:0.625	60	0.5	67	11242	1.07	1.67
PST2			1.0	71	11909	1.09	1.56
PST3			1.5	82	13742	1.16	1.54
PST4			2.0	92	15408	1.31	1.49
PST5			20	95	15908	1.38	1.40

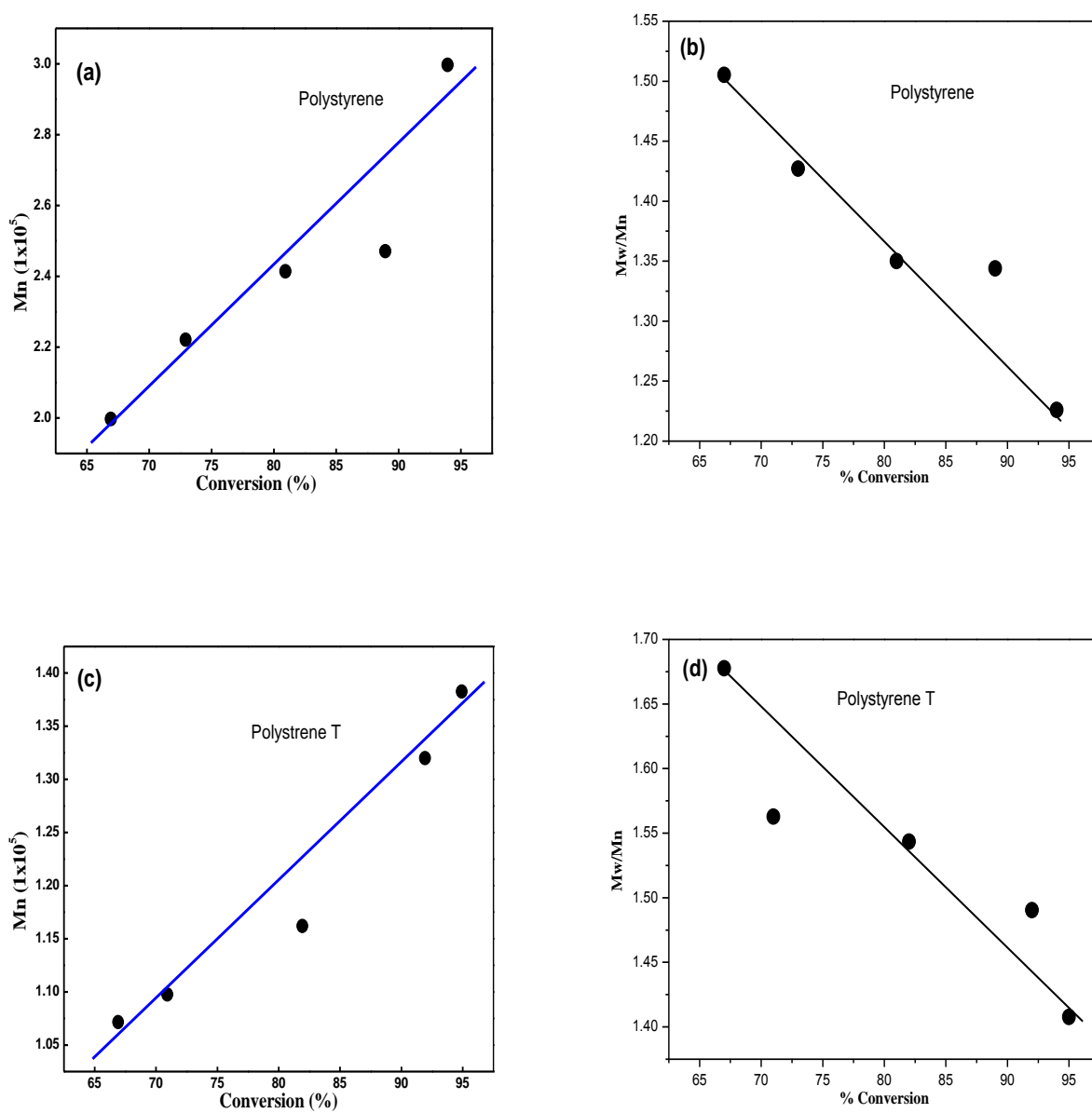


**Figure 5.18** (a) Mn as a function of %Conversion (b) PD as a function of %Conversion for polystyrene at room temperature (c) Mn as a function of %Conversion (b) PD as a function of %Conversion for polystyrene at high temperature:  $[M]_o/[M_t^sX]_o/[L]_o/I_o = [Polystyrene]_o/[Cu(1)Br]_o/[2,2' \text{ bipyridyl}]_o/[CH_3COCl]_o = 100:0.5:1:0.625$  and surfactant (Brij-98) concentration = 1.64gm/10 mL of distilled water.

The observed initiation by acyl radicals can be explained from the energetics of CO–X and Cu–X bonds, equilibrium and termination reactions at the initiation stage, and some side reactions for CO–Cl species. . High rate of bond dissociation and radical formation tendency in acetyl chloride may disturb the rate of propagation and termination. The formation of CH<sub>3</sub>CO· (acyl free radical ) from acetyl chloride can be explained to be taking place under effect of catalyst/ ligand complex as in conventional ATRP (where the catalyst/ligand complex extracts chlorine free radical from a molecule having a readily removable halogen atom, and combines with it). Formation of acyl radical can be explained from it's stability and ability to attack a carbon-carbon double bond. It has been reported that the acyl free radicals appear to react as units below 100°C and do not decompose into alkyl radicals and carbon monoxide<sup>213</sup>. It has been estimated that in the gas phase, the activation energy in reaction is 16±3 Kcal (Figure 5.19). Consequently the reverse reaction, of combination of carbon monoxide and alkyl radical has little or no activation energy.

This accounts for the fact that acyl radicals have sufficient stability at room temperatures and do not show any decomposition. In contrast to this at higher temperatures, acyl radicals decompose to give alkyl radicals and carbon monoxide. At temperatures lower than 100°C, these acyl radicals have ability attack at alkene carbon. In the above study it was confirmed that in a system containing carbon monoxide, alkyl free radicals and alkene, the reaction of alkyl radicals with ethylene has greater activation energy as compared to that of reaction of acyl free radical with alkene to undergo polymerization (Figure 5.20), and thus there is a rapid attack of acyl radical on double bond which helps in polymerization of ethylene.



**Figure 5.19** Activation energies for decomposition acyl radicals and formation of acyl radical.

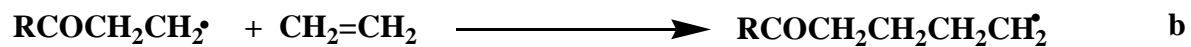


**Figure 5.20** Action of acyl radical on double bond(a) and subsequent propagation to help in polymerization of ethene(b).

Acyl free radicals at higher temperature could be made stable at very high pressures of 600-1000 atm<sup>214</sup>.  $\alpha$ -phenyl propionyl radicals have relatively less stability as compared to propionyl free radicals due to resonance stability in  $\alpha$ -phenyl ethyl radical, but still at low temperature the former shows good stability and rapid addition to double bonds to polymerize styrene<sup>215</sup>.

In presence of solvents such as water and methanol, there is some possibility of the reaction of complexed radical with solvent (for example, methanol) to form an acylated product and hydrogen radical, which then can attack double bond, to form polymer.

The presence of  $\text{CH}_3\text{CO-}$  as one of the terminal groups was confirmed by presence of peaks in range  $177\text{-}178\text{cm}^{-1}$  in  $^{13}\text{C}$  NMR of polystyrene prepared by using acetyl chloride as initiator show that, though hydrogen radical is formed due to reaction of solvent and acyl radical in some amount, there is sufficient acyl radical available to cause polymerization. The activation energy for reaction of acyl radical with double bonds is less than the activation energy of reaction for combination of acyl radical with solvent and release of hydrogen radical. So polymerizations of MMA and Styrene with a appreciable yield was obtained using these initiator in ATRP. However this polymerization leads to a highly cross-linked structure with higher MW's as compared to the theoretical values(as confirmed by GPC ). One reason for the high MW's could be that the termination reaction by combination of two acyl radicals does not interrupt the reaction, since the formation of  $\alpha,\alpha$ -diketones is relatively slow, and they can only add to the monomer and initiate polymerization.

## 5.6 Conclusions

Polymerization is fast with acetyl chloride ( $\text{CH}_3\text{COCl}$ )/CuCl as the catalytic system. The linear plots of  $\ln[M]_0/[M]$  with time confirm the process to follow first order kinetics. The linear variation of polydispersity and average molecular weight with %conversion also account to formation of a polymer with good molecular weight distribution. But at the same time uncontrolled radical dissociation of acetyl chloride in ATRP of MMA and Styrene leads to formation of highly cross linked structures with very high molecular weights. Molecular weights do not follow the theoretical values; however,  $\text{CH}_3\text{COCl}$ /CuCl as catalysts give high conversion rates presumably due to the transfer process. Polydispersities decrease with conversion for these systems, and they are the lowest for systems with less surfactant concentration. The polydispersities follow similar trend with high surfactant concentration at high temperatures ( $60^\circ\text{C}$ ), but abnormally high polydispersities are found at low conversions, which are reduced to nearly one at the end of reaction. The phenomena observed can be explained by the energetics of  $\text{CO-X}$  and  $\text{Cu-X}$  bonds, equilibrium and termination reactions at the initiation stage, and some side reactions for  $\text{CO-Cl}$  species. Acetyl chloride is easily activated to form high concentrations of radicals. The formed acyl radicals have stability at temperatures below  $100^\circ\text{C}$  owing to high activation energy for decomposition reaction, and thus formed stable acyl free radicals rapidly take part in polymerization reaction. However, acetyl ( $\text{CH}_3\text{CO}\cdot$ ) radicals do not terminate bimolecularly, since the formation of  $\alpha,\alpha$ -diketones is relatively slow. Thus, they can only add to the monomer and initiate polymerization.

## Summary of thesis

Carbon nanotubes (CNTs) are wonder materials and new allotropes of carbon a very high aspect ratio. These cylindrical carbon molecules have unusual properties, which are valuable for nanotechnology, electronics, optics and other fields of materials science and technology. Due to their extraordinary thermal conductivity and mechanical and electrical properties, carbon nanotubes find applications as additives to various structural materials. CNTs can be used to prepare novel materials such as hydrogen storage materials, super conductors, reinforced materials etc.

They have very large surface areas, and large exposed surface areas show tremendous adsorption ability. Adsorption heterogeneity and hysteresis are two widely recognized features of organic chemical-CNT interactions. Different mechanisms mainly hydrophobic interactions, pi-pi bonds, electrostatic interactions, hydrogen bonds, and adsorption of organic chemical adsorption on CNTs may account for adsorption behavior. Adsorption mechanisms will be better understood by investigating the effects of properties of both CNTs and organic chemicals along with environmental conditions. Due to their adsorption characteristics CNTs have potential applications in separation sciences and water treatment.

This thesis describes the various methods of synthesis of various types of CNTs and their basic properties, basically related to adsorption behavior.

This thesis also explains the water crises in India and the available water recourses. The various technologies used for water purification as sulfide precipitation, carbonate precipitation, solvent extraction, cementation, ultrafiltration and nanofiltration membrane processes, reverse osmosis etc. have been described. Thus use of nanotubes as an advancement over conventional methods has been described.

The use of carbon nanotubes in pure or composite forms forms the major base of present study. The nanosize materials also have the capacity of altering the pore diameters of polymeric membranes. This property has been used for heavy metal rejection studies using only carbon nanotubes and CNT/Polysulfone nanocomposite membranes, where effect of addition of CNTs to polysulfone has been recorded in terms of porosity and hydrophilicity variation.

This thesis also explains the water crises in India and the available water recourses. The various technologies used for water purification as sulfide precipitation, carbonate precipitation, solvent extraction, cementation, ultrafiltration and nanofiltration membrane processes, reverse osmosis etc. have been described.

## **Chapter 2**

This chapter describes the metal rejection behavior of CNT's without functional groups and with different functional groups such as oxidized, acylated, reduced, amide and azide functionalized CNT's. Cleaned nanotubes were treated with various chemical reagents to introduce  $-\text{COOH}$ ,  $-\text{OH}$ ,  $-\text{COCl}$ ,  $-\text{CONHCH}_2\text{CH}_2\text{NH}_2$  groups respectively onto CNT surface. The overall rate constant for physisorption reaction for all metal ions onto CNT's with varying functional groups have been studied and compared.

Batch adsorption isotherm studies have been conducted by using five concentrations (900, 1000, 1500, 1750 and 2500  $\mu\text{g/L}$ ) of Chromium solution at pH 3.5 and  $25\pm 1^\circ\text{C}$ . The amount of metal ion adsorbed by amide and azide functionalized CNTs per gram ( $Q_e$  mg/g) was calculated.

It was confirmed that % removal is a function of time and continuously increases with time of contact, upto a point where equilibrium is reached. At equilibrium the adsorption process becomes steady and does not increase with increase in contact period. Maximum adsorption and thus

percentage removal is observed for Chromium followed by that of Lead. It has been observed that the Freundlich model is more suitable to fit the adsorption data than Langmuir model since the correlation coefficients are higher.

### Chapter 3

In this chapter, we perform a systematic analysis of the chemical oxidation of MWNT's treated by various reagents that possess different degrees of oxidation power. The cleaned graphitic surfaces were treated with acid mixture ( $\text{H}_2\text{SO}_4$ ,  $\text{HNO}_3$ ), acid piranha ( $\text{H}_2\text{SO}_4$ ,  $\text{H}_2\text{O}_2$ ), base piranha ( $\text{NH}_4\text{OH}$ ,  $\text{H}_2\text{O}_2$ ) and  $\text{KMnO}_4$ ,  $\text{CH}_3\text{COOH}$  in presence of a phase transfer catalyst. All the reactions were performed at room temperature for 1-2 h. All these processes gave different results in respect to degree and type of functionalization, cutting of lengths and damage of sidewalls, which have been reported in this chapter. The surface morphology and surface concentration of functional groups were determined by various analytical techniques such as SEM, FT-IR, Raman and Titration analysis. The functionalized CNT's material were quantitatively analyzed by titration analysis using a standard strong acid-base titration procedure to determine the  $-\text{COOH}$  concentrations on their surface of the treated CNTs. TGA curves with different degradation points were obtained, according to various functional groups and have been included in this chapter to account for the presence variation in degree and type of functionalization. Oxidation with  $\text{H}_2\text{SO}_4/\text{HNO}_3$  under extreme conditions (reflux) increases the defect formation, shortens the length and gives highest degree of functionalization. The degree of defect formation and functionalization followed the trend  $\text{H}_2\text{SO}_4/\text{HNO}_3 > \text{Base piranha} > \text{Acid piranha} > \text{KMnO}_4$ . Use of non-acidic treatments such as the mixture of  $\text{NH}_4\text{OH}$  and  $\text{H}_2\text{O}_2$ , facilitates the complete removal of carbonaceous materials and gives good number of functional groups, though less as compared to treatment with acid mixture but better as compared to acid piranha.

## Chapter 4

In this chapter various studies related to flux improvement, pore structure and size control have made polysulfone/CNT composite membranes. In the present study modified CNT's (oxidized, amide and azide functionalized) were used to enhance the interaction with the polysulfone matrix. The prepared composite membranes were characterized by FT-IR, SEM, TGA.

Pore size and contact angle measurements have been carried out to show that presence of MWNT's remarkably decrease the pore size and contact angle, and increase the hydrophilicity of membranes.

The FTIR spectra of blend membranes have been shown to confirm the presence of hydrogen bond interaction between functional groups of CNT's and sulfonic groups of polysulfone membrane.

MWNTs owing to their high mechanical and heat resistance, offer increased heat tolerance to composite membranes. Heavy metal rejection studies have been carried out for  $\text{Cr}^{+6}$ ,  $\text{Cd}^{+2}$ ,  $\text{Pb}^{+2}$ ,  $\text{Cu}^{+2}$  and  $\text{As}^{+3}$  at different pressures for all composite membranes.

Amide and azide functionalized carbon nanotubes gave better results as compared to oxidized CNTs at acidic pH 2.6 and pressure 4.90 bars, which was better than plain unfunctionalized CNTs. All the observations with results make an important part of this chapter.

## Chapter 5

In present study we report the use of novel initiators "Acyated carbon nanotubes" and various alkanoyl chlorides for ATRP of PMMA and polystyrene.

In a typical experiment, CuCl and bidentate ligand 2,2'-bipyridyl were mixed in RBF, equipped with a magnetic stirring bar and to this, emulsion of monomer was transferred by means of cannula using vacuum. To this system initiator was injected dropwise under nitrogen purging. The reaction mixture

was stirred at room temperature and at 60°C. The reaction was quenched by intensive cooling and diluted with tetrahydrofuran (THF). The formed polymer was recovered by precipitation in a non-solvent.

PMMA as well as Polystyrene have been prepared and analyzed by FT-IR, <sup>13</sup>C NMR, TGA, SEC and DSC techniques. The number average molecular weights (M<sub>n</sub>), weight average molecular weights (M<sub>w</sub>) and polydispersities were determined by GPC. The GPC results show that formed polymers have high molecular weights as compared to M<sub>theo</sub>. The linear plots of ln[M]<sub>0</sub>/[M] with time confirm the process to follow first order kinetics. The linear variation of polydispersity and average molecular weight with %conversion also account to formation of a polymer with good molecular weight distribution. It concludes that Acylated carbon nanotubes” and acetyl chloride can be used as initiators for ATRP, and that reducing the surfactant concentration gives a better control over molecular weights.

## References

- [1] Wang, X.; Li, Q.; Xie, J.; Jin, Z.; Wang, J.; Li, Y.; Jiang, K.; Fan, S. *Nano Letters* **2009**, *9*, 3137–3141.
- [2] Flahaut, E.; Bacsá, R.; Peigney, A.; Laurent, C. *Chemical Communications* **2003**, *12*, 1442–1443.
- [3] Cumings, J.; Zettl, A. *Science* **2011**, *289*, 602–604.
- [4] Treacy, M.M.J.; Ebbesen, T.W.; Gibson, J.M. *Nature* **1996**, *381*, 678–680.
- [5] Zavalniuk, V.; Marchenko, S. *Low Temperature Physics* **2011**, *37*, 337
- [6] Liu, L.; Guo, G.; Jayanthi, C.; Wu, S. *Phys. Rev. Lett.* **2002**, *88*, 217206.
- [7] Huhtala, M.; Kuronen, A.; Kaski, K. *Computer Physics Communications* **2002**, *146*, 30.
- [8] Yu, Kehan; Lu, G.; Bo, Z.; Mao, S.; Chen J. *J. Phys. Chem. Lett.* **2011**, *2*, 1556–1562..
- [9] Stoner, B.R.; Raut, A.S.; Brown, B.; Parker, C.B.; Glass, J.T. *Appl. Phys. Lett.* **2011**, *99*, 183104.
- [10] Hsu, Hsin-Cheng; Chen-Hao Wang, Nataraj, S.K.; Huang, H.C.; Du, He-Y.; Chang, S.T.; Chen, Li-C.; Chen K.H. *Diamond and Related Materials* **2012**, *25*, 176–9.
- [11] Parker, C.B.; Raut, A.S.; Brown, B.; Stoner, B.R.; Glass, J.T. *J. Mater. Res.* **2012**, *27*, 1046–53.
- [12] Cui, Hong-tao; O. Zhou, O.; Stoner, B.R. *J. Appl. Phys.* **2000**, *88*, 6072–4.
- [13] Yin, L.W.; Bando, Y.; Li, M.S.; Liu, Y.-X.; Qi, Y.X. *Adv. Mater.* **2003**, *15*, 1840–1844.
- [14] Q.X. Guo, Y. Xie, X.J. Wang, S.Y. Zhang, T. Hou, S.C. Lv, *Chem. Commun.* **2004**, *1*, 26–27.
- [15] Smith, B.W.; Luzzi, D.E. *Chem. Phys. Lett.* **2000**, *321*, 169–174.
- [16] Liu, Q.; Ren, W.; Chen, Zhi-Gang; Yin, L.; Li, F.; Cong, H.; Cheng, Hui-Ming *Carbon* **2009**, *47*, 731–736.
- [17] Zhao, X.; Liu, Y.; Inoue, S.; Suzuki, T.; Jones, R.; Ando, Y. *Phys. Rev. Lett.* **2004**, *92*, 125502.

- [18] Nikolaev, P.; Bronikowski, M. J.; Bradley, R. K.; Rohmund, F.; Colbert, D.T.; Smith, K. A.; Smalley, R. E. *Chemical Physics Letters* **1999**, *313*, 91–97
- [19] Ebbesen, T. W.; Ajayan, P. M. *Nature* **1992**, *358*, 220–222.
- [20] Prasek, J.; Drbohlavova, J.; Chomoucka, J.; Hubalek, J.; Jasek, O.; Adamc, V.; Kizek, R. *J. Mater. Chem.* **2011**, *21*, 15872–15884.
- [21] Ebbesen T.W.; Ajayan, P.M. *Nature* **1992**, *358*, 220–222.
- [22] Zhao, X.; Ohkohchi, M.; Shimoyama, H.; Ando, Y. *J. Cryst. Growth* **1999**, *198*, 934–938.
- [23] Saito, Y.; Okuda M.; Koyama, T. *Surf. Rev. Lett.* **1996**, *3*, 863–867.
- [24] Guo, T.; Nikolaev, P.; Thess, A.; Colbert, D.T.; Smalley, R.E. *Chem. Phys. Lett.* **1995**, *243*, 49–54.
- [25] Ikegami, T.; Nakanishi, F.; Uchiyama M.; Ebihara, K. *Thin Solid Films* **2004**, *457*, 7–11.
- [26] Kim, K.S.; Cota-Sanchez, G.; Kingston, C.; Imris, M.; Simard, B.; Soucy, G. *Journal of Physics D: Applied Physics* **2007**, *40*, 2375.
- [27] Narkiewicz, U.; Podsiadly, M.; Jedrzejewski, R.; Pelech, I. *Appl. Catal.* **2010**, *384*, 27–35.
- [28] Y. Shirazi, Y.; Tofighy, M.A.; Mohammadi, T.; Pak, *Appl. Surf. Sci.* **2011**, *257*, 7359–7367.
- [29] Yong, Z.; Fang, L.; Zhi-hua, Z. *Micron*, **2011**, *42*, 547–552.
- [30] Afolabi, A. S.; Abdulkareem, A. S.; Mhlanga, S. D.; Iyuke, S. E. *J. Exp. Nanosci.* **2011**, *6*, 248–262.
- [31] Zhu, J.; Yudasaka, M.; Iijima, S. *Chem. Phys. Lett.* **2003**, *380*, 496–502.
- [32] Zhang, D. S.; Shi, L. Y.; Fang, J. H.; Dai, K.; Li, X. K. *Mater. Chem. Phys.* **2006**, *97*, 415–419.
- [33] Liu, Y. C.; Sun, B. M.; Ding, Z. Y. in *Advanced Polymer Science and Engineering*, ed. Wang, C. H.; Ma, L. X.; Yang, W. **2011**, pp. 545–549.
- [34] Yu, M.F.; Lourie, O.; Dyer, M.J.; Moloni, K.; Kelly, T.F.; Ruoff, R.S. *Science* **2000**, *287*, 637–640.

- [35] Zhang, M.; Fang, S.; Zakhidov, A.A.; Lee, S.B.; Aliev, A.E.; Williams, C.D.; Atkinson, K.R.; Baughman, R.H. *Science* **2005**, *309*, 1215–1219.
- [36] Miaudet, P.; Badaire, S.; Maugey, M.; Derré, A.; Pichot, V.; Launois, P.; Poulin, P.; Zakri, C. *Nano Letters* **2005**, *5*, 2212–2215.
- [37] Sitharaman, B.; Shi, X.; Walboomers, X. F.; Liao, H.; Cuijpers, V.; Wilson, Lon J.; Mikos, A. G.; Jansen, John A. *Bone* **2008**, *43*, 362–370.
- [38] Postma, H. W. Ch.; Teepen, T.; Yao, Z.; Grifoni, M.; Dekker, C. *Science* **2011**, *293*, 76–9.
- [39] Bradley, K.; Gabriel, J. C. P.; Grüner, G. *Nano Letters* **2003**, *3*, 1353–1355.
- [40] Guldi; Dirk, M.; Rahman, G.M.A.; Prato, M.; Jux, N.; Qin, S.; Ford W. *Angewandte Chemie* **2005**, *117*, 2051–2054.
- [41] Dillon, A. C.; Jones, K. M.; Bekkedahl, T.A.; Klang, C. H.; Bethune, D. S.; Heben, M. J. *Nature* **1997**, *386*, 377–379.
- [42] Halber, Deborah. MIT LEES on Batteries. Lees.mit.edu. Retrieved on **2012-06-06**.
- [43] Bourzac, Katherine. "Nano Paint Could Make Airplanes Invisible to Radar." Technology Review. MIT, 5 December **2011**.
- [44] Stafiej, A.; Pyrzynska, K. *Separation and purification technology* **2007**, *58*, 49-52
- [45] Abdel Salam, M. *Inter. J. Environmental Sci. and Techno.* **2013**, *10*, 677-688
- [46] Li, Y.H.; Di, Z.C.; Luan, Z. K.; Ding, J.; Zuo, H.; Wu, X. Q.; Xu, C.L.; Wu, D.H. *J. Environ. Sci.* **2005**, *17*, 175-6
- [47] Wang, J.; Ma, X.; Fang, G.; Pan, M.; Ye, X.; Wang, S. *J. Hazard. Mater.* **2011**, *186*, 1985-1992.

- [48] Dai, B.; Cao, M.; Fang, G.; Liu, B.; Dong, X.; Pan, M.; Wang, S. *J. Hazard. Mater.* **2012**, 219-220, 103-10.
- [49] Salvador-Morales, C.; Flahaut, E.; Sim, E.; Sloan, J.; Malcolm L. H. Green, Robert B. Sim *Molecular Immunology* **2006**, 43, 193–201
- [50] Kowalczyk, P.; Holyst, R. *Environ. Sci. Technol.* **2008**, 42, 2931–2936
- [51] Tofighy, M. A.; Mohammadi, T. *J. Hazard. Mater.* **2011**, 185, 140-147
- [52] Shu-Huei Hsieh and Jao-Jia Horng *J. University of Sci. and Techno.* **2007**, 14, 77-84
- [53] Doong, R.A.; Chiang, L.F. *Water Sci. Tech.* **2008**, 58, 1985-92.
- [54] Sharma, A.; Kumar, S.; Tripathi, B.; Singh, M. *Int. J. Hyd. Ener.* **2009**, 34, 3977-3982.
- [55] Medina-Gonzalez, Y.; Remigy, J-C. *Mat.Lett.* **2011**, 65, 229-232.
- [56] (a) Tang, B. Z.; Xu, H. *Macromolecules* **1999**, 32, 2569. (b) M. S. P. Shaffer, A. H. Windle, *Adv. Mater.* **1999**, 11, 937.
- [57] Kang, Y.; Taton, T. A. J. *J. Am. Chem. Soc.* **2003**, 125, 5650.
- [58] Kong, H.; Gao, C.; Yan, D. *J. Am. Chem. Soc.* **2004**, 126, 412-413
- [59] U.N. Millenium Project, Health, dignity and development: what will it take? Task force on Water and Sanitation (Earthscan, **2005**).
- [60] Mark A. Shanon and Raphael Semiat, *MRS Bulletin* **2008**, 33, 9-13.
- [61] Agency for Toxic Substance and Disease Registry (ATSDR), Department of Health and Human Services (US).
- [62] Jagdish Kumar et al., Arsenic Contamination in Groundwater: Hotspots Discovered Through GIS Model During Recent Survey in Bihar and UP, in: M.G.K. Menon and V.P. Sharma (Eds.), *Sustainable Management of Water Resources: Emerging Science and Technology Issues in South Asia*, Indian National Science Academy, New Delhi, **2009**, pp. 315-326.

- [63] Pershagen, G. *Environmental Health Perspectives* **1981**, *40*, 93-100.
- [64] United Nations Synthesis Report on Arsenic in Drinking Water, [http://who.int/water\\_sanitation\\_health/Arsenic/ArsenicUNReptoc.htm](http://who.int/water_sanitation_health/Arsenic/ArsenicUNReptoc.htm).
- [65] Information Brief on Arsenic Contamination in India, UNICEF India Country office (Newsletter).
- [66] Li, Y. H.; Wang, S.; Luan, Z.; Ding, J.; Xu, C.; Wu, D. *Carbon* **2003**, *41*, 1057-1062.
- [67] US Environmental Protection Agency, Drinking Water Health Advisories, *Reviews of Environmental Contamination and Toxicology*, **1989**, *107*, 1-184.
- [68] Srinivasan, K.; Balasubramaniam, N.; Ramakrishna, T.V. *Indian J. Environ. Health* **1988**, *30*, 376-397.
- [69] Alexeeff, G.V. et al. *Sci. Total Environ.* **1989**, *86*, 156.
- [70] Katz, S.J. et al. *J. Appl. Toxicol.* **1993**, *13*, 217.
- [71] Sanj, R. *J. Occup. Med.*, **1989**, *31*, 1013.
- [72] Domingo, J.L. et al. *Reviews of Environmental Contamination and Toxicology* **1989**, *108*, 105-132.
- [73] US Environmental Protection Agency, Evaluation of Potential Carcinogenicity of Lead and Lead Compounds: in support of Reportable Quantity Adjustments Pursuant to CERCLA, Section 102, USEPA, Washington DC **1989**, 142.
- [74] Fitzgerald, W.F. et al. *Environ. Sci. Technol.* **1998**, *32*, 1-7.
- [75] Uludong, Y. et al. *Journal of Membrane Science* **1997**, *129*, 93-99.
- [76] Beukema, A. et al. *Environmental Monitoring and Assessment* **1986**, *7*, 117-155.
- [77] Coogan, T.P. et al. *CRC Critical Reviews in Toxicology* **1989**, *19*, 341-384.
- [78] Chakraaborti, D. et al. *Current Science* **1998**, *4*, 74.

- [79] Sahu, K.C. et al. *Current Science* **2001**, 83, 21-22.
- [80] Kakabadse, G. Chemistry of Effluent Treatment, Applied Science Publishers Ltd., London **1979**.
- [81] Stem, W. et al., Aquatic Chemistry, John Willy and Sons, New York **1970**.
- [82] Patterson, J.W. Wastewater Treatment Technology, *Ann. Arbor. Science, Ann Arbor, Michigan* **1975**.
- [83] Kiff, R.F. General Inorganic Effluents, In: Surveys in Industrial Wastewater Treatment Manufacturing and Chemical Industries, Barnes, D.; Foster, C.F.; Hurdey, S.E. (eds) 3:, Longman, New York **1987**.
- [84] Bhattacharya, D. et al. *AICHE Symposium Series, Water Research* **1981**, 77, 31-42.
- [85] Patterson, J.W. et al. *J. Wat. Pollt. Control. Fed.* **1977**, 49, 2397-2410.
- [86] Branter K.A. et al. *Ind. Wast. Proc. 13th Mica. Atlantic Cont. Ann. Arbor Science* **1981**, 12, 43-50.
- [87] Beszedits, S. et al. Chromium Removal from Industrial Wastewaters, In Environmental Science and Technology, Nriagu J.O.; Nieboer, E. (eds.), John Willy and Sons, New York, **1988**, 20, 231-235.
- [88] Knocke, W.R. et al. Recovery of Metals from Electroplating Wastes, Proc. 33rd Purdue Industrial Waste Conf. **1978**, 33, 415-426.
- [89] Heen, P.V. The Regional American Chemical Society Meeting **1977**.
- [90] Namasivayam, C. et al. *Bioresource Technology* **1997**, 62, 123-127.
- [91] Zeman, L.J. et al. Microfiltration and Ultrafiltration, New York, Marcel Dekker, **1996**.
- [92] Wang, X. et al. *Journal of Membrane Science* **2006**, 278, 261-268.
- [93] Bessbousse, H. et al. *Journal of Membrane Science* **2008**, 307, 249-259.
- [94] Lee, H.S. *Desalination* **2008**, 219, 48-56.

- [95] Jain, S.K. Drinking water purification technologies using membranes and resins, in: Menon, M.G.K. and Sharma, V.P. (Eds.), Sustainable Management of Water Resources: Emerging Science and Technology Issues in South Asia, Indian National Science Academy, New Delhi, **2009**, 131-141.
- [96] Chian, E. S. K. *Water, AICRE Symp. Ser.* **1975**,71, 87-92.
- [97] U.S.E.P.A., Control Technology for Metal Finishing Industry- Evaporators, EPA-625/8/79/002, Cincinnati, OH **1977**.
- [98] Wing R.E. et al., Removal of Heavy Metals from Industrial Wastewater Using insoluble Starch Xanthate, EPA-600/2/78/085, A. S. EPA **1978**.
- [99] Seader J.D.; Henley, E.J. Separation Process Principles, Wiley, New York, USA, **1998**, 778-789.
- [100] Dakiky, M.; Khami, A.; Manannra A.; Mereb, M. *Adv. Environ. Res.* **2002**, 6, 533-540.
- [101] De Castro Dantas, T.N.; Dantas Neto, A.A.; De A. Moura, M.C.P. *Water Res.* **2011**, 35, 2219-2224.
- [102] Applegate, L.E. *Chem. Eng.* **1984**, 91, 64-89.
- [103] Sengupta A.K.; Clifford, D. *Environ. Sci. Technol.* **1986**, 20, 149-155.
- [104] Li, Y.H.; Ding, J.; Luan, Z.; Di, Z.; Zhu, Y.; Xu, C.; Wu D.; Wei, B. *Carbon* **2003**, 41, 2787-2792.
- [105] Lu C.; Chiu, H. *Chem. Eng. Sci.* **2006**, 61, 1138-1145.
- [106] Li, Y.H.; Wang, S.; Luan, Z.; Ding, J.; Xu C.; Wu, D. *Carbon* **2003**, 41, 1057-1062.
- [107] Fuhrman, H.G.; Wu, P.; Zhou, Y.; Ledin, A. *Desalination* **2008**, 226, 357-370.
- [108] Rengaraj, S.; Yoon, K.H.; Moon, S.H. *J. Radioanal. Nucl. Chem.* **2002**, 253, 241-245.
- [109] Singh, D.K.; Lal, J. *Indian Journal of Environmental Health* **1992**, 34, 108-113.
- [110] Rengaraj S.; Moon, S.H. *Water Res.* **2002**, 36, 1783-1793.
- [111] Tang, T. et al., *Angew. Chem. Int. Ed.* **2005**, 44, 1517-1520.

- [112] Dekker, C. *Physics Today* **1999**, 52, 22.
- [113] Peng, S. et al., *Mater. Lett.* **2005**, 59, 399-403.
- [114] Nora Savage, Mamadou S. Diallo, *J. Nanopart. Res.* **2005**, 7, 331.
- [115] Babel, S.; Kurniawani, T.A. *J. Hazardous Mater.* **2003**, 97, 219-243.
- [116] Bailey, S.E.; Olin, T.J.; Bricka, R.M. *Water Res.* **1999**, 33, 2469-2479.
- [117] Nabi, S.A.; Naushad, Mu.; Bushra, R. *Adsorpt. Sci. Technol.* **2009**, 27, 423 .
- [118] Kobya, M.; Demirbas, E.; Oncel, M.S.; Sencan, S. *Adsorpt. Sci. Technol.* **2002**, 20, 179.
- [119] Hashem, A.; Abdel-Halim, E.S.; El-Tahlawy, Kh. F.; Hebeish, A. *Adsorpt. Sci. Technol.* **2005**, 23, 367.
- [120] Abuilaiwi, F.A.; Atieh, M.A.; Ahmad, M.B.; Ibrahim, N.A.; Rahman, M.Z.A.; Yunus, W. Md. Z. W. *Adsorpt. Sci. Technol.* **2009**, 27, 661.
- [121] Zhao, X.; Holl, W.H.; Yun, G. *Water Res.* **2002**, 36, 851–858.
- [122] Henry, W.D.; Zhao, D.; Sen Gupta A.K.; Lange, C. *React. Funct. Polym.* **2004**, 60, 109–120.
- [123] Basso, M.C.; Cerrella E.G.; Cukierman, A.L. *Ind. Eng. Chem. Res.* **2002**, 41, 180–189.
- [124] Xianjia Peng, Luan, Z.; Ding, J.; Di, Z.; Li, Y.H.; Tian, B. *Mater. Lett.* **2004**, 59, 399.
- [125] Li, Y.H.; Ding, J.; Luan, Z.; Di, Z.; Zhu, Y.; Xu, C.; Wu, D.; Wei, B. *Carbon* **2003**, 41, 2787.
- [126] Ebbesen, T.W.; Ajayan, P.M.; Hiura, H.; Tanigaki, K. *Nature* **1994**, 367, 519.
- [127] Chen, Y.K.; Green, M.L.H.; Griffin, J.L.; Hammer, J.; Lago, R.M.; Tsang, S.K. *Adv. Mater.* **1996**, 8, 1012.
- [128] Hiura, H.; Ebbesen T.W.; Tanigaki, K. *Adv. Mater.* **1995**, 7, 275.
- [129] Tsang, S.C.; Chen, Y.K.; Harris P.J.F.; Green, M.L.H. *Nature* **1994**, 372, 159.
- [130] Chang, H.; Bard, A.J. *J. Am. Chem. Soc.* **1991**, 113, 5588.

- [131] Colbert, D.T.; Zhang, J.; McClure, S.M.; Nikolaev, P.; Chen, Z.; Hafner, J.H.; Owens, D.W.; Kotula, P.G.; Carter, C.B.; Weaver, J.H.; Rinzler, A.G.; Smalley, R.E. *Science* **1994**, *266*, 1218.
- [132] Tamura, R.; Tsukada, M. *Phys. Rev.* **1995**, *B 52*, 6015.
- [133] Bonard, J.M.; Stora, T.; Salvétat, J.P.; Maier, F.; Stöckli, T.; Duschl, C.; Forró, L.; de Heer, W.A.; Châtelain, A. *Adv. Mater.* **1997**, *827*, 9.
- [134] Dresselhaus, M.S.; Dresselhaus, G.; Saito, R.; Jorio, A. *Physics Reports* **2005**, *409*, 47-99
- [135] Zhang, H.B.; Lin, G.D.; Zhou, Z.H.; Dong, X.; Chen, T. *Carbon* **2002**, *40* 2429–2436
- [136] Antunes, E.F.; Lobo, A.O.; Corat, E.J.; Trava-Airoldi, V.J.; Martin, A.A.; Verissimo, C. *Carbon* **2006**, *44*, 2202–2211
- [137] Gupta, S.; Babu, B.V. *J. Environ. Man.* **2009**, *90*, 3013-3022.
- [138] Ho Y.S.; McKay, G. *Water Res.* **2000**, *34*, 735-742.
- [139] Hall, K.R.; Eagleton, L.C.; Acrivos, A.; Vermeulen, T. *Ind. Eng. Chem. Fundam.* **1966**, *5(2)*, 212–223 (1966).
- [140] Hu, H.; Zhao, B.; Itkis, M.E.; Haddon, R.C. *J. Phys. Chem. B* **2003**, *107*, 13838–13842.
- [141] Martinez, M.T.; Callejas, M.A.; Benito, A.M.; Cochet, M.; Seeger, T.; Anson, A.; et al. *Carbon* **2003**, *41*, 2247–2256.
- [142] Bower, C.; Kleinhammes, A.; Wu, Y.; Zhou, O. *Chem. Phys. Lett.* **1998**, *288*, 481–486.
- [143] Ziegler, K.J.; Gu, Z.; Peng, H.; Flor, E.L.; Hauge, R.H.; Smalley, R.E. *J. Ame. Chem. Soc.* **2005**, *127*, 1541–1547.
- [144] Datsyuk, V.; Kalyva, M.; Papagelis, K.; Parthenios, J.; Tasis, D.; Siokou, A.; Kallitsis, I.; Galiotis, C. *Carbon* **2008**, *46*, 833-840
- [145] Hou, P.; Liu, C.; Tong, Y.; Xu, S.; Liu, M.; Cheng, H.J. *Mater. Res.* **2001**, *16*, 2526–9.

- [146] Rinzler, A.G.; Liu, J.; Dai, H.; Nikolaev, P.; Huffman, C.B.; Macias, F.J.R. et al. *Appl. Phys. A* **1998**, *67*, 29–37.
- [147] Ajayan, P.M.; Ebbesen, T.W.; Ichihashi, T.; Iijima, S.; Tanigaki, K.; Hura, H. *Nature* **1993**, *362*, 522–4.
- [148] Dresselhaus, M.S.; Dresselhaus, G.; Saito, R.; Jorio, A. *Physics Reports* **2005**, *409*, 47–99
- [149] Zhang, H.B.; Lin, G.D.; Zhou, Z.H.; Dong, X.; Chen, T. *Carbon* **2002**, *40*, 2429–2436
- [150] Antunes, E.F.; Lobo, A.O.; Corat, E.J.; Trava-Airoldi, V.J.; Martin, A.A.; Verissimo, C. *Carbon*, **2006**, *44*, 2202–2211
- [151] Haibin, C.; David, S.S. *J. Mem. Sci.* **2006**, *269*, 152–160.
- [152] Kim, S.; Joerg, R.; Jinschek, H.C.; David, S.; Sholl, E.M. *Nano letters* **2007**, *7*, 2806–2811.
- [153] Deng, J.; Zhang, X.; Wang, K.; Zou, H.; Zhang, Q.; Fu, Q. *J. Mem.Sci.* **2007**, *288*, 261–267.
- [154] Roy, S.; Ntim, S.A.; Mitra, S.; Sirkar, K.K. *J.Memb.Sci.* **2011**, *375*, 81–87.
- [155] Sharma, A.; Kumar, S.; Tripathi, B.; Singh, M.; Vijay, Y.K. *Int. J. Hyd. Ener.* **2009**, *39*, 3977–3982.
- [156] Medina-Gonzalez, Y.; Remigy, J.C. *Mat.Lett.* **2011**, *65*, 229–232.
- [157] Lee, K.W.; Seo, B.K.; Nam, S.T.; Han, M.J. **2003**, *159*, 289.
- [158] Ahmad, A.L.; Sarif, M.; Ismail, S. *Desalination* **2005**, *179*, 25.
- [159] Han, M.J.; Nam, S.T. *J. Memb. Sci.* **2002**, *202*, 55–61.
- [160] Zhao, Z.P.; Wang, Z.; Wang, S.C. *J.Memb. Sci.* **2003**, *217*, 151–158.
- [161] Möckel, D.; Staude, E.; Guiver, M.D. *J.Memb. Sci.* **1999**, *158*, 63–75.
- [162] Higuchi, A.; Mishima, S.; Nakagawa, T. *J.Memb. Sci.* **1991**, *57*, 175–185.
- [163] Robert Y.M. Huang, Rajinder Pal, Go Young Moon, *J.Memb. Sci.* **1999**, *160*, 17–30
- [164] Klein, E.; Eichholz, E.; Don H.; Yeager *J.Memb. Sci.* **1994**, *90*, 69–80.
- [165] Zhao, S.; Wang, Z.; Wei, X.; Zhao, B.; Wang, J.; Yang, S.; Wang, S. *J.Memb. Sci.* **2011**, *385*, 251–262.

- [166] Nyström, M.; Järvinen, P. *J.Memb. Sci.* **1987**, *60*, 275-296.
- [167] Rodemann, K.; Staude, E. *J.Memb. Sci.* **1994**, *88*, 271-278.
- [168] Zhao, C.; Liu, X.; Rikimaru, S.; Nomizu, M.; Nishi, N. *J.Memb. Sci.* **2003**, *214*, 179-189.
- [169] Rucka, M.; Poźniak, G.; Turkiewicz, B.; Trochimczuk, W. *Enzyme and Microbial Technology* **1996**, *18*, 477-481.
- [170] Kim, K.S.; Lee, K.H.; Cho, K.; Park, C.E. *J.Memb. Sci.* **2002**, *199*, 135-145.
- [171] Kim, S.; Chen, L.; Johnson, J.K.; Marand, E. *J.Memb. Sci.* **2007**, *294*, 147-158.
- [172] Ahn, J.; Chung, W.-J.; Pinnau, I.; Guiver, M.D. *J.Memb. Sci.* **2008**, *314*, 123-133.
- [173] Ge, L.; Zhu, Z.; Rudolph, V. *Sep. Puri. Tech.* **2011**, *78*, 76-82.
- [174] Lei, G.; Zhonghua, Z.; Feng, L.; Shaomin, L.; Li, W.; Xuegang, T.; Victor, R.J. *Phys. Chem. C.* **2011**, *115*, 6661-6670.
- [175] Celik, E.; Liu, L.; Choi, H. *Water Res.* **2011**, *45*, 5287-5294.
- [176] Qiu, S.; Wu, L.; Panc, X.; Zhanga, L.; Chena, H.; Gao, C. *J. Memb. Sci.* **2009**, *342*, 165-172.
- [177] Choi, J.-H.; Jegal, J.; Kim, W.-N. *J.Memb. Sci.* **2006**, *284*, 406-415.
- [178] Qiu, S.; Wu, L.; Pan, X.; Zhang, L.; Chen, H.; Gao, C. *J.Memb. Sci.* **2009**, *342*, 165-172.
- [179] Bonard, J.M.; Stora, T.; Salvetat, J.P.; Maier, F.; Stockli, T.; Duschl, C.; Forro, L.; de Heer, W.A.; Chatelain, A. *Adv. Mater.* **1997**, *9*, 827-831.
- [180] Jena, A.K.; Gupta, K.M. *J. Power Sources* **1999**, *80*, 46.
- [181] Jena, A.K.; Gupta, K.M. *J. Power Sources* **2001**, *96*, 214.
- [182] Celik, E.; Park, H.; Choi, H.; Choi, H. *Water Res.* **2011**, *45*, 274.
- [183] Rong, C.; Ma, G.; Zhang, S.; Song, L.; Chen, Z.; Wang, G.; Ajayan, P.M. *Compos. Sci. Techno.* **2010**, *70*, 380.
- [184] Wang, J.S.; Matyjaszewski, K. *Macromolecules* **1995**, *28*, 7901
- [185] Wang, J.S.; Matyjaszewski, K. *J. Am. Chem. Soc.* **1995**, *117*, 5614.
- [186] Kato, M.; Kamigato, M.; Sawamoto, M.; Higashimura, T. *Macromolecules* **1995**, *28*, 1721

- [187] Destarac, M.; Bessiere, J.M.; Boutevin, B.J. *Polym. Sci. Part A: Polymer Chemistry* **1998**, *36*, 2933-2947.
- [188] Davis, K.A.; Matyjaszewski, K. *Adv. Polym. Sci.* **2002**, *159*, 1–13
- [189] Coessens, V.; Pintauer, T.; Matyjaszewski, K. *Prog. Polym. Sci.* **2001**, *26*, 337–377
- [190] Pyun, J.; Matyjaszewski, K. *Chem. Mater.* **2001**, *13*, 3436–3448
- [191] Matyjaszewski, K.; Xia, J. *Chem. Rev.* **2001**, *101*, 2921
- [192] Kamigaito, M.; Ando, T.; Sawamoto, M. *Chem. Rev.* **2001**, *101*, 3689
- [193] Ritz, a P.; La´talova,´ a P.; Janata, a M.; Toman, a L.; Kr´ı´z,ˇ a J.; Genzer, b J.; Vlcˇek, a P. *Science Direct Reactive & Functional Polymers* **2007**, *67*, 1027–1039
- [194] Qifeng Chen, Zhenbiao Zhang, Nianchen Zhou, Zhengping Cheng, Jian Zhu, Wei Zhang, Xiulin Zhu *J. Polym. Sci. Part A: Polym. Chem.* **2011**, *49*, 3588-3594.
- [195] Peng Liu and Zhixing Su *Polymer Bulletin* **2005**, *55*, 41-417
- [196] Dnyaneshwar V. Palaskar; Prakash S. Sane; Prakash P. Wadgaonkar *Reactive and Functional Polymers* **2010**, *70*, 931-937
- [197] Haddleton, D.M.; Jasieczek, C.B.; Hannon, M.J.; Shooter, A.J. *Macromolecules* **1997**, *30*, 2190–2193
- [198] Haddleton, D.M.; Crossman, M.C.; Dana, B.H.; Duncalf, D.J.; Heming, A.M.; Kukulj, D.; Shooter, A.J. *Macromolecules* **1999**, *32*, 2110–2119
- [199] Moineau, G.; Granel, C.; Dubois, P.; Jerome, R.; Teyssie, P. *Macromolecules* **1998**, *31*, 542–544
- [200] Uegaki, H.; Kotani, Y.; Kamigaito, M.; Sawamoto M. *Macromolecules* **1997**, *30*, 2249–2253
- [201] Kotani, Y.; Kamigaito, M.; Sawamoto, M. *Macromolecules* **1999**, *32*, 2420–2424
- [202] Percec, V.; Barboiu, B.; Neumann, A.; Ronda, J.C.; Zhao, M. *Macromolecules* **1996**, *29*, 3665–3668

- [203] Percec, V.; Barboiu, B. *Macromolecules* **1995**, *28*, 7970–7972
- [204] Aleksandra Malinowska, Petr Vlček, Jaroslav Kříž, Luděk Toman, Petra Látalová, Miroslav Janata, Bohumil Masař *Polymer* **2004**, *46*, 5-14
- [205] Miroslav Janata, Bohumil Masař, Luděk Toman, Petr Vlček, Petra Polická, Jiří Brus, Petr Holler *Reactive and Functional Polymers* **2001**, *50*, 67-75
- [206] Yong Gao, Songqing Li, Huaming Li, Xiayu Wang *European Polymer Journal* **2005**, *41*, 2329-2334
- [207] Hao Kong, Chao Gao, Deyue Yan *J. Material Chemistry* **2004**, *14*, 1401-1405
- [208] Guoyong Xu, Wei-Tai Wu, Yusong Wang, Wenmin Pang, Qingren Zhu, Pinghua Wang, Yezi You *Polymer* **2006**, *47*, 5909-5918
- [209] Armand Soldera *Macromol. Symp.* **1998**, *133*, 21-32
- [210] Karasz, F.E.; MacKnight, W.J. *Macromolecules* **1968**, *6*, 537-540
- [211] O'Reilly, J.M.; Mosher, R.A. *Macromolecules* **1981**, *14*, 602
- [212] Hao Kong, Chao Gao, Deyue Yan *J. Materials. Chem.* **2004**, Doi:10.1039/B401180E
- [213] Richard Cramer **1957**, *79*, 6215-6219
- [214] Faltings, K. *Ber.* **1939**, *73B*, 1207
- [215] Huisgen, R.; Jacob, F. *Ann.* **1954**, *690*, 37

## List of Publications & Presentations

### *Publications*

- 1) **Prachi Shah, C. N. Murthy\*** “Studies on the porosity control of MWCNT/polysulfone composite membrane and its effect on metal removal”, *J.Memb. Sci.*, **2013**, 437, 90-98

### *Presentations*

- 1) DAE-BRNS Theme meeting on “**Membrane Separations for Fuel Cycle Applications**” (**MEMSEP-2013**) on 16-17<sup>th</sup> September, 2013 at Bhabha Atomic Research Centre, Mumbai
- 2) National Conference **AMPM-13** on 6<sup>th</sup> April, 2013 at Faculty of Technology and Engineering, M. S. University of Baroda, Vadodara.
- 3) **Gujarat Science Congress** on 26<sup>th</sup> February, 2012 at Geology Department, Faculty of Science, M. S. University of Baroda, Vadodara.
- 4) National Conference on “**Advances in Polymer Science & Nanotechnology: Design and Structure**” (**PSNDS-11**) on 16-17<sup>th</sup> December, 2011 at Faculty of Technology and Engineering, M. S. University of Baroda, Vadodara.
- 5) DAE-BRNS 3<sup>rd</sup> **International Symposium Materials Chemistry (ISMC-2010)** on 7-11<sup>th</sup> December, 2010 at Bhabha Atomic Research Centre, Mumbai.
- 6) **Sixth All Gujarat Research Scholars Meet (AGRSM-VI)** on 31<sup>st</sup> January, 2010 at Dept. of Chemistry, Faculty of Science, M. S. University of Baroda, Vadodara.
- 7) National Conference on “**Water: Membranes and other Purification Technologies**” on 9-10<sup>th</sup> January, 2010 at Faculty of Technology and Engineering, M. S. University of Baroda, Vadodara.

## **List of Awards**

- 1) **Best Poster Award** at National Conference **AMPM-13** on 6<sup>th</sup> April, 2013 at Faculty of Technology and Engineering, M. S. University of Baroda, Vadodara.
- 2) **Best Oral Presentation** at **Gujarat Science Congress** on 26<sup>th</sup> February, 2012 at Geology Department, Faculty of Science, M. S. University of Baroda, Vadodara.
- 3) **Best Paper Award** at DAE-BRNS 3<sup>rd</sup> **International Symposium Materials Chemistry (ISMC-2010)** on 7-11<sup>th</sup> December, 2010 at Bhabha Atomic Research Centre, Mumbai.

**THANK YOU**